JÉSSICA BORELI DOS REIS LINO

ENHANCING NMR QUANTUM COMPUTATION BY OPTIMIZING SPECTROSCOPIC PARAMETERS OF POTENTIAL QUBIT MOLECULES

LAVRAS-MG
2021

JÉSSICA BORELI DOS REIS LINO

ENHANCING NMR QUANTUM COMPUTATION BY OPTIMIZING SPECTROSCOPIC PARAMETERS OF POTENTIAL QUBIT MOLECULES

Tese apresentado à Universidade Federal de Lavras, como parte das exigências do Programa de Pós-Graduação em Agroquímica, área de concentração em Química/Bioquímica, para obtenção do título de Doutor.

Dr. Teodorico de Castro Ramalho
Orientador

LAVRAS-MG
2021

Ficha catalográfica elaborada pelo Sistema de Geração de Ficha Catalográfica da Biblioteca Universitária da UFLA, com dados informados pelo(a) próprio(a) autor(a).

Lino, Jéssica Boreli dos Reis.
Enhancing NMR quantum computation by optimizing spectroscopic parameters of potential qubit molecules / Jéssica Boreli dos Reis Lino. - 2021.
103 p. : il.

Orientador(a): Teodorico de Castro Ramalho.

Tese (doutorado) - Universidade Federal de Lavras, 2021.
Bibliografia.

1. Cálculos de parâmetros de NMR. 2. Computação quântica. 3. Informação quântica. I. Ramalho, Teodorico de Castro. II. Título.

JÉSSICA BORELI DOS REIS LINO

ENHANCING NMR QUANTUM COMPUTATION BY OPTIMIZING SPECTROSCOPIC PARAMETERS OF POTENTIAL QUBIT MOLECULES

Tese apresentado à Universidade Federal de Lavras, como parte das exigências do Programa de Pós-Graduação em Agroquímica, área de concentração em Química/Bioquímica, para obtenção do título de Doutor.

APROVADA em 16 de dezembro de 2021.

Dr. André Farias de Moura	UFSCar
Dr. Moisés Porfírio Rojas Leyva	UFLA
Dra. Paula Homem de Mello	UFABC
Dr. Sérgio Scherrer Thomasi	UFLA

Prof. Dr. Teodorico de Castro Ramalho
Orientador

LAVRAS - MG
2021

Dedicated to my family

ACKNOWLEDGMENTS

The realization of this work was only possible thanks to the collaboration, both professional and affective, of many people. I would like to express my sincere gratitude to all of you who in any way helped me in this journey.

I would like to thank the destiny for being always so generous with me, blessing my steps and filling up my way with extraordinary people.

My dear and beloved family, my husband Vinícius, my two years old son Inácio, especially my little baby, who I am expecting in March; my sister Jaqueline and my parents, Rogério and Andréia, thank you all for the unconditional love and incessant incentive for the sake of my knowledge achievement and triumph. And all my family, who always believed and encouraged me.

Professor Teodorico de Castro Ramalho, to whom I am grateful for the trust, opportunity, and teachings. Certainly, I was privileged to have you as my supervisor and counselor.

All the friendships that UFLA and Lavras city blessed me with; without you all, this journey would have been certainly more arduous.

Colleagues from the Computational Chemistry Laboratory for support and assistance.

All the professors and people from the Chemistry Department, for dedication, attention, friendship, and teaching.

The Federal University of Lavras and to the Chemistry Department for the opportunities.

In special, I would like to thank Professor Stephan P. A. Sauer, who welcomed me with open arms, with whom I had the honor to learn very much more than I could ever imagine. Thank you sincerely for everything!

Sauer's group, who also welcomed and helped me a lot during my stay in Denmark.

To Denmark's friends, especially Fernanda, who cheered me up when I needed more and became my dear and loved friend.

The Copenhagen University and the Chemistry Department for the opportunity and financial support.

The Coordination for the Improvement of Higher Education Personnel (CAPES) for the scholarship and support; also, FAPEMIG and CNPq for support.

This study was financed in part by the Coordenação de Aperfeiçoamento de Pessoal de Nível Superior – Brasil (CAPES) – Finance Code 001

To everyone who contributed directly or indirectly to the conclusion of this degree,

THANK YOU SO MUCH!

"We are currently in the midst of a second quantum revolution. The first one gave us new rules that govern physical reality. The second one will take these rules and use them to develop new technologies." (Dowling and Milburn, 2003)

RESUMO GERAL

A computação quântica é o campo da ciência que usa fenômenos da mecânica quântica, como superposição e emaranhamento, para realizar operações em dados. A unidade de informação básica usada na computação quântica é o bit quântico ou qubit. Sabe-se que os computadores quânticos poderiam teoricamente ser capazes de resolver problemas muito mais rapidamente do que qualquer computador clássico. Atualmente, a ressonância magnética nuclear (RMN) no estado líquido enriquece o processamento da informação quântica (PIQ), inspirando novas ideias para sua investigação teórica e experimental, desenvolvendo tecnologias para demonstrar a computação quântica em pequenos sistemas físicos. Não obstante, as moléculas que permitem implementações de muitos quantum bits (qubits) no PIQ via RMN devem atender a algumas condições em relação às suas propriedades espectroscópicas. Em primeiro momento, constantes de acoplamento através do espaço (TS) de ^{31}P-^{31}P excepcionalmente grandes observados em 1,8-difosfanaftalenos (PPN) e em nafto[1,8-cd]-1,2-ditiole fenilfosfinas (NTP) foram propostas e investigadas com intuito de fornecer um controle mais preciso no PIQ por RMN em grande escala. Propriedades espectroscópicas de derivados de PPN e NTP, como deslocamento químicos e acoplamentos spin-spin através do espaço foram exploradas por estratégias teóricas. A partir de nossos resultados, os derivados PPN_o-F, PPN_o-etil e PPN_o-NH_2 foram os melhores candidatos para processamento de informação quântica via RMN, na qual a elevada constante de acoplamento TS poderia contornar a necessidade de longos tempos nas implementações de portas quânticas. O que poderia, em princípio, superar as limitações naturais relacionadas ao desenvolvimento do PIQ via RMN em larga escala. No segundo artigo, relatamos uma estratégia de design computacional para pré-seleção de complexos recentemente sintetizados de cádmio, mercúrio, telúrio, selênio e fósforo (chamados complexos MRE) como moléculas qubit adequadas para o PIQ via RMN. Deslocamentos químicos e constantes de acoplamento spin−spin em cinco complexos MRE foram examinados usando a aproximação regular de ordem zero (ZORA) a nível DFT (Teoria do funcional de densidade) e a abordagem relativística de quatro componentes de Dirac−Kohn−Sham. Usados juntos com os qubits mais comumente utilizados em experimentos de computação quântica via RMN, núcleos de spin-1/2, como ^{113}Cd, ^{199}Hg, ^{125}Te e ^{77}Se, podem alavancar as futuras arquiteturas de computadores quânticos escaláveis, permitindo muitos qubits heteronucleares para implementações do PIQ via RMN.

Palavras-chave: Cálculos de parâmetros de NMR. Computação quântica. Informação quântica.

GENERAL ABSTRACT

Quantum computing is the field of science that uses quantum-mechanical phenomena, such as superposition and entanglement, to perform operations on data. The fundamental information unit used in quantum computing is the quantum bit or qubit. It is well known that quantum computers could theoretically be able to solve problems much more quickly than any classical computers. Currently, liquid state nuclear resonance magnetic (NMR) enriches quantum information processing (QIP) by inspiring new ideas for theoretical and experimental investigation, leading to technology for demonstrating quantum computing in small physical systems. Notwithstanding, molecules that enable many qubits NMR QIP implementations should meet some conditions regarding their spectroscopic properties. First, exceptionally large through-space (TS) P-P SSCCs observed in 1,8-diphosphanaphthalenes (PPN) and in naphtho[1,8-cd]-1,2-dithiole phenylphosphines (NTP) were proposed and investigated to provide more accurate control within large-scale NMR QIP. Spectroscopic properties of PPN and NTP derivatives, as chemical shifts and through-space spin-spin couplings were explored by theoretical strategies. From our results, the derivatives PPN_o-F, PPN_o-ethyl and PPN_o-NH_2 were the best candidates for quantum information processing via NMR, where the large TS J could circumvent the need of long-time quantum gate implementations. Which could, in principle, overcome natural limitations related to the development of large-scale NMR QIP. In the second paper, we report a computational design strategy for prescreening recently synthesized complexes of cadmium, mercury, tellurium, selenium, and phosphorus (called MRE complexes) as suitable qubit molecules for NMR QIP. Chemical shifts and spin–spin coupling constants in five MRE complexes were examined using the spin–orbit zeroth order regular approximation (ZORA) at the density functional theory level and the four-component relativistic Dirac–Kohn–Sham approach. Assembled together with the most common qubits used in NMR quantum computation experiments, spin-1/2 nuclei, such as ^{113}Cd, ^{199}Hg, ^{125}Te, and ^{77}Se, could leverage the prospective scalable quantum computer architectures, enabling many and heteronuclear qubits for NMR QIP implementations.

Keywords: NMR parameters calculations. Quantum computation. Quantum information.

SUMMARY

FIRST PART

1 INTRODUTION

Quantum mechanics has a reputation for being not only mysterious but also far removed from our daily life. But there is a high-quality device in a chemistry laboratory called nuclear magnetic resonance (NMR) spectrometer, whose operation is described using language usually utilized for describing elementary quantum systems. However, NMR spectrometer operates on macroscopic samples of ordinary liquids, usually organic compounds in inert solvents. Of course, a complete explanation of any spectroscopic experiment requires quantum mechanics. But only in NMR, the lifetimes of multiparticle quantum states are often long enough to appreciate the complexity of the dynamics of such states.

Moreover, NMR was one of the early platforms and still has been used to perform experimental demonstrations of quantum information processing (QIP). These demonstrations are the first step toward realizing the dreamed quantum computer: a device that harnesses the complexity of quantum dynamics to solve computational problems that are and will remain forever beyond the reach of classical computers. The success of NMR as a testbed of experimental QIP may be attributed to the well-established theory of NMR and availability of extremely sophisticated NMR instruments.

The fundamental information-processing elements used in NMR are two-level nuclear spins, called qubits, which are bound together in a single molecule. A liquid NMR sample contains a macroscopic number of molecules, each of which functions as an independent information-processing unit. The molecules are initially in thermal equilibrium at high enough temperature that the nuclear spins are only weakly polarized along the direction of a strong magnetic field. NMR techniques cannot control the quantum states of individual molecules, and the measurements performed in NMR detect the average magnetization of the entire sample[1].

Meanwhile, the advancement of the aimed NMR large-scale quantum processors depends mainly on two challenges; first, the accurate and efficient control of the quantum system states, and second, the construction of systems containing a large number of qubits[2]. The former has been augmented by the development of algorithms which are able to manipulate, with high fidelity, the quantum states of relatively large systems[3]. Recently,

---

[1] MENICUCCI, N. C.; CAVES, C. M. Local Realistic Model for the Dynamics of Bulk-Ensemble NMR Information Processing. **Physical Review Letters**, v. 88, n. 16, p. 167901-167905, Apr. 2002.

[2] VIND, F.; FOERSTER, A.; OLIVEIRA, I. *et al*. Experimental realization of the Yang-Baxter Equation via NMR interferometry. **Scientific Reports**, v. 6, n. 20789, p. 1-8, Feb. 2016.

[3] LU, D. *et al*. Enhancing quantum control by bootstrapping a quantum processor of 12 qubits. **npj Quantum Information**, v. 3, n. 45, p. 1-7, Oct. 2017.

Peterson et al.[4] have designed a fast and scalable algorithm for controlling the quantum states of systems containing 100 qubits.

These recent algorithms combined with modern NMR equipments, and sophisticated theoretical techniques make possible the manipulation of the nuclear spin system states through magnetic radio-frequency (RF) pulses, which are used to implement quantum gates, the basic computational step[4].

Regarding the second challenge, chemistry can leverage the development of NMR large-scale quantum systems, once it depends especially on the design of a qubit molecule containing numerous suitable spin-1/2 nuclei, which acts as the qubits. In this way, theoretical chemistry can speed up the sharpening of the potential qubit molecule concerning its physical requirements[5], towards a specially synthesized system, giving resolvable spectra to the upcoming large-scale NMR quantum processor.

Computational Chemistry is the branch of chemical knowledge that makes use of computer-based methods to understand and predict the behavior of molecular systems. In this scenario, our work aimed to highlight the relevant aspects of QIP via NMR from a chemical point of view, emphasizing the importance and role of spectroscopic properties related to qubit molecules, as well as the possibility of studying these molecules theoretically through Computational Chemistry, in order to lead us to advances in scientific research related to quantum computing for new paradigms.

It should be kept in mind that qubit molecules must meet some specific conditions related to their structural and electronic parameters, as well as spectroscopic properties. In this perspective, detailed computational work on this subject could potentially be adopted in the discovery and optimization of newly designed qubit molecules for the processing of quantum information.

This work is divided into two parts, the first one carefully discusses quantum computation via NMR, as well as theoretical calculations of chemical displacement and scalar spin-spin coupling constant. The aim was to make the text and the connections between the subjects clear to readers, especially chemists, since the theme of this work is generally more common by physicists.

---

[4] PETERSON, J. P.S.; SARTHOUR, R. S.; LAFLAMME, R. Enhancing Quantum Control by Improving Shaped-Pulse Generation. **Physical Review Applied**, v. 13, n. 5, p. 054060-1-054060-12, May 2020.

[5] DIVINCENZO, D. P. The Physical Implementation of Quantum Computation. **Fortschritte der Physik**, v. 48, n. 771-783, p. 771-783, Oct. 2000.

The second part consists of two articles, in the first paper, derivatives of two molecules *1,8-di(phosphinyl)naphthalene* and *naphtho[1,8-cd]-1,2-dithiole phenylphosphines* were theoretically tested aiming to maximize the spin-spin coupling constants, as well as the chemical shift range between the coupled nuclei. Exceptionally large through-space coupling (TS) J coupling constants (^{31}P, ^{31}P) were observed in the two molecules cited above. This remarkably large TS coupling is a potential resource to overcome the natural limitations related to the development of large-scale quantum computers via NMR, circumventing the need for long quantum gates implementations. Furthermore, several levels of DFT theory were studied for the calculation of chemical shift and scalar coupling constant for the proposed derivatives.

In the second paper, we report a computational design strategy for prescreening recently synthesized complexes of cadmium, mercury, tellurium, selenium, and phosphorus (called MRE complexes) as suitable qubit molecules for NMR QIP. Chemical shifts and spin−spin coupling constants in five MRE complexes were examined using the spin−orbit zeroth order regular approximation (ZORA) at the density functional theory level and the four-component relativistic Dirac−Kohn−Sham approach. Assembled together with the most common qubits used in NMR quantum computation experiments, spin-1/2 nuclei, such as ^{113}Cd, ^{199}Hg, ^{125}Te, and ^{77}Se, could leverage the prospective scalable quantum computer architectures, enabling many and heteronuclear qubits for NMR QIP implementations.

2 THEORETICAL BACKGROUND

2.1 Computational NMR Spectroscopy

Quantum mechanics has a reputation for being not only mysterious, but also far removed from our daily life. But there is a device in a chemistry laboratory called nuclear magnetic resonance (NMR) spectrometer, whose operation is described using language usually utilized for describing elementary quantum systems. However, NMR spectrometer operates on macroscopic samples of ordinary liquids, usually organic compounds in inert solvents. Of course, a complete explanation of any spectroscopic experiment requires quantum mechanics. But only in NMR, the lifetimes of multiparticle quantum states are often long enough to appreciate the complexity of the dynamics of such states.

NMR uses radio-frequency radiation to observe and manipulate the magnetic dipoles associated with the spins (intrinsic angular momenta) of the atomic nuclei in molecules. It was first demonstrated by the groups of Felix Bloch at Stanford and Edward Purcell at Harvard in the

late 1940s, for which they shared the 1952 Nobel prize in physics. Since its discovery, NMR has many applications in chemical analysis and biological imaging. Nevertheless, NMR has been used to perform the first experimental demonstrations of quantum information processing (QIP)[6,7]. These demonstrations are the first step toward realizing the dreamed quantum computer: a device that harnesses the complexity of quantum dynamics to solve computational problems that are and will remain forever beyond the reach of classical computers[8].

NMR spectroscopy observes nuclear spin transitions in molecules and is one of the spectroscopic techniques mostly used for elucidation of molecular structure. NMR measures the interaction of an oscillating radio-frequency electromagnetic field with a collection of nuclei immersed in a strong external magnetic field. At some particular field values the energy difference matches the electromagnetic frequency and the transition (nuclear magnetic resonance) is observed. Which gives rise to an NMR spectrum that provides detailed information about the molecular structure and dynamics, ranging from simple organic species to biopolymers[9].

The widespread application of NMR has tremendously benefited many areas in natural and life sciences[10]. NMR was first demonstrated in 1945, commercialized in the 1960's and by the end of this decade, NMR was routinely used by chemists[11]. Thenceforward, magnetic resonance spectroscopy has experienced decades of engineering evolution and accumulating tremendous growth, becoming an important analytical tool of modern chemistry and befitting as an ideal testbed for exploring ideas about quantum control for quantum information processing purposes[12].

---

[6] CORY, David G.; FAHMY, Amr F.; HAVEL, Timothy F. Ensemble quantum computing by NMR spectroscopy. **Proceedings of the National Academy of Sciences**, v. 95, n 5, p. 1634-1639, Mar. 1997.

[7] JONES, J.; MOSCA, M.; HANSEN, R. Implementation of a quantum search algorithm on a quantum computer. **Nature**, v. 393, n. 6683, 344–346, May 1998.

[8] HAVEL, T. F. *et al*. Quantum information processing by nuclear magnetic resonance spectroscopy. **American Journal of Physics**, v. 70, n. 3, p. 345-362, Feb. 202.

[9] ATKINS, P. W.; DE PAULA, J. **Physical Chemistry**. 10 ed. Oxford University Press, 2014.

[10] KAUPP, M.; BÜHL, M. **Calculations of NMR and EPR: theory and applications**, 1a. ed. Wiley-VCH: Weinheim, 2004.

[11] GRANDINETTI, P. J. **Nuclear Magnetic Resonance for the People**, 2011.

[12] RYAN, C. A.; LAFOREST, M; LAFLAMME, R. Randomized benchmarking of single- and multi-qubit control in liquid-state NMR quantum information processing. **New Journal of Physics**, v. 11, n. 1, p. 1-18, Jan. 2009.

2.1.1 Nuclear Interactions in External Magnetic Field

The NMR signals is due the fact that the atomic nuclei have a quantum mechanical property called nuclear spin (I). Because the nucleus is a charged particle, its spinning gives rise to a magnetic moment ($\boldsymbol{m}$). In the semi-classical picture, the nucleus spin behaves like the dipolar moment of a magnet possessing angular momentum ($\boldsymbol{J}$) parallel to its magnetic moment. A nucleus K of spin I_K and magnetogyric ratio γ_K is characterized by a magnetic moment[13] (Equation (**1**)):

$$\boldsymbol{m}_K = \gamma_K \boldsymbol{J}_K = \gamma_K \hbar I_K, \tag{1}$$

where $\hbar$ is the reduced Plank's constant. In a macroscopic sample and in the absence of an external magnetic field, normally the nuclear magnetic moments are randomly oriented, and the vector sum of all nuclear magnetic moments is zero, making the net sample magnetization equal to zero. When placed in an external magnetic field B_0, pointing by convention to the z direction, the nuclear magnetic moment can either be aligned with the external magnetic field or anti-aligned with it, but the majority is aligned with it, Figure 1. Therefore, the net magnetization will be aligned with B_0. Nonetheless, magnetic moments are not statically aligned exactly parallel or antiparallel to the external magnetic field. Instead, they are forced to remain at a certain angle to B_0, and this causes them to "wobble" around the axis of the field at a fixed frequency. This periodic wobbling motion is called precession. Each nuclear magnetic moment in a sample precesses around the external magnetic field with a frequency ω_0 which is called Larmor frequency (Equation (**2**))[14].

$$\omega_0 = \gamma_k B_0 \tag{2}$$

[13] OLIVEIRA, I. S. *et al*. **NMR Quantum Information Processing.** Elsevier and Amsterdam, 2007.
[14] MORAN, Robert F.; DAWSON, Daniel M.; ASHBROOK, Sharon E. Exploiting NMR spectroscopy for the study of disorder in solids. **International Reviews in Physical Chemistry**, v. 36, n. 1, p. 39-115, Feb. 2017.

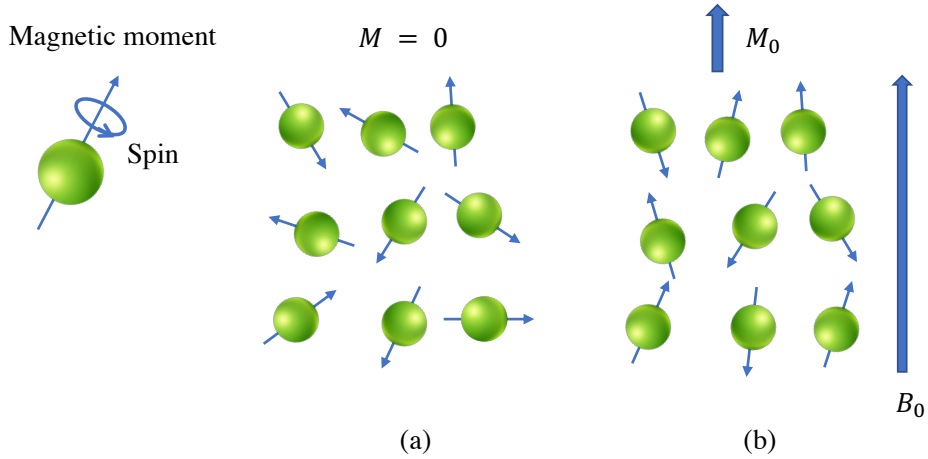

Figure 1 A nucleus with an unpaired proton has spin and will have a net magnetic moment or field. The nuclear magnetic moment direction is: (a) in the absence of an external magnetic field and (b) in the presence of an external magnetic field.

The Hamiltonian of NMR spin system is comprised of the system Hamiltonian and the control Hamiltonian, $H = H_S + H_C$. The system Hamiltonian, H_S, describes the interactions among the spins and the interaction between the spins and an external magnetic field. The control Hamiltonian, H_C, describes the interaction between the spins and an oscillating radio frequency field. The most common nuclei observed in NMR spectroscopy have spin-1/2 because they have two discrete energy levels, which are the target nuclei of this work. Some examples of them are ^{1}H, ^{13}C, ^{15}N,^{19}F and ^{31}P[15].

The time evolution of a spin-1/2 particle subject to a static magnetic field $\vec{B}_0$ along the $\hat{z}$-axis is governed by the Hamiltonian[13] in Equation (**3**).

$$H_0 = -\mu.B = -\hbar\gamma B_0 I_Z = -\hbar\omega_0 I_z = \begin{bmatrix} -\frac{\hbar\omega_0}{2} & 0 \\ 0 & \frac{\hbar\omega_0}{2} \end{bmatrix}, \quad (3)$$

where I_x, I_y, and I_z (x, y and z components of the nuclear spin angular momentum operators) relate to the well-known Pauli matrices as (Equation (**4**)):

[15] GAUGLITZ, Günter; VO-DINH, Tuan. **Handbook of Spectroscopy**. WILEY-VCH Verlag GmbH & Co. KGaA, Weinheim, 2003.

$$I_x = \frac{1}{2}\sigma_x, \qquad I_y = \frac{1}{2}\sigma_y, \qquad I_z = \frac{1}{2}\sigma_z, \tag{4}$$

where in matrix symbolism (Equation (**5**)),

$$\sigma_x = \begin{bmatrix} 0 & 1 \\ 1 & 0 \end{bmatrix}, \qquad \sigma_y = \begin{bmatrix} 0 & -i \\ i & 0 \end{bmatrix}, \qquad \sigma_z = \begin{bmatrix} 1 & 0 \\ 0 & -1 \end{bmatrix}. \tag{5}$$

The eigenvalues of the Hamiltonian are the energies of to the spin states which are proportional to the eigenvalues of the operator I_Z, given by Equation (**6**):

$$E_m = -m\hbar\omega_0. \tag{6}$$

Therefore, for a nucleus with spin I, there are $2I + 1$ energy levels spaced by the amount $\hbar\omega_0$. Hence, Equations (**3**) and (**6**) show that the spin-1/2 has two-discrete energy eigenstates - $|0\rangle$ or $|\uparrow\rangle$ (the spin is aligned with the static magnetic field, i.e. “spin-up" and $m = \frac{1}{2}$) and $|1\rangle$ or $|\downarrow\rangle$ (the spin is anti-aligned with the static magnetic field, i.e. “spin-down" and $m = -\frac{1}{2}$). Furthermore, the $|0\rangle$ state, whose energy is given by $\langle 0|H|0\rangle$, has $\hbar\omega_0$ less energy than the $|1\rangle$ state, which the energy state is given by $\langle 1|H|1\rangle$. This energy splitting is called as the Zeeman splitting (Figure 2 (a)). The energy separation between the two spin states ($|0\rangle$ and $|1\rangle$) is proportional to the strength of the external magnetic field and increases as the magnetic field strength is increased (Figure 2 (b)). In the absence of external magnetic field, these two spin states ($|0\rangle$ and $|1\rangle$) have the same energy[13].

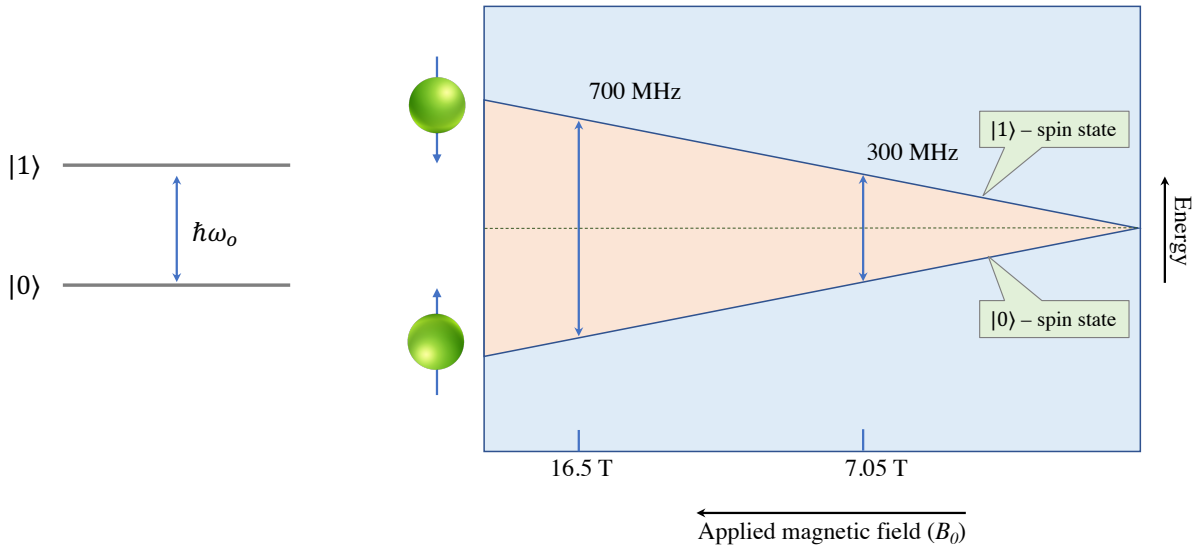

(a) (b)

Figure 2 (a) Energy diagram or Zeeman splitting for a spin-1/2 particle subject to a static magnetic field. (b) The energy difference between the two states depends on the strength of the external magnetic field.

For liquid-state NMR, the values of the magnetic field B_0 vary from 5-20 Tesla, resulting in precession frequencies ω_0 in the radio-frequency range.

The frequency of the Larmor frequency, Equation (**2**), is dependent on the external magnetic field, the nuclear isotope γ_K and its chemical environment within the molecule[16]; the last mentioned happens because when a molecule is placed in a magnetic field, the electronic cloud around nucleus K creates an induced magnetic field B_{ind} proportional to the electronic current (Biot et Savart law), creating their own magnetic field proportional to the external magnetic field, according to the Equation (**7**)[14]:

$$B_{ind} = -\sigma_K . B_0, \tag{7}$$

where σ_K is the chemical shielding tensor of the nucleus K. The induced field of electrons deshields the external magnetic field and the effective magnetic field at the nucleus K differs from the applied field. So, the total magnetic field at the nucleus K is (Equation (**8**)):

[16] BAUGH, J.*et al*. Quantum information processing using nuclear and electron magnetic resonance: review and prospects, 2007. eprint: arxiv:quant-ph/0710.1447. Accessed in 28 Sept. 2021.

$$B_{total} = B_0 + B_{ind} = (1 - \sigma_K).B_0. \quad (8)$$

Therefore, the nuclear spin Hamiltonian for a molecule consisting of *N* uncoupled nuclei (Equation (**9**)) and the total energy (Equation (**10**)) become:

$$H_0 = -\sum_{K=0}^{N} \hbar(1 - \sigma_K)\gamma B_0 I_Z^K = -\sum_{K=0}^{N} \hbar\omega_0^K I_Z^K, \quad (9)$$

$$E = -m_K.B_{total} = -m_K.(1 - \sigma_K)B_0. \quad (10)$$

For this reason, even though same nuclear species have equal gyromagnetic ratio, they can in principle experience different effective magnetic fields in the molecule, due to the diversity of the chemical and structural environments. In other words, the same species of nucleus can either have the same Larmor frequency or a different one, depending on the molecular symmetry. On the other hand, different species of nuclei possess different gyromagnetic ratio and have differences in Larmor frequency on the order of MHz when placed in constant magnetic fields[17].

From an experimental point of view, a relative scale, called chemical shift δ, was introduced to solve two main issues: the fact that the resonance frequency depends on the magnitude of the magnetic field, which implies that the resonance frequencies acquired at different magnetic fields must be scaled and also, that the absolute frequency scale (~106 Hz) is not appropriate for reporting the NMR spectra. The chemical shift can be calculated for any nucleus according to Equation (**11**) and can vary between few Hz to several kHz.

$$\delta_K = \frac{\nu_0 - \nu_k}{\nu_0} \quad (11)$$

In Equation (**11**), $\nu_K = \omega_K/2\pi$ is the resonance frequency of nucleus K for which the chemical shift δ_K is calculated and ν_0 is the resonance frequency of a given nucleus in a standard substance. However, the Larmor frequency emitted by the nucleus K of spin $I_K = 1/2$ can be expressed in terms of the chemical shielding of the nucleus K as in Equation (**12**), and

[17] LESZCZYNSKI, J. **Handbook of Computational Chemistry**. 2. ed. Switzerland: Springer International Publishing, 2017.

then the chemical shift can be expressed as the difference between chemical shieldings of the reference nucleus and nucleus K like in the Equation (**13**).

$$\omega_K = -\gamma_K(B_0(1-\sigma_K)) \tag{12}$$

$$\delta_K = \frac{\sigma_0 - \sigma_K}{1-\sigma_0} \approx \sigma_0 - \sigma_K \tag{13}$$

In Equation (**13**), the assumption $1-\sigma_0 \approx 1$ was made, σ_0 being $\sim 10^{-5}$. Chemical shieldings and shifts are usually scaled with 'ppm' (parts per million).

Typical liquid-state NMR experiments involve an ensemble of around 10^{20} identical molecules dissolved in a solvent, whose effect on the nuclear magnetic moments of the molecules can be neglected[16].

When two spins are close in the space, there is an interaction between their dipolar moments. The strength of this coupling is dependent on the distance separating the two spins and their relative orientation with respect to the external magnetic field. In a liquid, the molecules move and rotate around each other on a much shorter time scale than the interactions occurring between them. This causes the intermolecular and intra-molecular dipolar interactions average to zero on the NMR time scale (i.e., the Larmor period time scale). Within the same molecule, there are still other interactions between the spins. If the wave-functions of bonding electrons overlap spatially within a pair of nuclear spins, the electron mediates an effective interaction between the nuclear spins. This interaction is independent of the external magnetic field, its direction and the orientation of the molecule, which inspires its name: scalar coupling (also called indirect spin-spin coupling or J-coupling).

Indirect NMR spin–spin coupling constants provide a wealth of structural information as well as detailed insight into the bonding of an atom to its neighbors[18]. The strength of the J-coupling is dependent on the nuclear-electron and electron-electron interactions, and on additional parameters like the geometry of the molecule and the gyromagnetic ratio of the nuclei. If the nuclear-electron and electron-electron interactions are strong, then the J-coupling is strong. This interaction is the most important NMR parameter for the application of NMR to QIP.

---

[18] AUTSCHBACH, Jochen; LE GUENNIC, Boris. Analyzing and Interpreting NMR Spin–Spin Coupling Constants Using Molecular Orbital Calculations**. Journal of Chemical Education**, v. 84, n. 1, p. 156-171, Jan. 2007.

The Hamiltonian for scalar J-coupling of a molecule containing N spin-1/2 coupled nuclei is given by Equation (**14**):

$$H_J = \hbar \sum_{K<L}^{N} \frac{\pi J_{KL} \sigma^K \sigma^L}{2} = \hbar \sum_{K<L}^{N} \frac{\pi J_{KL} \left(\sigma_x^K \sigma_x^L + \sigma_y^K \sigma_y^L + \sigma_z^K \sigma_z^L \right)}{2}, \tag{14}$$

where J_{KL} is the coupling strength between the spins K and L. In Equation (**12**) the system is said to be strongly coupled. When the frequency separation between the spins is large compared to their coupling strength, i.e. when $2\pi \, |J_{KL}| \ll |\omega_K - \omega_L|$, we can simplify Equation (**12**) to

$$H_J = \hbar \sum_{K<L}^{N} \frac{\pi J_{KL} \sigma_z^K \sigma_z^L}{2}. \tag{15}$$

When the condition $|\omega_K - \omega_L| \gg 2\pi J$ applies, the spectra are also said to be first order and the system is said to be weakly coupled. This condition is easily satisfied for heteronuclear spins and for small homonuclear molecules when the chemical shift between the nuclei is sufficiently large[13].

Summing up, the system Hamiltonian of N nuclear spins in an isotropic solution and with first order spectra is given by Equation (**16**):

$$H = -\sum_{K=0}^{N} \frac{\hbar \omega_0^K \sigma_Z^K}{2} + \hbar \sum_{K<L}^{N} \frac{\pi J_{KL} \sigma_z^K \sigma_z^L}{2}. \tag{16}$$

In addition to the static magnetic field, each spin “sees" another magnetic field along $\pm \hat{z}$ produced by neighboring spins. The resonance frequency ω_K of each spin K is shifted by $-J_{KL}/2$ when spin K is in the $|0\rangle$ state, and by $+J_{KL}/2$ when spin L is in the $|1\rangle$ state. A molecule with two spins that are coupled with strength J would then have two resonance frequencies for each spin (the frequency spectrum of spin K consists of two lines separated by J_{KL} and centered around ω_0^K). We can associate each with the state of the other spins, either $|0\rangle$ or $|1\rangle$.

The magnitude of the couplings can be measured directly in the spectrum. The coupling strength J can be from few or tenths of Hertz to few hundreds of Hertz, for couplings through

three or four bonds and couplings through a single bond, respectively. The coupling does not need to be positive, and the relative signs of the couplings can be determined by pulse sequences as soft-COSY, for example[19].

Due to the importance of NMR spectroscopy in modern chemical research, the shielding and spin–spin coupling constants are undoubtedly the most important properties which depend on the nuclear spin[17].

2.1.2 Non-relativistic NMR calculations

Magnetics parameters, like chemical shifts and spin-spin coupling constants can be calculated in electronic structure calculations, using wave function methods and density functional methods. In this work we have investigated chemical shifts and spin-spin coupling using density functional theory (DFT). The basic argument of DFT is that ground state energy is determined by electron density[20], and the properties of the system can be predicted by the ground state electron density ρ of a chemical system with interacting electrons in the presence of external potential. DFT theory significantly reduces the complexity of computing system properties by making the problem three-dimensional[21,22].

According to Hohenberg and Kohn[20], the energy functional of a system is given by Equation (**17**).

$$E[\rho] = \langle \psi_0 | \hat{T} + \hat{V} + \hat{U} | \psi_0 \rangle, \tag{17}$$

where ρ is the ground state electron density and the operators are: $\hat{T}$ for kinetic energy; $\hat{V}$ for electron-nuclear attraction; and $\hat{U}$ for electron-electron repulsion. The variational principle in quantum chemistry establishes that $E[\rho] = E_0$, i.e. there is a solution for the electron density function with a global minimum at the ground state density. Kohn-Sham theory mimics wave

[19] ERNST, R. R; BODENHAUSEN, G.; WOKAUN, A. **Principles of Nuclear Magnetic Resonance in One and Two Dimensions**. Clarendon Press and Oxford, 1990.
[20] HOHENBERG, P.; KOHN, W. Inhomogeneous Electron Gas. **Physical Review**, v. 136, n. 3B, p. B864-B871, 1964.
[21] JENSEN, F. **Introduction to Computational Chemistry**. 2. ed. John Wiley & Sons Ltd, 2007.
[22] KOCH, W.; Holthausen Max C. **A Chemist's Guide to Density Functional Theory**. 2. ed. Wiley-VCH Verlag GmbH, 2001.

function theory in its usage of orbitals[21]. This allows choosing a basis set and set up one-electron orbitals, and to generate trial density to optimize against energy E (Equation (**18**)):

$$\rho(\vec{r})\sum_{k=1}^{N}|\chi_k(\vec{r})|^2\,; \qquad \chi_k(\vec{r}) = \sum_n a_{kn}\varphi_n(\vec{r}), \tag{18}$$

where $\chi_k(\vec{r})$ are one electron orbitals, $\varphi_n(\vec{r})$ are the basis set functions and a_{kn} are coefficients.

The model, introduced by Kohn and Sham[23], has similar mathematics to the Hartree-Fock (HF) method, possessing the same formula for kinetic, electron-nuclear, and Coulomb energies except for the exchange-correlation term. The equation for a single electron orbital is

$$\left[-\frac{\hbar^2}{2m}\nabla^2 + \hat{V}(\vec{r})\right]\chi_k(\vec{r}) = \varepsilon_k\chi_k(\vec{r}), \tag{19}$$

where $-\frac{\hbar^2}{2m}\nabla^2$ is the kinetic energy term, $\hat{V}(\vec{r})$ is the potential energy term and ε_k is the energy eigenvalue. The term which is not known in DFT is the exchange-correlation energy, in which the remaining energy is absorbed. This term can be written as in Equation (**20**).

$$E_{XC}[\rho] = \int \rho(\vec{r})\varepsilon_{XC}[\rho(\vec{r})]dv, \tag{20}$$

where $\rho(\vec{r})$ is the density, indicating the number of electrons per unit volume and $\varepsilon_{XC}[\rho(\vec{r})]$ is the exchange-correlation energy density, representing energy per electron.

Within DFT, an important research area is to derive exchange-correlation functional approximations. The functional catches a function and returns a scalar. They are denoted as $F[f]$ in quantum chemistry. There exists a diversity of exchange-correlation functionals in DFT, which employs different approximations and all aim to increase the method accuracy. For example, the well-known hybrid XC functional B3LYP (Becke, 3-parameter, Lee–Yang–Parr) is a three-parameter functional defined by Equation (**21**):

[23] KOHN, W.; Sham, L. J. Self-Consistent Equations Including Exchange and Correlation Effects. **Physical Review**, v. 140, n. 4A, p. A1133-A1138, 1965.

$$E_{XC}^{B3LYP} = (1-a)E_X^{LSDA} + aE_X^{HF} + b\Delta E_X^B + (1-c)E_C^{LDA} + cE_C^{LYP}, \quad (21)$$

where a, b and c are 0.20, 0.72, and 0.81 respectively. E_X^B is a generalized gradient approximation, the Becke 88 exchange functional and the correlation functional of Lee, Yang and Parr for B3LYP, and E_C^{LDA} is the Vosko-Wilk-Nusair (VWN) local spin density approximation to the correlation functional.

Alternatively, the generalized gradient functional PBE0, also known as PBE1PBE, mixes Perdew–Burke-Ernzerhof (PBE) exchange energy and Hartree–Fock exchange energy in a set 3:1 ratio, along with the full PBE correlation energy (Equation (**22**)):

$$E_{XC}^{PBE0} = \frac{1}{4}E_X^{HF} + \frac{3}{4}E_X^{PBE} + E_C^{PBE}, \quad (22)$$

where E_X^{HF} is the Hartree–Fock exact exchange functional, E_X^{PBE} is the PBE exchange functional, and E_C^{PBE} is the PBE correlation functional.

Accurate spin-spin coupling calculations require large basis set[24] this is partly because of the Fermi Contact contribution, which requires an accurate description of the nuclear region that is not offered by normal basis sets[25].

In this work, one of the basis sets employed in the calculation of the NMR parameters is cc-pVTZ, which stands for correlation consistent polarized Valence Triple Zeta[26]. By convention, correlation consistent is denoted as (cc) lower case letters to avoid confusion with coupled cluster (CC) method. Correlation consistent[26] basis sets are developed by Dunning et al. and employ a smaller set of primitives to achieve similar or better accuracy than the "STO-nG" type basis sets. STO-nG – stands for Slater Type Orbitals with n is the number of Gaussian Type Orbitals that are linearly combined to mimic an STO. The Slater Type and Gaussian Type functions for STO and GTO are, respectively,

$$s(\vec{r}) = e^{-\zeta|r|}, \qquad g(\vec{r}) = e^{-\zeta r^2}, \quad (23)$$

[24] LESZCZYNSKI, J. **Computational Chemistry**: Reviews of Current Trends, World Scientific, 2004.
[25] HELGAKER, T., JASZUŃSKI, M.; RUUD, K. Ab Initio Methods for the Calculation of NMR Shielding and Indirect Spin-Spin Coupling Constants. **Chemical Reviews**, v. 99, n. 1, p. 293-352, Dec. 1999.
[26] DUNNING, T.H., Gaussian basis sets for use in correlated molecular calculations. I. The atoms boron through neon and hydrogen. **The Journal of Chemical Physics**, v. 90, n. 2, p. 1007, Aug. 1989.

where $\vec{\boldsymbol{r}}$ is coordinate vector and ζ controls the width of orbitals. Correlation consistent basis sets are designed in a way that recovers correlation energy of valence electrons. However, with the addition of core functions, nuclear properties such as magnetic shielding and spin-spin couplings, can also be calculated.

2.1.2.1 NMR parameter calculations

Early in the 1950s, Ramsey presented the theoretical methods that quantum chemistry needed to evaluate the main parameters of the NMR spectrum, the shielding constants[27] and the indirect spin–spin coupling constants[28] These parameters are obtained from an effective NMR Hamiltonian, H^{NMR}, which describes the interactions of nuclear magnetic moments in a molecule with the external magnetic field $\boldsymbol{B}$ and the mutual interactions of these moments[29].

The NMR operator acts in the space defined by all possible arrangements of the nuclear spins. The eigenvalues of H^{NMR}determine the transition energies as the differences between different nuclear spin states in the molecule and the eigenvectors determine the arrangement of the nuclear spins with respect to the external field[17]. The effective NMR Hamiltonian is written as[30] (Equation (**24**)):

$$H^{NMR} = -\sum_K \boldsymbol{B}^T(\mathbf{1}-\boldsymbol{\sigma}_K)\boldsymbol{m}_K + \frac{1}{2}\sum_{K\neq L}\boldsymbol{m}_K^T(\boldsymbol{D}_{KL}+\boldsymbol{K}_{KL})\boldsymbol{m}_L, \tag{24}$$

where $\boldsymbol{\sigma}_K$ is the shielding tensor, $\boldsymbol{D}_{KL}$ is the direct interaction of the magnetic dipoles, the direct spin–spin coupling, $\boldsymbol{K}_{KL}$ is the reduced indirect spin–spin coupling tensor and the superscript T denotes the matrix transpose. $\boldsymbol{m}_K$ is the nuclear magnetic dipole moment and it is related to the nuclear spin, $\boldsymbol{I}_K$ as (Equation (**25**)):

$$\boldsymbol{m}_K = \hbar\gamma_K\boldsymbol{I}_K = \mu_N g_K \boldsymbol{I}_K, \tag{25}$$

---

[27] RAMSEY, N. F. Magnetic Shielding of Nuclei in Molecules, **Physical Review**, v. 78, n. 6, p. 699, Jun. 1950.
[28] RAMSEY, N. F. Electron Coupled Interactions between Nuclear Spins in Molecules, **Physical Review**, v. 91, n. 2, p. 303, Jul. 1953.
[29] JACKOWSKI, Karol; JASZUNSKI, Michal. **Gas Phase NMR**, The Royal Society of Chemistry, 2016.
[30] ABRAGAM, A. **Principles of Nuclear Magnetism**. Oxford University Press, 1961.

where γ_K is the nuclear magnetogyric ratio, $\mu_N = e\hbar/2m_p$ is the nuclear magneton, m_p the proton mass, and g_K is the g factor of nucleus K, unique for each isotope[17].

The effective NMR Hamiltonian H^{NMR} has no explicit dependence on the electronic structure. H^{NMR} acts within the space of the accessible nuclear spin states[29]. It includes two electron-independent contributions, the nuclear Zeeman term $-\boldsymbol{B}^T.\boldsymbol{m}_K$ and the classical direct dipolar coupling of the nuclear magnetic moments $\boldsymbol{m}_K^T\boldsymbol{D}_{KL}\boldsymbol{m}_L$. All the effects of the electronic structure are incorporated in the nuclear magnetic shielding tensors $\boldsymbol{\sigma}_K$, and the reduced indirect nuclear spin–spin coupling tensors $\boldsymbol{K}_{KL}$[17,29].

In standard quantum chemical calculations, to calculate the shielding and indirect spin–spin coupling tensors, the perturbation expansion of the molecular Hamiltonian is employed. In the perturbation expansion of the Schrödinger equation, we must consider all contributions that are either linear or bilinear in $\boldsymbol{B}$ and $\boldsymbol{m}_K$ for the shielding constants, and those linear or bilinear in $\boldsymbol{m}_K$ and $\boldsymbol{m}_L$ for the indirect spin–spin coupling constants, as indicated by Equation (**24**). Since the perturbing operators are time independent, both the shielding and spin–spin coupling tensors can be expressed as energy derivatives.

In an isotropic medium, the NMR spin Hamiltonian for a rotating molecule may be written as (assuming $\boldsymbol{B}$ oriented along the Z axis) (Equation (**26**)):

$$H_{iso}^{NMR} = -\sum_K B(1-\sigma_K)m_{K,Z} + \frac{1}{2}\sum_{K\neq L} K_{KL}\boldsymbol{m}_K^T.\boldsymbol{m}_L. \tag{26}$$

As mentioned in the Section 2.1.1 Nuclear Interactions in External Magnetic Field, the direct spin–spin couplings D_{KL} are purely anisotropic and vanish in the rotational averaging. On the other hand, the averaging of the shielding and indirect spin–spin coupling tensors leads to what is known as the nuclear shielding constants σ_K (Equation (**27**)) and the reduced indirect nuclear spin–spin coupling constants K_{KL} (Equation (**28**)):

$$\sigma_K = \frac{1}{3}Tr\ \boldsymbol{\sigma}_K, \tag{27}$$

$$K_{KL} = \frac{1}{3}Tr\ \boldsymbol{K}_{KL}. \tag{28}$$

For closed-shell molecules, the nuclear magnetic shielding and reduced indirect nuclear spin-spin coupling tensors, $\boldsymbol{\sigma}_K$ and $\boldsymbol{K}_{KL}$, can be defined as second derivatives of the energy in

the presence of an external magnetic induction $\boldsymbol{B}$ and a nuclear magnetic moment $\boldsymbol{m}_K$ or two nuclear magnetic moments $\boldsymbol{m}_K$ and $\boldsymbol{m}_L$. The nuclear magnetic shielding tensor can be determined as[31] in Equation (**29**).

$$\sigma_K = \left.\frac{\partial^2 E(\boldsymbol{B},\ \boldsymbol{m}_K)}{\partial \boldsymbol{B}\ \partial \boldsymbol{m}_K}\right|_{\boldsymbol{B}=\boldsymbol{m}_K=0} \tag{29}$$

And the reduced indirect nuclear spin-spin coupling tensor as in Equation (**30**).

$$\boldsymbol{K}_{KL} = \left.\frac{\partial^2 E(\boldsymbol{m}_K,\ \boldsymbol{m}_L)}{\partial \boldsymbol{m}_K \partial \boldsymbol{m}_L}\right|_{\boldsymbol{m}_K=\boldsymbol{m}_L=0} \tag{30}$$

Using the perturbation theory expression for the perturbed energy, taking the derivatives and writing the contributions in terms of expectation values and response functions one finds for closed-shell systems:

$$\sigma_K = \left\langle 0\middle|\widehat{H}^{B,K}\middle|0\right\rangle + \langle\langle \widehat{H}^{B}; \widehat{H}^{B(PSO)} \rangle\rangle = \sigma_K^{dia} + \sigma_K^{para}. \tag{31}$$

Equation (**31**) indicates that there are two contributions to the nuclear magnetic shielding tensor, they are called diamagnetic σ_K^{dia}, which is obtained as the expectation value $\left\langle 0\middle|\widehat{H}^{B,K}\middle|0\right\rangle$, and paramagnetic terms σ_K^{para}, calculated as a linear response function $\langle\langle \widehat{H}^{B}; \widehat{H}^{B(PSO)} \rangle\rangle$.

The diamagnetic contribution arises from the ability of the applied field to generate a circulation of charge in the ground-state electron distribution of the atom. This charge circulation generates a magnetic field that opposes to the applied field and hence shields the nucleus. σ_K^{dia} magnitude depends on the average distance of the electrons from the nucleus in question and on the electron density close to the nucleus. For this reason, the diamagnetic contribution is broadly proportional to the electron density of the atom containing the nucleus of study[32]. It follows that the shielding is decreased if the electron density on the atom is reduced by the influence of an electronegative atom nearby. That reduction in shielding translates into

[31] SAUER, Stephan P. A. **Molecular Electromagnetism:** A Computational Chemistry Approach, Oxford University Press, 2011.

[32] ATKINS, Peter, DE PAULA, Julio, FRIEDMAN, Ronald S. **Physical Chemistry**: Quanta, Matter, and Change. 2. ed. USA: Oxford University Press.

an increase in deshielding, and hence to an increase in the chemical shift δ as the electronegativity of a neighboring atom increases.

The paramagnetic contribution arises from the interaction of the nucleus with the field generated by the paramagnetic currents and, therefore, it depends on the ability of the applied field to mix excited states into the ground state[33]. In other words, σ_K^{para} contribution arises from the ability of the applied field to force electrons to circulate through the molecule by making use of orbitals that are unoccupied in the ground state. So, the paramagnetic contribution reinforces the applied magnetic field and deshields the nucleus in question[32].

Therefore, $\sigma_K^{dia} > 0$, and $\sigma_K^{para} < 0$. The total local contribution is positive if the diamagnetic contribution dominates and is negative if the paramagnetic contribution dominates[32].

The shielding constant is dimensionless and is expressed in ppm (parts per million). This unit reflects the role of the shielding compared to the electron independent direct Zeeman interaction of the nuclear magnetic moment with the external field (Equation (**26**)). As described in Section 2.1.1 Nuclear Interactions in External Magnetic Field, the physical understanding of the nuclear shielding comes from considering that the electrons in the molecule create an additional magnetic field, acting as a correction proportional to the external field and leading to the local magnetic field[17] (Equation (**32**)).

$$\boldsymbol{B}_K^{loc} = (1 - \sigma_K)\boldsymbol{B} \tag{32}$$

When σ_K is positive, it means that the presence of electrons leads to a decreased local magnetic field experienced by the nuclear magnetic moments; that is, the electron density shields the nuclear magnetic moments from the external magnetic field, a concept that explains the origins of the term shielding constant[17]; while a negative shielding constant implies that the nucleus is deshielded and the local magnetic induction at the nucleus is larger than the external field[31].

A direct comparison of calculated shielding constants with experiment is hampered by the difficulty in experimentally determining the absolute shielding constants calculated by theory[17]. Advantageously, the shielding constant can be considered as a measure of the local field experienced by a nuclear magnetic moment due to the shielding of the external magnetic

[33] ATKINS, Peter, FRIEDMAN, Ronald S. **Molecular Quantum Mechanics**. USA: Oxford University Press, 2010.

field by the electron density. The relative difference in the local magnetic fields around different nuclei provides similar information and for this reason experimental NMR studies report the so-called chemical shift δ_K (Equation (**33**)).

$$\delta_K = \frac{\sigma_K(reference) - \sigma_K(sample)}{1 - \sigma_K(reference)} \cong \sigma_K(reference) - \sigma_K(sample) \tag{33}$$

The chemical shifts are taken relative to the shielding in a selected molecule, called as *reference* molecule. The trends for the absolute shielding are thus reversed to those for the chemical shift; when $\sigma_K < \sigma_L$, the nucleus K is more shielded than nucleus L[17].

Regarding the spin-spin coupling, also using the perturbation theory expression for the perturbed energy and applying the second derivatives in Equation (**30**), the quantum mechanical expression for the reduced indirect nuclear spin-spin coupling tensor is[31] (Equation (**34**))

$$\boldsymbol{K}_{KL} = \boldsymbol{K}_{KL}^{DSO} + \boldsymbol{K}_{KL}^{PSO} + \boldsymbol{K}_{KL}^{FC} + \boldsymbol{K}_{KL}^{SD} + \boldsymbol{K}_{KL}^{\overline{SD}^{FC}}. \tag{34}$$

It consists of five contributions, which include the so-called diamagnetic spin-orbit $\boldsymbol{K}_{KL}^{DSO}$, the paramagnetic spin-orbit $\boldsymbol{K}_{KL}^{PSO}$, the Fermi contact $\boldsymbol{K}_{KL}^{FC}$, spin–dipolar $\boldsymbol{K}_{KL}^{SD}$, and the mixed Fermi contact-spin dipolar terms $\boldsymbol{K}_{KL}^{\overline{SD}^{FC}}$[31]. However, the last contribution, the Fermi contact-spin dipolar cross-term is purely anisotropic and does not contribute to the trace of the tensor (Equation (**28**)) and thus to the coupling constant[31].

The total value of indirect spin–spin coupling are sums of contributions arising from three different electron–nuclear interactions, the spin–orbital (SO), spin–dipolar (SD), and Fermi-contact (FC) mechanisms. The diamagnetic spin orbit (DSO) and the paramagnetic spin orbit (PSO) represent the interactions of the magnetic field of the nuclei mediated by the electron orbital motion. The third term, spin dipole (SD) describes the interactions between the nuclear magnetic moments mediated by the electronic spin angular moment. The last term and most well-known is the Fermi-contact (FC), which is, in most of the time, the major contributor to isotropic indirect spin–spin coupling constants, the FC is also a response property and reflects the interaction between the electron spin magnetic moment close to the nucleus and the

magnetic field at the nucleus. For an accurate quantum chemical description of SSCCs all the terms in Equation (**38**) must be considered[34].

According to Ramsey's non-relativistic theory, the coupling tensor may be calculated using second order perturbation theory[28,35] (Equation (**35**)).

$$K_{KL} = \left\langle 0 \middle| \widehat{H}_{KL}^{DSO} \middle| 0 \right\rangle - 2 \sum_{K_S \neq 0} \frac{\left\langle 0 \middle| \widehat{H}_K^{PSO} \middle| K_S \right\rangle \left\langle K_S \middle| \left(\widehat{H}_L{}^{PSO} \right)^T \middle| 0 \right\rangle}{E_{K_S} - E_0} - 2 \sum_{K_T} \frac{\left\langle 0 \middle| \widehat{H}_K{}^{FC} + \widehat{H}_K^{SD} \middle| K_T \right\rangle \left\langle K_T \middle| \left(\widehat{H}_L{}^{FC} \right)^T + (\widehat{H}_L^{SD}) \middle| 0 \right\rangle}{E_{K_T} - E_0} \tag{35}$$

The first summation is over all excited singlet states with energy E_K, while the second summation is over all triplet states with energy E_{K_T}. The operators for the four mechanisms in atomic units are (Equation (**36**)):

$$\begin{aligned} \widehat{H}_{KL}^{DSO} &= \alpha^4 \sum_i \frac{\boldsymbol{r}_{in}^T \boldsymbol{r}_{im} \boldsymbol{I}_3 - \boldsymbol{r}_{in} \boldsymbol{r}_{im}^T}{\boldsymbol{r}_{in}^3 \boldsymbol{r}_{im}^3}, \\ \widehat{H}_K^{PSO} &= -i\alpha^2 \sum_i \frac{\boldsymbol{r}_{in} \times \nabla_i}{\boldsymbol{r}_{in}^3}, \\ \widehat{H}_K^{FC} &= \frac{8\pi\alpha^2}{3} \sum_i \delta(\boldsymbol{r}_{in}) s_i, \\ \widehat{H}_K^{SD} &= \alpha^2 \sum_i \frac{3\boldsymbol{r}_{in}^T s_i \boldsymbol{r}_{in} - \boldsymbol{r}_{in}^2 s_i}{\boldsymbol{r}_{in}^5}, \end{aligned} \tag{36}$$

where α is the fine structure constant[10], $\boldsymbol{r}_{in}$ is the position of electron with respect to nucleus, $\delta(\boldsymbol{r}_{in})$ is the Dirac delta function, $\boldsymbol{I}_3$ is a three-by-three unit matrix, and s_i is spin of electron. All the summations in Equation (**36**) are over all electrons in the system. Again, the superscript T shows that the vectors are transposed.

---

[34] SOARES, B. Almeida et al. Experimental and NMR theoretical methodology applied to geometric analysis of the bioactive clerodane trans-dehydrocrotonin. **Journal of the Brazilian Chemical Society**, v. 25, n. 4, p. 629-638, Apr. 2014.

[35] HELGAKER, T.; JASZUŃSKI, M.; PECUL, M. The quantum-chemical calculation of NMR indirect spin-spin coupling constants. Progress in Nuclear Magnetic Resonance Spectroscopy, v. 53, n. 4, p. 249-268, Nov. 2008.

The NMR spin Hamiltonian is usually expressed in terms of the indirect spin–spin coupling tensors $\boldsymbol{J}_{KL}$, which are related to the reduced tensors as[29] in Equation (**37**).

$$\boldsymbol{J}_{KL} = \frac{1}{h}\mu_N g_K \mu_N g_L \boldsymbol{K}_{KL} \tag{37}$$

The reduced coupling tensors $\boldsymbol{K}_{KL}$ are independent of the nuclear g factors, and therefore, in contrast to $\boldsymbol{J}_{KL}$, can compare the strengths of the couplings between nuclei with different g_K values. Therefore, using the relation in the Equation (**37**) and considering the isotropic value of the spin–spin coupling constant, the indirect spin–spin coupling can be expressed as the sum of four contributions[17] (Equation (**38**)).

$$J_{KL}^{iso} = J_{KL}^{DSO} + J_{KL}^{PSO} + J_{KL}^{SD} + J_{KL}^{FC} \tag{38}$$

The unit of J^{iso} is Hz, the sign can be either positive or negative, though NMR experiments typically only provide the absolute value of J^{iso}. If the indirect spin–spin coupling interaction stabilizes the antiparallel arrangement of the nuclear spins, then J is positive[29].

Chemical and physical properties of atoms and molecules are predicted differently within non-relativistic and relativistic theory. Electrons in heavy element molecules move so fast that relativistic effects become important. Thus, for heavy element systems the relativistic effects can have a particularly strong impact on calculated NMR parameters[36].

2.2 Relativistic effects

The impact of relativistic effects in chemistry is a wide research area. Nature is relativistic due to the finite rather than an infinite speed of light[37]. But, unlike the usual observables of quantum theory such as position, momentum and energy, the relativistic effects are generally not observable. Nevertheless, in chemistry and physics of heavy elements compounds, manifestations of relativistic effects are predominantly[37]. For example, relativistic effects explain why gold presents yellow color and the liquid nature of mercury at room

[36] AUTSCHBACH, J. Calculating NMR Chemical Shifts and J-Couplings for Heavy Element Compounds. *In*. MEYERS, R. A. **Encyclopedia of Analytical Chemistry**, John Wiley & Sons, Ltd, 2014.
[37] AUTSCHBACH, J. Perspective: Relativistic effects. **The Journal of Chemical Physics** v. 136, n. 150902, p. 1-15, Apr. 2012.

temperature[37,38] Although gravitational effects on chemical phenomena can be neglected at the size scale of atoms and molecules, and given the small masses of protons, neutrons and electrons, relativistic effects become apparent as the velocities of the particles approach the speed of light c[37]. In this way, in relativistic quantum chemistry one needs to deal with Einstein's special relativity.

According to the Einstein's theory of special relativity, all physical laws and equations must be invariant under Lorentz transformation. The many-body Schrodinger's equation is not invariant under such a transformation. Therefore, one needs another set of equations to account the relativistic effects in chemical applications[39].

In the 1970s, it was realized that (nonrelativistic) Schrödinger quantum mechanics reproduces results on molecular properties far from experimental results. And, especially when heavy elements are involved, this divergence can be so large that qualitative chemical reasoning and understanding is affected[39]. Such effects arise from the high speed of electrons in the vicinity of heavy nuclei. One distinguishes between scalar relativistic effects, associated with the relativistic mass increase of electrons, and the spin-orbit interaction, generated by magnetic induction, a mechanism that cannot be described within a non-relativistic framework[40].

Relativistic effects are introduced through the choice of Hamiltonian. There are many relativistic Hamiltonians on the market, but they can all be defined with respect to the generic form of the electronic Hamiltonian within the Born–Oppenheimer approximation (Equation (**39**)):

$$H = \sum_i \hat{h}\,(i) + \frac{1}{2}\sum_{i \neq j} \hat{g}(i,j) + V_{NN}, \tag{39}$$

where V_{NN} is the classical repulsion of clamped nuclei. The basic formulas of present molecular electronic structure methods can be developed without specification of the one-electron operator $\hat{h}$ and the two-electron operator $\hat{g}$, which implies that the various non-relativistic methods available today can be carried over into the relativistic domain, albeit with possible adaptions.

---

[38] ZIEGLER, T.; SNIJDERS, J. G.; BAERENDS, E. J. Relativistic Effects on Bonding. **Journal of Chemical Physics**, v. 74, n. 2, p. 1271-1284, Aug. 1981.

[39] REIHER, M.; WOLF A. **Relativistic Quantum Chemistry**: The Fundamental Theory of Molecular. 2. Ed. Science: Wiley-VCH, 2015.

[40] SAUE, T. Spin-Interactions and the Non-relativistic Limit of Electrodynamics. **Advances in Quantum Chemistry**, v. 48, p. 383-405, Oct. 2005.

Relativistic effects are usually separated into spin-orbit coupling (SO) interactions and scalar relativistic (SR) effects, where the SR are relativistic effects at the one-electron level and the SO are relativistic effects that affect the electron-electron interactions in many-electron systems. There are many fully and quasi-relativistic methods available for quantum chemical calculations. For instance, all-electron relativistic quantum chemical calculations can be carried out with a Hamiltonian that only includes SR terms or including both SR and SO. The latter approach is in principle more accurate[41].

The introduction of relativistic Hamiltonians increases the computational cost, independent of system size. This happens because the non-relativistic one-electron operator is a scalar operator, whereas the fully relativistic Dirac Hamiltonian is a 4 x 4 matrix operator. Dirac equation explicitly includes spin and describes two kinds of particles: the electron and its anti-particle, the positron, with an entangled existence, what increases the dimension of the corresponding one-electron wave functions (orbitals)[42].

Among scalar non-relativistic and four-component relativistic one-electron Hamiltonians there are two-component relativistic Hamiltonians where the positronic degrees of freedom have been frozen. SR effects can be introduced into a non-relativistic computer code with essentially no extra computational cost, but the description of SO interaction requires at least a two-component formalism and will increase computational cost because of the transition from real to complex algebra and the general reduction of symmetry.

2.2.1 Dirac equation

The starting point for relativistic quantum chemistry is the equation proposed by Dirac in 1928[43]. The Dirac equation is perhaps the most important equation of modem physics, being the fundamental equation of relativistic quantum mechanics and quantum electrodynamics[44]. Converting the classical relativistic energy-momentum relation (Equation (**40**)):

$$E = \sqrt{c^2p^2 + m^2c^4}, \tag{40}$$

[41] AUTSCHBACH, J.; ZHENG, S. Relativistic Computations of NMR Parameters from First Principles: Theory and Applications, **Annual Reports on NMR Spectroscopy**, v. 67, p. 1-95, 2009.
[42] SAUE, T. Relativistic Hamiltonians for Chemistry: A Primer. **ChemPhysChem**, v. 12, n. 17, p. 3077-3094, Nov. 2011.
[43] DIRAC, P. A. M., The quantum theory of the electron. **Proceedings of the Royal Society of London Series a-Containing Papers of a Mathematical and Physical Character**, v. 117, n. 778, p. 610-624, Feb. 1928.
[44] SCHWERDTFEGER, P. **Relativistic Electronic Structure Theory**: Fundamentals, v. 11, 1. Ed. Elsevier Science, 2002.

into a quantum-mechanical equation by replacing the momentum p with a differential operator $-i\hbar\Delta$ acting on suitable wave functions, leads to the Hamiltonian (relativistic Hamiltonian for a free particle) in Equation (**41**):

$$H = \sqrt{-c^2\hbar^2\Delta + m^2c^4}. \tag{41}$$

The time-dependent free Dirac equation, wrote in the familiar "Schrödinger form", as a quantum-mechanical evolution equation is (Equation (**42**)):

$$i\hbar\frac{d}{dt}(t, \boldsymbol{x}) = H_0\psi(t, \boldsymbol{x}), \qquad \psi(t_0, \boldsymbol{x}) = \psi(\boldsymbol{x}). \tag{42}$$

The Dirac equation describes the quantum-mechanical motion of particles with spin-l/2 according to the requirements of the special theory of relativity. Correspondingly, it contains the following scalar parameters: Planck's constant $\hbar$, which sets the scale of quantum phenomena, the velocity of light c, which sets the scale for relativistic effects, and m, the rest-mass of the particle.

In Equation (**41**), one gets a wave equation upon the canonical substitution of momentum with its operator form. However, this resulting equation is still not Lorentz invariant because the orders of the derivatives for space and time coordinates are different. At this point, Dirac realized that Equation (**40**) could be linearized by introducing matrices, giving rise to the Dirac operator for free particles (Equation (**43**)):

$$H_0 = \sqrt{c^2p^2 + m^2c^4} = c\boldsymbol{\alpha}.\boldsymbol{p} + \boldsymbol{\beta}mc^2. \tag{43}$$

H_0 is a matrix-differential operator and Equation (**42**) describes particles with an inner Dirac operator H_0 is often called the operator of kinetic energy, but one should be aware that it describes the relativistic energy of a free particle including the rest energy mc^2.

In equation (**43**), the differential operator $\boldsymbol{p} = -i\hbar\nabla$ is the usual momentum operator and the operators $\boldsymbol{\alpha}$ and $\boldsymbol{\beta}$ are the 4×4 Dirac matrices which are expressed in the block matrix form by the following expressions (Equation (**44**)):

$$\boldsymbol{\alpha} = \begin{pmatrix} 0_2 & \boldsymbol{\sigma} \\ \boldsymbol{\sigma} & 0_2 \end{pmatrix}; \qquad \boldsymbol{\beta} = \begin{pmatrix} I_2 & 0_2 \\ 0_2 & -I_2 \end{pmatrix}, \tag{44}$$

where $\boldsymbol{\sigma}$ ($\boldsymbol{\sigma} = \sigma_x, \sigma_y, \sigma_z$) are 2 × 2 Pauli spin matrices and I_2 is the 2 × 2 identity matrix and 0_2 is the 2 × 2 zero matrix. In this form, Dirac's equation can be written, after some rearrangements, in atomic units as[45] in Equation (**45**).

$$H^D \Psi^D = \begin{pmatrix} V & c\boldsymbol{\sigma}.\boldsymbol{p} \\ c\boldsymbol{\sigma}.\boldsymbol{p} & V - 2c^2 \end{pmatrix} = E\Psi^D \tag{45}$$

The Equation (**45**) is the Dirac equation in an external field. As in nonrelativistic quantum mechanics, the influence of an external field is described by a potential-energy $V(\boldsymbol{x})$ that is added to the kinetic energy H_0. The operator H^D is intended to describe the energy of a particle in a given external field and is obtained by replacing the free Dirac operator H_0 with an external field as in Equation (**46**).

$$H^D = H_0 + V(\boldsymbol{x}) \tag{46}$$

As mentioned above, there are two important aspects of Equation (**45**). First, the spin of the electron is incorporated in Dirac's equation explicitly through the introduction of Pauli matrices in the linearization of the Hamiltonian in Equation (**43**). In contrast, electron spin can be introduced into the non-relativistic quantum mechanics only by an *ad-hoc* assumption. The other important aspect of Equation (**45**) is the fact that it has both positive and negative energy solutions. The negative energy solutions of Dirac's equation eventually led to the idea of the existence of anti-particle states of electrons, called positrons. Nowadays, we consider this the birth of quantum field theory, although Dirac initially dismissed the negative-energy solutions of the problem when it was first published.

In non-relativistic quantum mechanics, the variation principle is a very useful concept. In the Dirac theory, the formulation of such a variational formalism is problematic because if the negative energy continuum is empty, electrons will fall into it under emission of photons. Dirac resolved this dilemma in 1929 by postulating that the negative energy states are

[45] VAN LENTHE, E.; BAERENDS, E. J.; SNIJDERS, J. G., Relativistic total energy using regular approximations, **Journal of Chemical Physics**, v. 101, n. 11, p. 9783-9792, Dec. 1994.

completely filled[46]. If an electron is excited from the negative energy continuum, a 'hole' is left behind. The hole behaves as a particle with the same mass as an electron, but with opposite charge. The negative energy states are therefore connected with positrons. The filling of the negative energy continuum implies that the 'vacuum' is infinitely charged and has an infinite energy. This awkward property can be solved by going one step further and using normal ordered operators, which means that the vacuum expectation value of the corresponding operator is subtracted from the operator. The effect is that, although filled, the charge and energy of the vacuum are zero.

In quantum chemistry, we generally seek the solutions of Equation (**45**) that correspond to the positive-energy spectrum. In non-relativistic quantum chemistry, it is common to talk about 'orbitals', 1-component 1-electron wavefunctions. The solution of the Dirac equation is a four-component vector, it is common to use in this case the term 'spinor' instead of orbital. As we see below, the solutions may be grouped into two components, the so-called large and small components. As an approximation, it is often typical that one seeks the positive-energy solutions only with the large components.

2.2.2 Four-Component and Two-Component Relativistic Methods

Due to the 4×4 matrix form of Equation (**45**), the eigenvector solutions of this equation are composed of four components[37] (Equation (**47**)):

$$\Psi^D = \begin{pmatrix} \psi_1 \\ \psi_2 \\ \psi_3 \\ \psi_4 \end{pmatrix} = \begin{pmatrix} \psi_L \\ \psi_S \end{pmatrix}; \qquad \psi_L = \begin{pmatrix} \psi_1 \\ \psi_2 \end{pmatrix}, \qquad \psi_S = \begin{pmatrix} \psi_3 \\ \psi_4 \end{pmatrix}. \tag{47}$$

In Equation (**47**), the eigenvector solution of the Dirac wave function is grouped into the large component, (ψ_L) and the small component (ψ_S).

If the Dirac equation is solved for a free particle, i.e. $V = 0$ for all r, one gets two kinds of solutions: solutions with eigenvalues less than $-mc^2$ and solutions with eigenvalues greater

[46] DIRAC, P. A. M., A theory of electrons and protons. **Proceedings of the Royal Society of London. Series A**, v. 126, n. 801, p. 360-365, Jan. 1930.

than $+mc^2$. For quantum chemistry, the main interest is in the positive energy solutions. For the positive energy solutions, the upper components (ψ_L) have a large amplitude and the lower components (ψ_S) have a small amplitude.

For the positive-energy spectrum, the contribution of the small component is much smaller than that of the large component. If Equation (**45**) and (**47**) are combined, the following expressions are obtained:

$$V\psi_L + c\boldsymbol{\sigma}.\boldsymbol{p}\psi_S = E\psi_L, \tag{48}$$

$$c\boldsymbol{\sigma}.\boldsymbol{p}\psi_L + (V - 2c^2)\psi_S = E\psi_S. \tag{49}$$

In Equations (**48**) and (**49**), the small and large components of the Dirac wave function are coupled by the following relation.

$$\psi_S = \frac{1}{2c} k\boldsymbol{\sigma}.\boldsymbol{p}\psi_L \tag{50}$$

$$k = \left(1 - \frac{V - E}{2c^2}\right)^{-1} \tag{51}$$

In the four-component relativistic formalism, one seeks solutions to both small and large components via simultaneous solutions of the Equations (**48**) and (**49**). However, early attempts with an auxiliary basis set suffered from the so called 'variational collapse'[47,48] when small and large components were varied independently. This problem can be overcome by relating the basis sets for small and large components via e Equation (**50**), which is referred as the kinetic balance approximation[49]. Using Equations (**50**) and (**51**), one eliminates the small component of the Dirac wave function and sees solutions for only the large component. This approach yields the following eigenvalue equation for the large component only:

$$\left[V + \frac{1}{2}\boldsymbol{\sigma}.\boldsymbol{p}k\boldsymbol{\sigma}.\boldsymbol{p}\right]\psi_L = E\psi_L. \tag{52}$$

---

[47] SCHWARZ, W. H. E.; WALLMEIER H. Basis set expansions of relativistic molecular wave-equations. **Molecular Physics**, v. 46, n. 5, p. 1045-1061, Feb. 1982.

[48] SCHWARZ, W. H. E.; WECHSELTRAKOWSKI E. The 2 problems connected with Dirac-Breit-Roothaan calculations. **Chemical Physics Letters**, v. 85, n. 1, p. 94-97, Jan. 1982.

[49] STANTON, R. E.; HAVRILIAK, S. Kinetic Balance: A partial solution to the problem of variational safety in Dirac calculations. **Journal of Chemical Physics**, v. 81, n. 4, p. 1910-1918, May 1984.

This equation is not practical since the Hamiltonian operator depends on k (and E). At this point, one may decouple the small and large components completely by employing Foldy-Wouthuysen transformations[50], which leads to exact two- component relativistic methods. Another approach is to construct approximate decoupling schemes by expanding k in a power series. This formalism leads to quasi-relativistic two-component methods. A famous example of such a method is called the zeroth order regular approximation (ZORA)[45,51,52], which is discussed in the following sub-section.

2.2.2.1 Zeroth Order Regular Approximation

It is possible to obtain a more practical expression for the Hamiltonian in Equation (**52**) by employing a power series expansion for k.

$$k = \left(1 - \frac{V - E}{2c^2}\right)^{-1} = 1 + \sum_{n=1}^{\infty} \left(\frac{V - E}{2c^2}\right)^n \tag{53}$$

At the first order of this expansion, one gets the Pauli Hamiltonian after some manipulation.

$$H^{Pauli} = V + \frac{p^2}{2} - \frac{p^4}{8C^2} + \frac{Vp^2}{8c^2} + \frac{i}{4c^2}\boldsymbol{\sigma}.(\boldsymbol{\nabla}\mathrm{V} \times \boldsymbol{p}) \tag{54}$$

In Equation (**54**), first two terms on the right-hand side recover the non-relativistic Hamiltonian. The third term is called the mass-velocity operator, which yields relativistic corrections to the kinetic energy due to the mass-increase effect in special relativity. The fourth term is the Darwin term, which gives a correction to the potential near the nucleus. The last term is the spin-orbit coupling term. It should be noted that the Pauli Hamiltonian transforms to the non-relativistic Hamiltonian at the limit ($c \rightarrow \infty$).

Another expansion[51] can be made for k by the following relation (Equation (**55**)):

---

[50] FOLDY, L. L.; WOUTHUYSEN, S. A. On the Dirac theory of spin 1/2 particles and its non-relativistic limit. **Physical Review**, v. 78, n. 1, p. 29-36, Apr. 1950.

[51] VAN LENTHE, E.; BAERENDS, E. J.; SNIJDERS, J. G. Relativistic regular two-component Hamiltonians. **Journal of Chemical Physics**, v. 99, n. 6, p. 4597- 4610, Jun. 1993.

[52] VAN LENTHE, E.; BAERENDS, E. J.; SNIJDERS, J. G., The zero-order regular approximation for relativistic effects: The effect of spin-orbit coupling in closed shell molecules. **Journal of Chemical Physics**, v. 105, n. 15, p. 6505-6516, Jul. 1996.

$$k = \frac{c^2}{2c^2 - V}\left(1 + \frac{E}{2c^2 - V}\right)^{-1} = \frac{c^2}{2c^2 - V} + \left(\frac{c^2}{2c^2 - V}\right)\sum_{n=1}^{\infty} -1^n \left(\frac{E}{2c^2 - V}\right)^n . \quad (55)$$

At the zeroth order of this expansion series, one can get the ZORA Hamiltonian after some arrangements, which is expressed by Equation (**56**).

$$H^{ZORA} = V + \frac{1}{2}\boldsymbol{\sigma}.\boldsymbol{p}\left(\frac{c^2}{2c^2 - V}\right)\boldsymbol{\sigma}.\boldsymbol{p} = V + \frac{1}{2}\boldsymbol{p}\left(\frac{c^2}{2c^2 - V}\right)\boldsymbol{p} + \frac{i}{2}\left(\frac{c^2}{2c^2 - V}\right)^2 \boldsymbol{\sigma}.(\boldsymbol{\nabla}\mathrm{V} \times \boldsymbol{p}) \quad (56)$$

The ZORA Hamiltonian includes the familiar spin-orbit coupling term even at the zeroth order of expansion. The complete Hamiltonian in Equation (**56**) is referred as the ZORA/spin-orbit Hamiltonian. If the spin-orbit coupling term is neglected, one gets the ZORA/scalar Hamiltonian.

ZORA is two-component method if spin-orbit coupling is included and one-component method if only scalar-relativistic effects are considered, and both Hamiltonians are essentially as expensive to use as than their non-relativistic counterpart. The ZORA Hamiltonian gives valence-shell properties and orbital energies of heavy elements, as can four-component relativistic methods[52]. In general, it can be said that ZORA method reproduces most of the relativistic effect, also if heavy elements are present, and are very cost-effective alternatives to the 4-component Dirac-Coulomb (DC) Hamiltonian.

2.3 Quantum computing

For long outstanding, computation devices were built entirely based on classical physics. From abacus to digital microprocessors, these tools summarize the fact that laws of physics support computation. In the 1970s and 1980s, the possibility of building a quantum

computing device started to gain some attention when Feynmann[53], Deutsch[54], Benioff[55], and Bennett[56] proposed the idea of using quantum mechanics to perform calculation. At that time, they launched the potential of a quantum computer model, which spread the field of research now called quantum computing.

A quantum computer benefits from quantum mechanical phenomena such as superposition and entanglement to realize calculations[57]. This superposition phenomena allows quantum computers to execute operations on many values at one fling whereas a classical computer usually must perform these operations sequentially. Consequently, quantum algorithms provide exponential speedups over their classical counterparts for certain problems.

What for some time was an idea, today is an attractive and fruitful research area for companies, governments and intelligence agencies. In 2020, a total of roughly 1 billion USD in private capital invested into the entire Quantum Information Science space[58]. Moreover, quantum chemistry will be directly impacted with the development of quantum computation and quantum information, the new device will solve problems dealt by chemists and physicists which cannot be resolved the classical computers.

Chemists face one fundamental problem, the resolution of the Schrödinger equation, reaching the exact solution. This is a challenging task because the dimension of the Hilbert space increases exponentially with the number of particles in the system, what demands exponential amount of computational resource[59,60]. Paul Dirac[61] mentioned that with the Schrödinger equation, "the underlying physical laws necessary for the mathematical theory of a large part of physics and the whole of chemistry are thus completely known and the difficulty

---

[53] FEYNMANN, R. P. Simulating physics with computers. **International Journal of Theoretical Physics**, v. 21, n. 6, p. 467-488, Jun. 2008.

[54] DEUTSCH, D. Quantum theory, the Church-Turing principle and the universal quantum computer. **Proceedings of The Royal Society of London, Series A**, v. 400, n. 1818, p. 97–117 Jul. 1985.

[55] BENIOFF, P. Quantum-mechanical Hamiltonian models of Turing-machines. **Journal of Statistical Physics**, v. 29, n. 3, p. 515–546, Nov. 1982.

[56] BENNETT, C. H.; BRASSARD, G. Quantum cryptography: Public key distribution and coin tossing. **Proceedings of IEEE International Conference on Computers Systems and Signal Processing**, Bangalore, India, pp. 175-179, Dec 1984.

[57] NIELSEN, M. A.; CHUANG, I. L., **Quantum Computation and Quantum Information**, Cambridge University Press, Cambridge, UK, 2000.

[58] KÖNIG, André M. Quantum Computing: Paradigm shift or slow death? | Current state (part 1). **Weekly Quantum World Detangled**, Jun. 2021. *In*. https://quantumcomputing.substack.com/p/quantum-computing-paradigm-shift. Accessed in 30 Sept. 2021.

[59] AARONSON, S. Why quantum chemistry is hard. **Nature Physics**, v. 5, n. 10, p. 707-708, Oct. 2009.

[60] SCHUCH, N.; VERSTRAETE, F. Computational complexity of interacting electrons and fundamental limitations of density functional theory. **Nature Physics**, v. 5, n. 10, p. 732-735, Jul. 2009.

[61] DIRAC, P. A. M. Quantum mechanics of many-electron systems. **Proceedings of the Royal Society A**, v. 123, n. 792, p. 714-733, Apr. 1929.

is only that the exact application of these laws leads to equations too much complicated to be soluble".

Despite its remarkable promises, quantum computers is handling experimental difficulties of realizing one that really meets its theoretical potential. To circumvent its requirements, theoretical chemists, who have faced and explored quantum effects from the perspective of physical chemistry for decades, might merge their finds and insights with those of the quantum information community, leveraging the understanding of quantum computing[62].

There was proposed many models to physically realize a quantum processor, NMR, electron spin resonance (ESR), ion traps, atom traps, optics, superconducting devices and nitrogen-vacancy (NV) centers, among others[63]. Nowadays, a few of them are able to manipulate quantum bits, or qubits, the quantum systems whose observables are given by the Pauli matrices. A qubit encodes a fundamental unit of quantum information[16].

The improvement and realization of quantum computers is an interdisciplinary task. Thereby, NMR is one of the disciplines that supports the development of the quantum computer, in general quantum information processing (QIP). QIP is at the helm of the task of performing quantum algorithms or simulations and NMR plays an important role in pioneering experimental demonstrations of quantum computing algorithms[64,65]. Also, NMR-QIP takes advantage of the considerable experience of the NMR in probing nuclear spins in liquid solution with RF pulses. In addition, this technology is known for relatively high coherence time and capability to work at room temperature. This technology has proved simple to design NMR quantum systems with 2 or 3 qubits, and it has been natural that the first two-qubits quantum algorithm implementations used NMR technology[66].

2.3.1 NMR Quantum computers

As mentioned in Section 2.1 Computational NMR Spectroscopy, NMR employs radio-frequency radiation to observe and manipulate the magnetic dipoles associated with the spins,

---

[62] KAIS, S. Introduction to Quantum Information and Computation for Chemistry. *In*. KAIS, S. **Quantum Information and Computation for Chemistry**, 1. Ed., v. 154, New Jersey: John Wiley & Sons, Inc: Hoboken, 2014.

[63] LADD, T. D. *et al*. Quantum computers, **Nature**, v. 464, n. 7285, p. 45-53, Mar. 2010.

[64] CRIGER, B. et al. Recent advances in nuclear magnetic resonance quantum information processing. Philosophical Transactions of the Royal Society A, v. 370, n. 1976, p. 4620-4635, Oct. 2012.

[65] CRIGER, B.; PARK, D.; BAUGH, J. Few-qubit magnetic resonance quantum information processors: simulating chemistry and physics *In*. KAIS, S. **Quantum Information and Computation for Chemistry**, 1. Ed., v. 154, New Jersey: John Wiley & Sons, Inc: Hoboken, 2014.

[66] GRUSKA, J. **Quantum Computing**. McGraw-Hill Book Co Ltd, Apr. 2000.

the "intrinsic angular momentum" of the atomic nuclei in molecules. Its first demonstration gathered the physics Nobel prize in 1952, which was shared by Bloch and Edward Purcell. Because of the many applications NMR has in chemistry, it is most encountered in chemical and medical research laboratories than it is in physics. However, this scenario is changing because NMR has been successfully used to perform experimental demonstrations of quantum information processing (QIP)[7,67,68]. These demonstrations are the first step toward realizing dreamed quantum computer: a device that exploits the complexity of quantum dynamics to solve computational problems that are and will remain forever beyond the reach of classical computers[8].

Currently, liquid state NMR enriches QIP by inspiring new ideas for theoretical and experimental investigation, leading to technology for demonstrating quantum computing in small physical systems[16]. In a sample containing N spin-1/2 for each molecule, the natural Hamiltonian of this system in a large homogeneous magnetic field $\vec{B}_0$ pointing in the z direction is given by Equation (**16**). Considering the Larmor frequency ($\nu_i^L = \frac{\omega_i^L}{2\pi} = \gamma_i|\vec{B}_0|$), the natural Hamiltonian becomes:

$$H_{nat} = \frac{1}{2}\sum_{i=1}^{N} 2\pi\nu_i^L\sigma_z^i + \frac{\pi}{2}\sum_{i<j}^{N} J_{ij}\sigma_z^i\sigma_z^j, \tag{57}$$

where ν_i^L is the Larmor frequency of the i^{th} nucleus with gyromagnetic ratio γ_i, J_{ij} is the coupling strength between nucleus i and j, and σ_z^i is the z Pauli matrix of the i^{th} spin.

The first term in the Equation (**57**) describes the precession of the spins due to their coupling to the external magnetic field, while the second term describes the J-coupling between pairs of nuclei. As mentioned in Section 2.1.1 Nuclear Interactions in External Magnetic Field, this Hamiltonian corresponds to the weak coupling limit, where we assume that the chemical shifts between coupled spins are much greater than their respective couplings, i.e., $\left|\nu_i^L - \nu_j^L\right| \gg J_{ij}/2$. Whether this approximation is not valid, one needs to use the full coupling Hamiltonian $\sigma_x^i\sigma_x^j + \sigma_y^i\sigma_y^j + \sigma_z^i\sigma_z^j$ instead of $\sigma_z^i\sigma_z^j$. The exact values of the Hamiltonian parameters are determined by fitting experimental data.

---

[67] CHUANG, I. L. *et al*., Bulk quantum computation with nuclear magnetic resonance: Theory and experiment, **Proceedings of the Royal Society A**, v. 454, n. 1969 p. 447–467, Jan. 1998.

[68] CORY, D. G.; PRICE, M. D.; HAVEL, T. F. Nuclear magnetic resonance spectroscopy: An experimentally accessible paradigm for quantum computing, **Physica D**, v. 120, n. 1-2, p. 82–101, Sept. 1998.

2.3.2 NMR Qubits

Information is something that can be encoded in the state of a physical system. If the physical system follows classical laws of physics, the information stored there is of "classical" nature, as in the classical computer. To quantify information, the concept of bit was introduced and defined as the basic unit of information. A bit of information stored in a classical computer is a value 0 or 1 kept in a certain location of the memory unit. The computer is able to measure the bit and retrieve the information without changing the state of the bit. If during the measurement, the bit is at the same state every time, it will yield the same results. A bit can also be copied and one can prepare another bit with the same state. A string of bits represents one single number[62]. All these properties of bits seem trivial, but in the domain of quantum information processing, this is no longer true, as we will see below.

Otherwise, the basic unit of quantum information is a quantum bit – qubit. Physically, a qubit can be represented by the state of a two-level quantum system of various forms, be it an ion with two accessible energy levels or a photon with two states of polarization[62]. Nuclear spins (I = 1/2) in molecules are quantum systems with two well–characterized states, which therefore can act naturally as a qubit[63,69,70].

Differently from classical bits, a qubit cannot be only in the states $|0\rangle$ and $|1\rangle$, but also in a superposition of both: $\alpha|0\rangle + \beta|1\rangle$. In the latter case, a measurement of the superposed state will collapse the state to either one of its component states $|0\rangle$ or $|1\rangle$, which is a widely observed phenomenon in quantum physics. This means that even the state of the qubit that is measured is identical each time, the measurement outcomes would most probably be different. For example, if one repetitively does the following: prepare a qubit in the same state $\alpha|0\rangle + \beta|1\rangle$ and then measure it with respect to the basis state $\{|0\rangle, |1\rangle\}$, one will get $|0\rangle$ in some measurements and $|1\rangle$ in the others[62].

Also, unlike classical bits that can be copied, a qubit cannot be copied due to the no-cloning theorem, which derives from the quantum mechanical nature of the qubit. This qubit no-cloning property has been used in the construction of security communication devices, because is impossible to eavesdrop a qubit of information. Concerning the information storage,

---

[69] LINO, J. B. d. R.; ROCHA, E. P.; RAMALHO, T. C. J. Value of NMR parameters and DFT calculations for quantum information processing utilizing phosphorus heterocycles. **The Journal of Physical Chemistry A**, v. 121, n. 23, p. 4486-4495, Apr. 2017.

[70] LINO, J. B. d. R.; RAMALHO, T. C. Quantum Information and Nuclear Magnetic Resonance Parameters. **Revista Virtual de Química**, v. 10, n. 4. p. 940-962, Jul. 2018.

once a qubit or an array of qubits could be in quantum superposition states such as $\alpha_{00}|00\rangle + \alpha_{01}|01\rangle + \alpha_{10}|10\rangle + \alpha_{11}|11\rangle$, a string of qubits is able to store several numbers $\alpha_{00}, \alpha_{01}, \ldots$ simultaneously, while a classical string of bits can only represent a single number. In this sense, n qubits encode not n bits of classical information, but 2^n numbers. Although none of the 2^n numbers are efficiently accessible because a measurement will destroy the state of superposition, this exponentially large information processing space combined with the peculiar mathematical structure of quantum mechanics still implies the formidable potential in the performance of some of the computational tasks exponentially faster than classical computers[62].

As mentioned in the section 2.1.1 Nuclear Interactions in External Magnetic Field, when placed in an external magnetic field, the atom nucleus magnetic moments result in discrete energy level systems that can be manipulated with resonant electromagnetic radiation leading to NMR[16]. Nuclear spins can serve as qubits, being addressed and read out using an NMR spectrometer. The first experimental quantum simulation of a harmonic oscillator was performed using NMR[62].

Nuclear spins (I = 1/2) in molecules are quantum systems with two well–characterized states, which therefore can act naturally as a qubit[63,69,70]. Although there is a limited number of different spin–1/2 nuclei, among which ^{1}H, ^{13}C, ^{19}F, ^{29}Si, and ^{31}P are the most common qubits used in NMR quantum computation experiments[63], other spin– 1/2 nuclei, such as ^{113}Cd, ^{199}Hg, ^{125}Te and ^{77}Se could in principle be used.

Most suitable spin systems are those wherein (i) each qubit has a resonance frequency sufficiently far from others, and (ii) each qubit is coupled to other qubits via spin-spin interaction. Here, (i) allows the addressability of qubits and (ii) allows the construction of quantum gates[71]. For a practical computer, the qubits must have long relaxation times to prevent quantum effects from decohering away. In liquid state NMR, the relaxation times are certainly long enough (around one second) for demonstration purposes[72].

The basis states for the two-dimensional Hilbert space of a qubit are denoted, as mentioned, by $|0\rangle$ and $|1\rangle$, in Dirac notation. General states are superpositions of these basis states: $|\psi\rangle = \psi_0|0\rangle + \psi_1|1\rangle$ (where ψ_0, $\psi_1$are complex numbers with $|\psi_0|^2 + |\psi_1|^2 = 0$). The basis states of an array of qubits are variously denoted by[8] Equation (**58**).

---

[71] MAHESH, T. S. Quantum information processing by NMR. **Resonance**, v. 20, v. 11, p. 1053–1065, Nov. 2015.

[72] JONES, J. A. Quantum computing and nuclear magnetic resonance. **PhysChemComm**, v. 4, n. 11, p. 49-56, 2001.

$$|\delta^1\rangle \otimes |\delta^2\rangle \otimes \ldots \otimes |\delta^N\rangle = |\delta^1\rangle|\delta^2\rangle \cdots |\delta^N\rangle = |\delta^1\delta^2 \cdots \delta^N\rangle, \tag{58}$$

where $\delta^n \in \{0,1\}$ $(n = 1, \ldots, N)$ and "$\otimes$" denotes the tensor (or Kronecker) product (Equation (**59**)):

$$\begin{aligned}&(\psi_0|0\rangle + \psi_1|1\rangle \otimes (\psi_0{}'|0\rangle + \psi_1{}'|1\rangle \\ &= \begin{bmatrix}\psi_0\\ \psi_1\end{bmatrix} \otimes \begin{bmatrix}\psi'_0\\ \psi'_1\end{bmatrix} = \begin{bmatrix}\psi_0\psi'_0\\ \psi_0\psi'_1\\ \psi_1\psi'_0\\ \psi_1\psi'_1\end{bmatrix}.\end{aligned} \tag{59}$$

It should be noted that the dimension of the tensor product space of *N* qubits grows exponentially as 2^N.

2.3.3 Single-spin control

To accomplish the QIP, one needs to be able to perform arbitrary single spin manipulations, which is equivalent to arbitrary rotations on any axis. As an example, consider the application of a magnetic field $\vec{B}_1$ perpendicular to the z axis which oscillates at the nuclear spin's Larmor frequency[16] (Equation (**60**)):

$$\vec{B}_1 = |\vec{B}_1|(\cos(\omega^{RF}t)\,\vec{x} + \sin(\omega^{RF}t)\vec{y}, \tag{60}$$

where $\omega^{RF} = 2\pi\nu^{RF}$ is the angular frequency of the field. In the rotating frame of the nucleus, i.e. the frame rotating at the same frequency as the spin, $\vec{B}_1$ appears as a constant field pointing along its rotating x axis and the spin starts to precess about this axis. By adjusting the phase of the $\vec{B}_1$ field, it is possible to create a rotation about any axis in the xy-plane; for example, $\omega^L t \rightarrow \omega^L t + \phi$ will create a rotation around the x axis making an angle ϕ with it. In the laboratory, such a rotating field can be applied by sending a RF pulse of a particular duration and phase to a conducting coil surrounding the sample, calculated according to the rotating wave approximation[16].

To better comprehend this phenomenon from the perspective of quantum mechanics, in the rotating frame picture: suppose the spin in the state $|\psi(t)\rangle$, and define the state in the rotating frame of the pulse with angular frequency ω^{RF}, as in Equation (**61**).

$$\begin{aligned} |\psi\rangle_r &= R_z(-\omega^{RF}t)|\psi(t)\rangle \\ &= R_z(-\omega^{RF}t)e^{-\frac{it}{\hbar}H_{nat}}|\psi(0)\rangle \\ &= e^{-\frac{it}{\hbar}\sigma_z\frac{\omega^{RF}}{2}t}\, e^{-\frac{it}{\hbar}H_{nat}}|\psi(0)\rangle \end{aligned} \tag{61}$$

In Equation (**61**), $|\psi\rangle_r = |\psi(0)\rangle$, for a single spin with $\omega^{RF} = \omega^L$. Applying a time derivative to Equation (**61**), the state $|\psi\rangle_r$ in the rotating frame evolves according to the Schrödinger equation with the new Hamiltonian[16] (Equation (**62**)).

$$H_r = R_z(-\omega^{RF}t)H_{nat}R_z(\omega^{RF}t) - \frac{\omega^{RF}}{2}\sigma_z \tag{62}$$

When an RF pulse with phase ϕ is applied to the spin, the laboratory frame Hamiltonian is[16] (Equation (**63**)):

$$H = \frac{\omega^L}{2}\sigma_z + \frac{\omega^{nut}}{2}(cos(\omega^{RF}t + \phi)\sigma_x + sin(\omega^{RF}t + \phi)\sigma_y), \tag{63}$$

where $\omega^{nut} = \pi\gamma_i|\vec{B}_1|$. In the rotating frame this becomes (Equation (**64**)):

$$H_r = \frac{1}{2}(\omega^L - \omega^{RF})\sigma_z + \frac{1}{2}\omega^{nut}(cos\ \phi\sigma_x + sin\ \phi\sigma_y). \tag{64}$$

Thus, if the RF pulse is at the same frequency as the spin, the spin will see a constant field in the xy plane and will precess about it. The rotation angle θ is determine by the interval τ during which the RF field is applied, according to $\theta = \omega_{nut}\tau$.

2.3.4 Two-spin control

It is also possible to independently control two spins with different Larmor frequencies. Applying a RF pulse at the frequency of the first spin, the rotating frame Hamiltonian is given by Equation (**65**).

$$\widetilde{H}_{nat} = \frac{1}{2}\omega_1^{nut}\sigma_x^1 + \frac{1}{2}\omega_2^{nut}\sigma_x^2 + \frac{1}{2}(\omega_2^L - \omega_1^L)\sigma_z^2 + \frac{\pi}{2}J_{12}\sigma_z^1\sigma_z^2 \tag{65}$$

Where we have set $\varphi = 0$ for simplicity. While the first spin undergoes a rotation around the x axis, the second spin experiences a field with an additional non-zero z component. This is called the off-resonance effect. If we consider the case where $\omega_2^L - \omega_1^L \gg \omega_1^{nut}$ then the second spin rotation around the x axis will average to zero during the time the first spin has completed its rotation. Typically, ω^{nut} is smaller than 1 MHz, so this condition is automatically satisfied if the two nuclei belong to different species. If the spins are of the same species, this condition can also be satisfied if a very low amplitude pulse is used due to the small nutation frequency. In this case, one drawback is that the pulse will necessarily take much longer to achieve the same angle of rotation, and if the two spins have a significant coupling constant J_{12}, coupling effects might introduce significant errors and, therefore, limit the control.

Fortunately, there are well-known techniques to address different nuclei of the same species with high precision. The most common technique is to control the spins using shaped pulses. The frequency response to the pulse will depend on the pulse shape (Fourier theorem) and so by applying the pulse with a time varying power we can control the power spectrum of the pulse. For example, if a Gaussian shaped pulse is applied at frequency ω^{RF}, then only spins within a Gaussian distribution of frequencies around ω^{RF} will respond to this RF field. Therefore, if the height and the length of the Gaussian pulse is carefully chosen, one spin can be "addressed", causing negligible effects to others. This technique permits control of spin pairs with smaller chemical shift differences in shorter periods of time, hence allowing stronger coupling. The length of a Gaussian pulse is proportional to the inverse of the chemical shift between the spins. Therefore, in the limiting case of small chemical shift differences and large J-coupling values, control of the qubits is more difficult.

For most liquid state experiments on a few spins, where chemical shifts are comparatively large and J-couplings are small, the use of Gaussian pulses is sufficient to achieve very high precision spin rotations. The situation becomes more complicated when there are more homonuclear spins (implying smaller chemical shift differences on average), or stronger coupling like in solid state or liquid crystal environments. It is still possible to

overcome these drawbacks by considering more complicated pulse shapes and phase modulation, which can implement any desired evolution by simulating the full quantum dynamics.

The strength of NMR technology is the remarkable control that can be implemented in multi-qubit systems. Many decades of RF engineering improvements today provide sufficient control for implementing experimental benchmarks such as quantum error correcting codes and simulations of quantum physics systems, among many others[16].

Finding more complex molecules is a challenge for scaling up liquid-state NMR quantum computers, although NMR spectroscopy is routinely performed on complex molecules with hundreds to thousands of resolvable nuclear resonances[11].

2.4 Designing enhanced qubit molecules

Nuclei like ^{1}H or ^{13}C are spin-1/2 quantum system and ideal qubits. The initial state of the system is obtained by allowing it to thermalize. By irradiating these nuclei at the appropriate frequency, it is possible to rotate their individual states one at a time leading to the so called single-qubit gates. Nuclei affect each other through interactions that can also be controlled, leading to two-qubit gates. By composing these two sets of gates we can reach any unitary transformation. This is known as universality[73]. After an algorithm consisting of a series of these gates, the final state can be observed by measuring the current induced by the rotating magnetic moments of the sample in a conducting coil. Algorithms should be performed on a timescale shorter than the characteristic decoherence time of the system, which is about 100 times the gate time in liquid state NMR[16].

The advancement of the aimed NMR large-scale quantum processors depends mainly on two challenges; first, the accurate and efficient control of the quantum system states, and second, the construction of systems containing a large number of qubits[2]. The former has been augmented by the development of algorithms which are able to manipulate, with high fidelity, the quantum states of relatively large systems[3]. This is a technological issue and has been the focus of many articles to date[74]. Recently, Peterson, Sarthour and Laflamme[4] have designed a fast and scalable algorithm for controlling the quantum states of systems containing 100 qubits.

---

[73] KAYE, P.; LAFLAMME, R.; MOSCA, M. **An introduction to quantum computing**, Oxford University Press, 2007.

[74] MAWHINNEY, Robert C.; SCHRECKENBACH, Georg. NMR quantum computing: applying theoretical methods to designing enhanced systems. **Magnetic Resonance in Chemistry**, v. 42, n. S1, p. S88-S98, May 2004.

These recent algorithms combined with modern NMR equipments, and sophisticated theoretical techniques make possible the manipulation of the nuclear spin system states through magnetic RF pulses, which are used to implement quantum gates, the basic computational step[4].

Regarding the second challenge, chemistry can leverage the development of NMR large-scale quantum systems, once it depends especially on the design of a qubit molecule containing a large number of suitable spin-1/2 nuclei, which will act as the qubits. In this way, theoretical chemistry can speed up the sharpening and strengthening of the physical requirements necessary by any potential qubit molecule[5], towards a specially synthesized system, giving resolvable spectra to the upcoming large-scale NMR quantum processor.

Outlining these physical requirements, the qubit molecule should meet these general design criteria[75,76,77]: (1) Nuclei having spin magnetic moment I=1/2 with either a high natural abundance, or using labelled samples, and having a relatively large sensitivity (the most common nuclei are ^{1}H, ^{13}C, ^{15}N, ^{19}F and ^{31}P); (2) compounds should be either soluble in some common NMR solvent or naturally found in a liquid state; (3) the differences in chemical shifts of the nuclei should be as large as possible (this is commonly achieved by using nuclei with a large range of chemical shifts, such as ^{13}C and ^{19}F, and/or heteronuclear spin systems since separate RF channels can be used for each nucleus); (4) spin-spin coupling between nuclei should be large; (5) the chosen nuclei, although not required to be mutually coupled, must form a contiguous network of couplings[74] (Figure 3); (6) the chosen system must have sufficiently long relaxation times to limit decoherence in addition to allowing for the evolution of implemented gates (spin–spin relaxation times, T_2, are typically shorter than spin-lattice relaxation times, T_1, and so it is the limiting factor; T_2 can be of the order of seconds, time enough for up to 10^{14} gates)[78].

---

[75] GLASER, S. J. NMR Quantum Computing. **Angewandte Chemie International**, v. 40, n. 1, p. 147-149, Jan. 2001.

[76] MADI, Z. L.; BRUSCHWEILER, R.; ERNST, R. R. One- and two-dimensional ensemble quantum computing in spin Liouville space. **The Journal of Chemical Physics**, v. 109, n, 24. p. 10603-10611, Dec. 1998.

[77] Cory D. G, et al. NMR based quantum information processing: achievements and prospects. **Fortschritte der Physik**, v. 48, n. 9-11, p. 875-907, 2000.

[78] VANDERSYPEN L, M. K.; CHUANG, I. NMR quantum computing: lessons for the future. **Quantum Information and Computation**, v. 1, n. 4, p. 134-142, Dec. 2001.

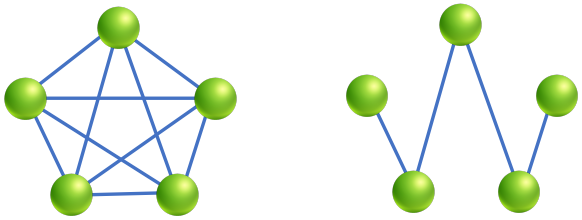

(a) (b)

Figure 3 a) Schematic representation of a system consisting of N = 5 pairwise-coupled spins (qubits). b) A linear coupling network is sufficient to realize all possible logic operations between arbitrary spins (qubits) in an N-spin system[76].

Using NMR parameter predictions from computational chemistry, in this work we study some possibilities to overcome natural limitations concerning the development of large-scale NMR, we first explore the large through-space spin-spin coupling constant, which could face the need of long-time quantum gates implementations. In principle, the large coupling could be useful to overcome potential sources of quantum information loss, suggesting the use of relatively short pulse sequences and affording an efficient manner to control two-qubit operations. Under these circumstances, coherence could likely be preserved[79].

Secondly, we suggest the use of spin-1/2 nuclei, such as ^{113}Cd, ^{199}Hg, ^{125}Te, and ^{77}Se as qubits. Heteronuclear qubit molecules for NMR QIP could face the challenges in single qubit control and multiqubit operations. These nuclei exhibit a large chemical shift range, allowing qubit addressability and exceptionally large spin-spin couplings, which could reduce the time of quantum gate operations and likely preserve the coherence. Hence, assembled with the most common qubits used in NMR quantum computation experiments, these nuclei could leverage the prospective scalable quantum computer architectures, enabling many and heteronuclear qubits for NMR QIP implementations[80].

[79] LINO, J. B. d. R; RAMALHO, T. C. Exploring through-space spin-spin couplings for quantum information processing: Facing the challenge of coherence time and control quantum states. **The Journal of Physical Chemistry A**, v 123, n. 7, p. 1372-1379, Jan. 2019.

[80] LINO, J. B. d. R.; SAUER, S. P. A. Enhancing NMR quantum computation by exploring heavy metal complexes as multiqubit systems: A Theoretical Investigation. **The Journal of Physical Chemistry A**, v 124, n. 24, p. 4946-4955, May. 2020.

SECOND PART

PAPER 1

Exploring Through-Space Spin-Spin Couplings for Quantum Information Processing: Facing the challenge of coherence time and control quantum states

Published article at The Journal of Physical Chemistry A

THE JOURNAL OF PHYSICAL CHEMISTRY A
Article
Cite This: J. Phys. Chem. A 2019, 123, 1372−1379
pubs.acs.org/JPCA

Exploring Through-Space Spin−Spin Couplings for Quantum Information Processing: Facing the Challenge of Coherence Time and Control Quantum States

Jéssica Boreli dos Reis Lino[†] and Teodorico Castro Ramalho*[,†,‡]

[†]Chemistry Department, Federal University of Lavras, 37200-000 Lavras, MG Brazil

[‡]Center for Basic and Applied Research, Faculty of Informatics and Management, University Hradec Kralove, 50003 Hradec Kralove, Czech Republic

Supporting Information

ABSTRACT: Nuclear magnetic resonance (NMR) is a powerful tool for studying quantum information processing (QIP). Recently quantum technologies have been proposed to overcome the challenges in large-scale NMR QIP. Furthermore, computational chemistry can promote its improvement. Nuclear spins-$^1/_2$ are natural qubits and have been used in most NMR quantum computation experiments. However, molecules that enable many qubits NMR QIP implementations should meet some requirements regarding their spectroscopic properties. Exceptionally large through-space (TS) P−P spin−spin coupling constants (SSCC or J) observed in 1,8-diphosphanaphthalenes (PPN) and in naphtho[1,8-*cd*]-1,2-dithiole phenylphosphines (NTP) were proposed and investigated to provide more accurate control within large-scale NMR QIP. Spectroscopic properties of PPN and NTP derivatives were explored by theoretical strategies using locally dense basis sets (LDBS). ^{31}P chemical shifts (δ) calculated at the B3LYP/aug-cc-pVTZ-J level and TS P−P SSCCs at the PBE1PBE/pcJ-2 (LDBS-1) level are very close to the experimental data for the PPN molecule. Differently, for the NTP dimer, PBE1PBE/pcJ-2 (LDBS-2) predicts more accurate ^{31}P δ, whereas PBE1PBE/Def2-TZVP (LDBS-1) forecasts more accurate TS P−P SSCCs. From our results, PPN$_o$-F, PPN$_o$-ethyl, and PPN$_o$-NH$_2$ were the best candidates for NMR QIP, in which the large TS SSCCS could face the need of long-time quantum gates implementations. Therefore, it could overcome natural limitations concerning the development of large-scale NMR.

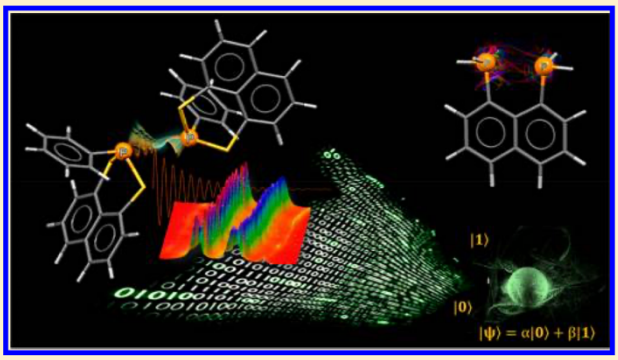

1. INTRODUCTION

The heightened development of quantum computers has been possible due to an interdisciplinary area of study, known as quantum information science, which combines communities of researchers in physics, engineering, chemistry, computer science, and mathematics.[1,2] Quantum information processing (QIP) aims at the study of storing and manipulating information in quantum-mechanical states in subunits (called qubits).[3]

Among all current QIP implementations, nuclear magnetic resonance (NMR) is a powerful tool for studying QIP and has had significant experimental progress.[2] Spin-$^1/_2$ systems, such as ^{1}H, ^{13}C, ^{19}F, ^{29}Si, and ^{31}P nuclear spins, are natural qubits used in most NMR quantum computation experiments.[4,5]

In recent years, researchers have become increasingly interested in building an NMR large-scale quantum processor, and the main challenge is the development of systems containing a large number of qubits combined with the ability to control their quantum states within enough coherence time.[1,6]

Recently, quantum technologies have been proposed to overcome the challenges in large-scale NMR QIP. In 2018, Devra et al.[7] encoded three fluorine (^{19}F) spins of the molecule iodotrifluoroethylene related to the design of high-fidelity three-qubit quantum gates. Also in 2018, Gaikwad et al.[8] experimentally demonstrated a two-qubit NMR QIP with high fidelity using the chloroform molecule as a quantum system (^{1}H and ^{13}C nuclei); their method was both selective and efficient. In 2017, Pande et al.[9] experimentally demonstrated a strong algorithmic cooling by two ^{29}Si spins of pentamethyldisilane, which allowed strong polarization enhancements.

Computational design strategies have been used for prescreening qubits molecules for NMR QIP, in which some quantum mechanical investigations of NMR values of qubits were made using *ab initio* and density functional theory (DFT) methods.[10−12] Chemistry can boost the development of

Received: September 26, 2018
Revised: January 21, 2019
Published: January 23, 2019

DOI: 10.1021/acs.jpca.8b09425
J. Phys. Chem. A 2019, 123, 1372−1379

quantum control in a large-scale NMR QIP; regarding sharpening and strengthening of the physical requirements, which must be satisfied by any potential qubit molecule, also known as DiVincenzo criteria.[13]

Any NMR QIP implementation using spin-1/2 nucleus (two-level qubits) is scalable in the total energy of the system because each spin-1/2 nucleus has two well-defined energy levels in a magnetic field, described by a two-dimensional Hamiltonian (eq 1):

$$\hat{H} = \frac{1}{2}(\hbar\gamma B_0 + \delta)\hat{Z} = \frac{1}{2}(\hbar\gamma B_0 + \delta)\begin{bmatrix} 1 & 0 \\ 0 & -1 \end{bmatrix} \quad (1)$$

where B_0 is the external magnetic field, γ is the nuclear gyromagnetic ratio, δ is the chemical shift term, and $\hat{Z}$ is the Pauli Z matrix.[1]

For multiple-spin systems, a well-defined qubit can be easily distinguished when the spin-1/2 nuclei of the qubit molecule possess a distinct and appropriately dispersed δ. This enables individual qubit addressing through radio frequency (RF) pulses. Moreover, two-qubit gates arise from spin−spin interactions. Thus, every pair of spins should be connected, either directly or indirectly, by a chain of usable coupling.[14]

Obtaining a larger qubit-system using liquid state NMR is challenging, mainly because the J coupling (the indirect coupling) is a relatively weak coupling mediated by the electron cloud in the molecule.[15,16]

Solid-state NMR spectroscopy allows more qubits than solution NMR;[17] additionally, the strongest dipolar coupling used in solid-state NMR QIP is enough to implement quantum gates in solid-state NMR quantum computers. Nevertheless, this coupling is quite slow, limiting quantum computers to nearest-neighbor interactions at slowed entangling gate speeds.[18]

Considering the NMR QIP, the couplings should be large,[19] since smaller couplings mean longer nonlocal gate operations,[20] with relatively long pulse sequences, and, therefore, bigger problems with decoherence.[3] Solid NMR provides advantages in using the dipolar coupling, but it also brings challenges facing the single qubit control and multiqubit operations. For two-qubit operations, this stronger coupling between spins reduces the time of quantum gate operations; however, when two qubits are recoupled for a logic gate, spurious couplings between nuclei could occur causing a small error in each logic gate.[17] This kind of uncontrolled dipolar coupling between nuclei is a source of decoherence.

A potential resource to overcome this challenge could be the remarkably large through-space (TS) coupling. In this case, the spin−spin coupling is transmitted through the interaction of overlapping lone pairs in molecules in which NMR active atomic nuclei are located in close proximity, but formally not bonded.[21−23] Exceptionally large TS $J(^{31}P,^{31}P)$ coupling constants have been observed in 1,8-diphosphanaphthalenes[16] (PPN) and in naphtho[1,8-*cd*]-1,2-dithiole phenylphosphines (NTP).[24] According to Reiter et al.[21] and Sanz Camacho et al.[24] there is no evidence of hydrogen bonding between phosphorus atoms in both PPN and NTP.

In principle, the large coupling could be useful to overcome potential sources of quantum information loss, suggesting the use of relatively short pulse sequences and affording an efficient manner to control two-qubit operations. Under these circumstances, coherence could likely be preserved.

To broaden the understanding of TS SSCCs transmission mechanisms, experimental and theoretical studies have been performed[25,26] and a recent review[27] discusses the understanding of through-space spin coupling known since the 1960s.[28] Contreras et al.[29] and Malkina et al.[23] called attention to evaluate the TS transmission of the Fermi contact (FC) term of J_{P-P} SSCCs by the overlapping of the P lone pairs. Those results strongly support the assumption that the TS lone-pair overlap of proximate phosphorus atoms is the main transmission mechanism of the TS SSCC.

The often termed "through-space" J couplings involve atoms that are often held close in space by rigid molecular architectures, leading to significant electron density between them, even though a formal covalent bond would not be drawn. High $^{TS}J_{F,F}$ values range around 170 Hz in rigid 4,5-difluorophenanthrenes molecules.[30] Nonbonded $J_{F,P}$ coupling constants above 130 Hz have been reported in *o*-CF_3-substituted naphthalene derivatives;[31] $^{TS}J_{P-P}$ above 150 Hz was found in 1,2-$C_6H_4(PPh_2)$−(PMePh);[32] about 240 Hz in arylphosphine−phosphonites;[33] and up to 120 Hz in 1,2-substituted ferrocenyl diphosphines.[34]

The success of DFT calculations in predicting the NMR parameters has led to the technique being extensively adopted to clarify the experimental results of these unusually high TS SSCCs values.[24,35−40] In 2018, TS J between ^{1}H formally separated by up to 18 covalent bonds in model helical molecules have been detected by NMR experiments and the existence of the through-space coupling phenomenon have been confirmed by DFT calculations.[41] Still in 2018, DFT calculations have been used to verify experimental findings and to provide additional insight into the hydrogen−hydrogen nonbonded through-space coupling on *in,in*-cyclophane.[42] Coupled cluster singles and doubles (CCSD),[26,41] second order polarization propagator approximation (SOPPA)[43] and second-order Møller−Plesset perturbation theory (MP2)[42] have also been employed for TS J calculations.

Despite its great importance, to our knowledge, this is the first application of TS $J(^{31}P,^{31}P)$ coupling as a resource for universal logic in NMR quantum computers. In fact, this strong TS J could suggest new experiments employing nuclear spins, which may be promising for future scalable quantum computer architectures.

In other instances, spin-$^1/_2$ nuclei systems are widely accepted as one of the most robust systems against the environment noise, providing them with relatively longer coherence time and allowing the accurate control of quantum gate operations.[16,44]

Given this scenario, this study aims at exploring the large through-space J $^{31}P-^{31}P$ couplings to provide tighter, more accurate control through large-scale NMR QIP. Theoretical strategies will be applied to explore the spectroscopic properties of 1,8-di(phosphinyl)naphthalene (Figure 1) and naphtho[1,8-*cd*]-1,2-dithiole phenylphosphine derivatives (Figure 2), as chemical shifts and through-space spin−spin couplings.

2. THEORETICAL METHODS

Crystallographic data for di(phosphinyl)naphthalene (PPN) were obtained from the Cambridge Crystallographic Data Centre database (CSD) and used for the geometry optimization *in vacuo* at DFT level of theory. B3LYP functional was employed among 6-311G(d,p), 6-31+G(d,p), or 6-31+G(3df,2pd) basis sets, which is called throughout this

DOI: 10.1021/acs.jpca.8b09425
J. Phys. Chem. A 2019, 123, 1372−1379

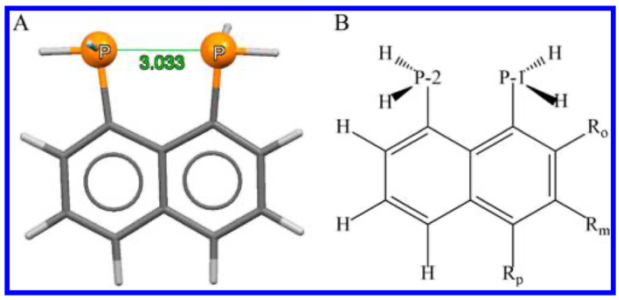

Figure 1. (A) 1,8-di(phosphinyl)naphthalene molecule, PPN. (B) Substituted molecule: $PPN_{o/m/p}$-F ($R_o/R_m/R_p$ = F), $PPN_{o/m/p}$-Cl ($R_o/R_m/R_p$ = Cl), $PPN_{o/m/p}$-Br ($R_o/R_m/R_p$ = Br), $PPN_{o/m/p}$-methyl ($R_o/R_m/R_p$ = methyl), $PPN_{o/m/p}$-ethyl ($R_o/R_m/R_p$ = ethyl), $PPN_{o/m/p}$-phenyl ($R_o/R_m/R_p$ = phenyl), $PPN_{o/m/p}$-NO_2 ($R_o/R_m/R_p$ = NO_2), and $PPN_{o/m/p}$-NH_2 ($R_o/R_m/R_p$ = NH_2).

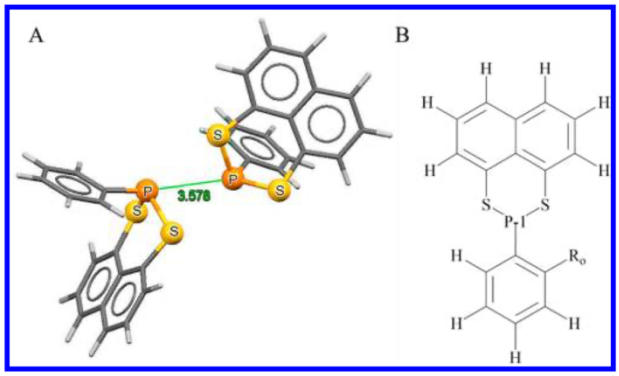

Figure 2. (A) Naphtho[1,8-cd]-1,2-dithiole phenylphosphine molecule, NTP dimer. (B) Substituted molecule: NTP_o-F (R_o = F), NTP_o-Cl (R_o = Cl), NTP_o-methyl (R_o = methyl), NTP_o-ethyl (R_o = ethyl), and NTP_o-NH_2 (R_o = NH_2).

paper as OP1, OP2 and OP3, respectively. The calculations were performed using the Gaussian 09 package.[45]

The OP1 geometry optimization method was performed for PPN derivatives; these were obtained through replacements in *ortho* (R_o), *meta* (R_m), and *para* (R_p) positions with respect to *P*-1, by F, Cl, Br, methyl, ethyl, phenyl, NO_2, and NH_2, in each position. They were named as follows: PPN_o-F if R_o= F, PPN_m-F if R_m= F, PPN_p-F if R_p = F, and so forth for the other substituents (Figure 1).

Naphtho[1,8-*cd*]-1,2-dithiole phenylphosphine (NTP) calculations were carried out using a dimer model proposed by Sanz Camacho and et al.[24] in which the NTP dimer model was extracted from DFT-optimized NTP crystal structures (Figure 2).

NTP derivatives were proposed taking the most suitable PPN derivative for the QIP into account. In other words, PPN derivatives in which replacements, proposed in this work, have fitted better to the NMR QIP requirements; this happened in PPN *ortho* position substituted. NTP derivatives were obtained by exchanging the H atom in the position *ortho* (R_o) related to *P*-1, by F, Cl, methyl, ethyl and NH_2. These derivatives were named NTP_o-F (R_o = F), NTP_o-Cl (R_o = Cl), NTP_o-methyl (R_o = methyl), NTP_o-ethyl (R_o = ethyl), and NTP_o-NH_2 (R_o = NH_2) (Figure 2).

All theoretical calculations were performed using the Gaussian 09 software.[45] Magnetic shieldings (σ) were computed for optimized geometries at the GIAO (gauge-including atomic orbitals) level. The σ and the spin−spin coupling constant (SSCC or J) calculations were carried out with the functionals, B3LYP and PBE1PBE, employing aug-cc-pVTZ-J,[46] Def2-TZVP,[47] IGLO-III,[48] or pcJ-2[49] basis sets. Furthermore, theoretical calculations were carried out within the locally dense basis sets (LDBS) scheme;[43,50−54] where one of the above-cited basis set was used on ^{31}P while either 6-31G or the corresponding basis set without the additional "-J" functions was employed for the remaining atoms, which are called throughout the article as the LDBS-1 and LDBS-2 scheme, respectively; see below for more details. ^{31}P NMR chemical shift (δ) was calculated relative to PH_3, optimized at the same level.

For the PPN derivatives, the SSCC values were computed for optimized geometries with the PBE1PBE functional and pcJ-2 within the LDBS-1 scheme. The σ values were carried out at the B3LYP/aug-cc-pVTZ-J level (an exception was taken when aug-cc-pVTZ-J was not available, as in the case of Bromine, in which aug-cc-pVTZ was employed instead).

NTP derivative SSCC values were calculated with PBE1PBE and Def2-TZVP within the LDBS-1 scheme. The σ values were obtained by PBE1PBE/pcJ-2 within the LDBS-2 scheme.

The ^{31}P chemical shift for both PPN and NTP derivatives was calculated relative to PH_3, as commented above. The absolute ^{31}P NMR shieldings for PH_3 were 555.51 ppm (PPN derivatives) and 557.24 ppm (NTP derivatives).

3. RESULTS AND DISCUSSION

3.1. Validation of the Theoretical Methodology.

Initially, the theoretical methodology was validated by taking the experimental data for ^{31}P of PPN[21,22] and NTP[24] molecules as references.

The OP1, OP2 and OP3 levels adopted for PPN geometry optimizations provided P···P intramolecular distance values of 3.033, 3.023, and 3.010 Å, respectively; which are very close to the experimental CSD value (2.985 Å) and to the values calculated by ref 22 (3.038 and 2.986 Å); the latter were performed with aug-cc-pVDZ and aug-cc-pVTZ, respectively, at the MP2 computational level. Therefore, the structure optimization theoretical levels used in this work remain adequate (Figure S1, Supporting Information).

As exemplified above, high-level *ab initio* calculations (MP2 and CCSD(T), e.g.) can accurately reproduce the experimental values, but these theoretical methods are very expensive computationally and, therefore may not be affordable for larger systems.

In this scenario, the use of the selected DFT method offered an efficient way of determining PPN geometries. Thus, DFT could provide a reasonable trade-off between cost and accuracy for modeling medium-sized to large molecules.

Currently, standard DFT methods seem to be sufficiently accurate for predictions of chemical shifts and SSCCs; however, the benchmarking of DFT methods could combine synergistically both computational costs and methodology precision. Indeed, there are many functionals, and while performance typically improves from LDA over GGA ongoing to hybrid functionals, *a priori* there is no substantial reason to prefer one functional from a given class over another.[55] With an appropriate basis set selection, DFT provides a highly accurate chemical shift and spin−spin coupling constant at a reasonable cost.[56,57]

The first NMR parameter evaluated was the ^{31}P chemical shift, in which case, the shielding values calculated for the P

DOI: 10.1021/acs.jpca.8b09425
J. Phys. Chem. A 2019, 123, 1372−1379

Table 1. ^{31}P Chemical Shifts δ (ppm) and P−P Through Space Coupling Constants TS J (Hz) for the P-1 and P-2 Atoms of PPN Molecule and NTP Dimer

	PPN molecule^{OP1}		NTP dimer		
theoretical level	δ P	TS $J_{P\text{-}1,P\text{-}2}$	δ P-1	δ P-2	TS $J_{P\text{-}1,P\text{-}2}$
B3LYP/aug-cc-pVTZ-J	−104.9	277.9	52.8	57.9	118
B3LYP/aug-cc-pVTZ-J$^{LDBS\text{-}1}$	−103.5	279.9	50.3	55.3	120
B3LYP/aug-cc-pVTZ-J$^{LDBS\text{-}2}$	−104.7	277.7	53.1	58.2	118
B3LYP/Def2-TZVP	−99.5	200.4	24.3	29.5	114
B3LYP/Def2-TZVP$^{LDBS\text{-}1}$	−104.0	203.7	57.5	62.9	103
B3LYP/IGLO-III	−102.4	279.9	20.0	26.3	133
B3LYP/IGLO-III$^{LDBS\text{-}1}$	−104.0	203.7	57.5	62.9	103
B3LYP/pcJ-2	−105.6	286.6	15.9	21.4	133
B3LYP/pcJ-2$^{LDBS\text{-}1}$	−113.8	263.2	47.1	51.8	126
B3LYP/pcJ-2$^{LDBS\text{-}2}$	−105.2	286.6	16.4	21.8	133
B3LYP/TZVP	−113.6	206.4	16.0	20.2	112
PBE1PBE/aug-cc-pVTZ-J	−110.1	250.8	3.8	9.4	109
PBE1PBE/aug-cc-pVTZ-J$^{LDBS\text{-}1}$	−109.3	252.8	36.7	41.6	111
PBE1PBE/aug-cc-pVTZ-J$^{LDBS\text{-}2}$	−110.0	250.6	3.6	8.9	108
PBE1PBE/Def2-TZVP	−105.4	179.7	11.1	16.3	107
PBE1PBE/Def2-TZVP$^{LDBS\text{-}1}$	−109.5	183.8	43.5	47.9	95
PBE1PBE/pcJ-2	−111.2	258.5	3.6	8.9	123
PBE1PBE/pcJ-2$^{LDBS\text{-}1}$	−119.3	236.4	32.8	37.4	116
PBE1PBE/pcJ-2$^{LDBS\text{-}2}$	−110.9	258.9	−3.1	2.2	123
PBE1PBE/TZVP	−118.6	184.8	3.8	7.9	105
experimental	*−104.9*[a]	*221.6*[a]	*−3.3*[b]	*0.6*[b]	*86*[b]

[a]From ref 21, CD_2Cl_2, 298 K. [b]From ref 24 at B_0 = 14.1 T, MAS rate = 7.5 kHz, 298 K.

atoms in the molecule were relatively shifted from a frequency of standard compound, 85% aqueous H_3PO_4 (see next session for more details).

Regarding the arrangement between the computational cost and methodology precision, the NMR parameters (δ and J) for PPN and NTP were evaluated at two hybrid GGA DFT functionals, B3LYP and PBE1PBE, following the classification given by Pudasaini and Janesko.[58]

The ^{31}P chemical shifts values (δ, ppm) and P−P TS SSCCs (Hz) at different theoretical levels for the PPN and NTP molecules are shown in Table 1.

B3LYP/aug-cc-pVTZ-J predicted the exact experimental value of ^{31}P δ for the PPN molecule, in both OP1 and OP3 levels; however, regarding the arrangement between the computational cost and methodology precision, OP1 level was chosen for further ^{31}P δ calculations of the PPN derivatives.

Concerning PPN molecule TS J calculations, PBE1PBE functional among pcJ-2 basis set within the LDBS-1 scheme, in OP1 optimization level, presented the highest accuracy of the theoretical levels employed (for TS J and δ values in OP2 and OP3, see Table S1in the Supporting Information).

In another instance, taking the NTP dimer into account, the accurate levels for δ calculations were PBE1PBE/pcJ-2 within the LDBS-2 scheme. Notwithstanding TS J, the most accurate calculation were using PBE1PBE functional when combined among the Def2-TZVP basis set within the LDBS-1scheme.

NTP derivative SSCC values were calculated with PBE1PBE and Def2-TZVP basis set within the LDBS-1 scheme. The σ values were obtained by PBE1PBE/pcJ-2 within the LDBS-2 scheme.

Sanz Camacho and et al.[24] employed periodic DFT PAW TS J calculations, upon NTP 2 × 1 × 1 supercell geometries and obtained values of 144 Hz, rising to 151 Hz with the inclusion of scalar relativity (implemented with ZORA approach). The SSCC computed in the work cited was significantly higher larger than the value measured experimentally (86 Hz). The authors also performed DFT J coupling calculations through the NTP dimer model; it was 123 Hz using PBE1PBE. They achieved a slight improvement of the TS J value predicted by the PBE1PBE functional against the one predicted by PAW TS J.

In this work, we gathered a highly accurate value for TS J upon NTP dimer using PBE1PBE functional and Def2-TZVP within the LDBS-1 scheme. This theoretical approach reduced the deviation between the theoretical and experimental values of the total coupling constant J from 67.4% to 10.5%. This is a very accurate result, concerning the magnitude of this coupling and its computational cost.

The methodology approach chosen in this work provided theoretical values that resemble the experimental data of ^{31}P TS J coupling and chemical shifts (Table 1). Additionally, in Table 2 are shown the values of the four nonrelativistic contributions to the total indirect nuclear SSCCs, first

Table 2. Fermi Contact (FC), Spin−Dipolar (SD), Paramagnetic Spin−Orbit (PSO) and Diamagnetic Spin−Orbit (DSO) Contributions to the Total P−P Through Space Coupling Constants TS J (Hz) for the P-1 and P-2 Atoms of PPN Molecule and NTP Dimer

	PPN molecule[a]	NTP dimer[b]
FC	233.5	94.7
SD	1.917	0.189
PSO	0.873	−0.148
DSO	0.137	0.283
total TS J	236.4	95.0

[a]From PBE1PBE/pcJ-2 within the LDBS-1 scheme calculation. [b]From PBE1PBE/Def2-TZVP within the LDBS-1 scheme calculation.

DOI: 10.1021/acs.jpca.8b09425
J. Phys. Chem. A 2019, 123, 1372−1379

suggested by Ramsey:[59] Fermi contact (FC), spin−dipolar (SD), paramagnetic spin−orbit (PSO), and diamagnetic spin−orbit (DSO) contributions to the total TS *J*. The FC, SD, PSO, and DSO contribution values were taken from the most accurate theoretical level for each SSCC calculation.

FC and SD contributions are transmitted by the interaction of the nuclear spins with the spins of the electrons; and, PSO and DSO contributions are transmitted by the interaction of the nuclear spins with the orbital angular momentum of the electrons.[43] In both structures, Total TS $J(^{31}P,^{31}P)$ is by far dominated by a large and positive FC term, while SD, PSO, and DSO contributions are smaller. Those results are in fair agreement with what is well-known nowadays, that the electron delocalization interactions are the main vehicle for transmitting the FC term for long-range SSCCs.[23,29,60]

The plot of calculated values versus experimental values ^{31}P TS *J* coupling and chemical shifts for PPN molecule NTP dimer gives a very good correlation (Figure 3). The plot is analyzed as a linear correlation with the square of the correlation coefficient, R^2 = 0.9997. This shows a very good agreement between theory and experiment.

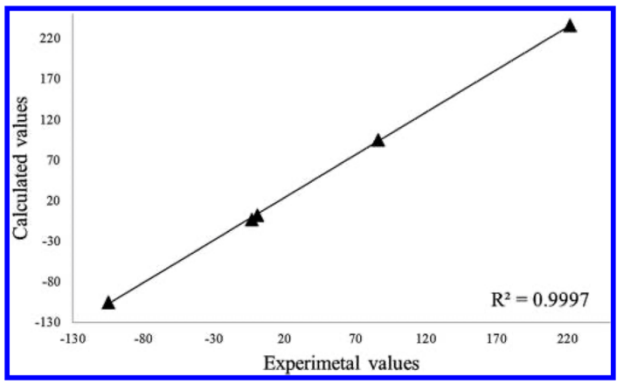

Figure 3. Calculated values versus experimental values ^{31}P TS *J* coupling and chemical shifts for PPN molecule NTP dimer. Data are from Table 1, and the correlation coefficient, R^2, is 0.9997.

3.2. NMR Parameters and Quantum Information Processing. Structural modifications have been performed in PPN and NTP replacing the H bonded to C in respective *ortho*, *meta*, and *para* positions related to the P-1 atom (Figure 1 and 2). The substituent groups were F, Cl, Br, methyl, ethyl, phenyl, NO_2, and NH_2, in each position once. Therefore, F, Cl, Br, and NO_2 are electron-withdrawing groups and methyl, ethyl, phenyl, and NH_2 are electron-donating groups. These modifications were carried out to investigate the structure−activity relationships and to propose molecules with improved performance for QIP.

This work concerns the ^{31}P nuclei as qubits on a large-scale NMR QIP and the spectroscopic properties calculated for the PPN and NTP derivatives with the best theoretical methods obtained in the validation of the calculation strategy are in Table 3.

The modifications performed in the PPN molecule enhanced the dispersion in the chemical shifts of P-1 and P-2 nuclei (Table S2, Supporting Information). From this result, it is possible to manipulate the nucleus by differentiating the qubits.[61] Foremost, the structural modifications had an auspicious effect on PPN derivatives, owing to the broken PPN symmetry. By analyzing all the chemical shifts (Table 3)

Table 3. Variation of ^{31}P Chemical Shifts [$\Delta\delta$ (ppm)] and P−P Through Space Coupling Constants [TS J (Hz)] for the Studied Molecules

compounds	$\Delta\delta_{P\text{-}1,P\text{-}2}$[a]	TS $J_{P\text{-}1,P\text{-}2}$
PPN	0.0	236.4
PPN_o-F	71.5	234.5
PPN_m-F	0.5	234.6
PPN_p-F	1.3	235.8
PPN_o-Cl	36.9	247.6
PPN_m-Cl	0.4	237.9
PPN_p-Cl	0.9	240.4
PPN_o-Br	13.8	238.3
PPN_m-Br	0.7	237.5
PPN_p-Br	0.8	240.6
PPN_o-methyl	44.3	255.2
PPN_m-methyl	1.1	234.7
PPN_p-methyl	0.4	236.3
PPN_o-ethyl	56.5	242.6
PPN_m-ethyl	0.5	233.1
PPN_p-ethyl	0.2	236.8
PPN_o-phenyl	10.3	235.6
PPN_m-phenyl	1.3	235.7
PPN_p-phenyl	0.7	242.8
PPN_o-NH_2	55.0	210.7
PPN_m-NH_2	0.4	231.3
PPN_p-NH_2	0.2	234.2
PPN_o-NO_2	32.7	249.0
PPN_m-NO_2	1.6	244.2
PPN_p-NO_2	1.2	249.7
NTP	5.3	95.0
NTP_o-F	2.0	94.8
NTP_o-Cl	4.8	83.3
NTP_o-methyl	2.5	89.0
NTP_o-ethyl	4.6	85.7
NTP_o-NH_2	3.9	86.5

in relation to the PPN reference molecule, the substitution generates a significant effect on $\Delta\delta_{P\text{-}1,P\text{-}2}$, which provided a notable increase, by 71.5 ppm in PPN_o-F, 56.5 ppm in PPN_o-ethyl, and by 55.0 ppm in PPN_o-NH_2. This effect could also occur to PPN_o-methyl, PPN_o-Cl, and PPN_o-NO_2, which rises to 44.3, 36.9, and 32.7 ppm, respectively. Furthermore, this effect is a bit smaller for PPN_o-Br and PPN_o-phenyl, which had their magnitude increased by 13.8 and 10.3, respectively. On the other hand, the substitutions in NTP dimers decrease the $\Delta\delta_{P\text{-}1,P\text{-}2}$ values (Table 3), meaning a small dispersion in the chemical shifts of P-1 and P-2 nuclei, thus limiting the manipulation of the nuclei at distinct frequencies, consequently not differentiating the qubits.

Regarding the theoretical values for chemical shifts, a critical point concerns the ^{31}P shielding scale. In fact, the standard reference compound for ^{31}P is 85% aqueous H_3PO_4, which shielding cannot be accurately estimated by theory. A more convenient reference is PH_3, but its gas-to-liquid shift, as large as 28 ppm,[62] must also be considered. Therefore, the ^{31}P absolute magnetic shielding calculated for a substance S was converted here to the chemical shift relative to 85% aqueous H_3PO_4 by using eq 2, where −266.1 ppm is the gas-phase chemical shift of PH_3.[63]

$$\delta(S, \text{calcd}) = \sigma(PH_3, \text{calcd}), -\sigma(S, \text{calcd}) - 266.1 \text{ ppm} \quad (2)$$

DOI: 10.1021/acs.jpca.8b09425
J. Phys. Chem. A 2019, 123, 1372−1379

Considering the TS SSCCs, the PPN derivatives have preserved the same magnitude order as the PPN large TS $J_{P,P}$. These unusual large TS SSCCs will be responsible for promoting the interaction among the individual qubits in the NMR QIP. Variations in SSCC against structural modifications should be expected; the values are in Table 3. As for the PPN molecule, TS SSCC was increased by 18.8 Hz in PPN_o-methyl, about 13 Hz in PPN_p-NO_2 and PPN_o-NO_2, 11.2 Hz in PPN_o-Cl, and about 8 Hz in PPN_m-NO_2.

It is important to stress that the ^{31}P nucleus presents T_2 adequate to retain the qubits in coherent phase, allowing the quantum operations to be coherently completed.[44,64,65] Furthermore, considering large-scale NMR QIP, the decoherence times must be preserved as the size of the system increases.

From the Table 3 and Figure 4, it was possible to rationalize the relation between J and $\Delta\delta$ values. Accordingly, the

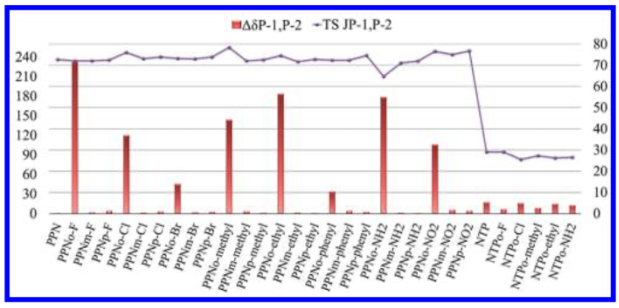

Figure 4. $\Delta\delta_{P\text{-}1,P\text{-}2}$ and TS $J_{P\text{-}1,P\text{-}2}$ values for the studied molecules.

derivative molecule that possesses larger TS $J_{P\text{-}1,P\text{-}2}$ as well as considerable $\Delta\delta_{P\text{-}1,P\text{-}2}$ will be a promising molecule for NMR QIP. PPN_o-F, PPN_o-ethyl and PPN_o-NH_2, have had both parameters optimized simultaneously: PPN_o-F with TS $J_{P\text{-}1,P\text{-}2}$ 234.5 Hz and $\Delta\delta_{P\text{-}1,P\text{-}2}$ 71.5 ppm; PPN_o-ethyl with TS $J_{P\text{-}1,P\text{-}2}$ 242.6 Hz and $\Delta\delta_{P\text{-}1,P\text{-}2}$ 56.5 ppm, and PPN_o-NH_2 with TS $J_{P\text{-}1,P\text{-}2}$ 210.7 Hz and 55.0 $\Delta\delta_{P\text{-}1,P\text{-}2}$ ppm. This means these derivatives could be considered as promising qubit molecules to be used in the NMR QIP. These molecules patterns can be useful to overcome the natural limitations concerning the development of large-scale NMR QIP using the large TS SSCCS facing the need of long-time quantum gate implementations.

4. CONCLUSIONS

The road of constructing a quantum computer is hard, but the alliance of interdisciplinary communities of researchers will be essential in any future effort toward experimental implementations of QIP. It is well-know that any classical circuit could, in principle, be designed as a quantum circuit with Toffoli gates. It should be kept in mind, however, that the practical benefits of quantum computers are deeply related to a processing power to solve problems that would be effectively impossible for regular computers. In fact, quantum computers could not do some tasks better than classical computers can. In addition, the quantum processors are unstable and the components for quantum computing are very expensive and hard to find, which is particularly challenging, both from the theoretical and experimental points of view. Essentially, that can limit quantum computers to research machines, at least over coming decades. In this work, we showed a way in which the computational chemistry resources can be leveraged and can enlighten researchers for the highly awaited quantum computer construction.

Through this outlook, PPN and NTP derivatives were proposed and investigated to develop new promising molecules able to provide more accurate control through large-scale NMR QIP.

Regarding the PPN molecule, geometry optimization was carried out employing the B3LYP functional among 6-311G(d,p), 6-31+G(d,p) or 6-31+G(3df,2pd) basis sets. B3LYP/6-311G(d,p) level have provided a good correlation between calculated and theoretical values.

Theoretical strategies were applied to explore the spectroscopic properties of 1,8-di(phosphinyl)naphthalene derivatives (Figure 1) and naphtho[1,8-*cd*]-1,2-dithiole phenylphosphines (Figure 2), as chemical shifts and through-space spin−spin couplings.

The spectroscopic parameters (δ and J) were calculated with B3LYP and PBE1PBE functionals for P-1 and P-2 atoms in both molecules. For speeding up the calculations, the "locally dense basis sets" approach was used.

For the PPM molecule, the B3LYP/aug-cc-pVTZ-J level showed better agreement with experimental data of ^{31}P chemical shifts and PBE1PBE functional among pcJ-2 within the LDBS-1 scheme was the most accurate level for TS $J(^{31}P,^{31}P)$ coupling. Differently, for the NTP dimer, PBE1PBE and pcJ-2 within the LDBS-2 scheme showed better agreement with the experimental data of ^{31}P chemical shifts; otherwise, for the TS $J(^{31}P,^{31}P)$ coupling, the most accurate methodology was using the PBE1PBE functional with the Def2-TZVP basis set within the LDBS-1 scheme.

Finally, our results have granted the best molecules for NMR-quantum information processing, which were PPN_o-F, PPN_o-ethyl, and PPN_o-NH_2. In addition, this study has reported a prominent application of these molecules in quantum computers. Their examples could be advantageous to overcome the natural limitations concerning the development of large-scale NMR QIP using the large TS SSCCS facing the need of long-time quantum gate implementations.

NMR QIP based on crystals provides a new opportunity to explore other potential sources for QIP. Employing these large TS SSCCs can circumvent the need of a long time for quantum gates operations. Our work introduced those derivatives toward suitable qubits molecules as a kick-off for the construction of more complex derivatives, which can meet the challenge of large-scale NMR QIP.

■ ASSOCIATED CONTENT

Supporting Information

The Supporting Information is available free of charge on the ACS Publications website at DOI: 10.1021/acs.jpca.8b09425.

Spectroscopic properties and geometries of the studied molecules (PDF)

■ AUTHOR INFORMATION

Corresponding Author

*(T.C.R.) E-mail: teo@dqi.ufla.br; teodorico.ramalho@gmail.com. Telephone: +55 35 3829-1522. Fax: +55 35 3829-1271.

ORCID

Jéssica Boreli dos Reis Lino: 0000-0002-2141-3440

Teodorico Castro Ramalho: 0000-0002-7324-1353

DOI: 10.1021/acs.jpca.8b09425
J. Phys. Chem. A 2019, 123, 1372−1379

Notes

The authors declare no competing financial interest.

■ ACKNOWLEDGMENTS

The authors wish to thank the Brazilian financial agencies Conselho Nacional de Desenvolvimento Científico e Tecnológico (CNPq), Fundação de Amparo ao Ensino e Pesquisa de Minas Gerais (FAPEMIG), and Coordenação de Aperfeiçoamento de Pessoal de Nível Superior/Ministério da Defesa (CAPES/MD) for financial support, and the Federal University of Lavras (UFLA) for providing the physical infrastructure and work space. This work was also supported by Excellence Project FIM UHK.

■ REFERENCES

(1) Olson, J.; Cao, Y.; Romero, J.; Johnson, P.; Dallaire-Demers, P.-L.; Sawaya, N.; Narang, P.; Kivlichan, I.; Wasielewski, M.; Aspuru-Guzik, A. *Quantum Information and Computation for Chemistry*. John Wiley & Sons, Inc.: Hoboken, NJ, 2014.

(2) Lu, D.; Xu, B.; Xu, N.; Li, Z.; Chen, H.; Peng, X.; Xu, R.; Du, J. Quantum Chemistry Simulation on Quantum Computers: Theories and Experiments. *Phys. Chem. Chem. Phys.* **2012**, *14*, 9411−9420.

(3) Suter, D.; Mahesh, T. S. Spins as Qubits: Quantum Information Processing by Nuclear Magnetic Resonance. *J. Chem. Phys.* **2008**, *128*, 052206−052206.

(4) Lu, D.; Brodutch, A.; Park, J.; Katiyar, H.; Jochym-O'Connor, T.; Laflamme, R. NMR Quantum Information Processing. *Biol. Magn. Reson.* **2016**, *31*, 193−226.

(5) Vind, F. A.; Foerster, A.; Oliveira, I. S.; Sarthour, R. S.; Soares-Pinto, D. O.; Souza, A. M.; Roditi, I. Experimental Realization of the Yang-Baxter Equation Via NMR Interferometry. *Sci. Rep.* **2016**, *6*, 1−8.

(6) Mitrikas, G.; Sanakis, Y.; Raptopoulou, C. P.; Kordas, G.; Papavassiliou, G. Electron Spin−Lattice and Spin−Spin Relaxation Study of a Trinuclear Iron(III) Complex and Its Relevance in Quantum Computing. *Phys. Chem. Chem. Phys.* **2008**, *10*, 743−748.

(7) Devra, A.; Prabhu, P.; Singh, H.; Arvind; Dorai, K. Efficient Experimental Design of High-Fidelity Three-Qubit Quantum Gates Via Genetic Programming. *Quantum Inf. Process.* **2018**, *17*, 67−67.

(8) Gaikwad, A.; Rehal, D.; Singh, A.; Dorai, K.; et al. Experimental Demonstration of Selective Quantum Process Tomography on an NMR Quantum Information Processor. *Phys. Rev. A: At., Mol., Opt. Phys.* **2018**, *97*, 1−8.

(9) Pande, V. R.; Bhole, G.; Khurana, D.; Mahesh, T. S. Strong Algorithmic Cooling in Large Star-Topology Quantum Registers. *Phys. Rev. A: At., Mol., Opt. Phys.* **2017**, *96*, 12330−12330.

(10) Lino, J. B. R.; Rocha, E. P.; Ramalho, T. C. Value of NMR Parameters and DFT Calculations for Quantum Information Processing Utilizing Phosphorus Heterocycles. *J. Phys. Chem. A* **2017**, *121*, 4486−4495.

(11) Mawhinney, R. C.; Schreckenbach, G. NMR Quantum Computing: Applying Theoretical Methods to Designing Enhanced Systems. *Magn. Reson. Chem.* **2004**, *42*, S88−S98.

(12) Tamulis, A.; Tamulis, V.; Ziriakoviene, A. Quantum Mechanical Design of Molecular Computers Elements Suitable for Self-Assembling to Quantum Computing Living Systems. *Solid State Phenom.* **2004**, *97−98*, 173−180.

(13) DiVincenzo, D. P. The Physical Implementation of Quantum Computation. *Fortschr. Phys.* **2000**, *48*, 771−783.

(14) Jones, J. A. Quantum Computing with NMR. *Prog. Nucl. Magn. Reson. Spectrosc.* **2011**, *59*, 91.

(15) Oliveira, I. S.; Bonagamba, T. J.; Sarthour, R. S.; Freitas, J. C. C.; deAzevedo, E. R. Perspectives for NMR Quantum Computation and Quantum Information. *NMR Quantum Information Processing* **2007**, *2*, 221−241.

(16) Xin, T.; Wang, B.-X.; Li, K.-R.; Kong, X.-Y.; Wei, S.-J.; Wang, T.; Ruan, D.; Long, G.-L. Nuclear Magnetic Resonance for Quantum Computing: Techniques and Recent Achievements. *Chin. Phys. B* **2018**, *27*, 020308−020308.

(17) Ladd, T. D.; Goldman, J. R.; Yamaguchi, F.; Yamamoto, Y.; Abe, E.; Itoh, K. M. All-Silicon Quantum Computer. *Phys. Rev. Lett.* **2002**, *89*, 017901−017901.

(18) Ladd, T. D. *Quantum Computing with Nuclear Spins in Semiconductors. Dissertation*; Stanford University: Stanford, CA, 2005.

(19) Marx, R.; Pomplun, N.; Bermel, W.; Zeiger, H.; Engelke, F.; Fahmy, A. F.; Glaser, S. J. Engineering of an All-Heteronuclear 5-Qubit NMR Quantum Computer. *Magn. Reson. Chem.* **2015**, *53*, 442−447.

(20) Negrevergne, C.; Mahesh, T. S.; Ryan, C. A.; Ditty, M.; Cyr-Racine, F.; Power, W.; Boulant, N.; Havel, T.; Cory, D. G.; Laflamme, R. Benchmarking Quantum Control Methods on a 12-Qubit System. *Phys. Rev. Lett.* **2006**, *96*, 170501.

(21) Reiter, S. A.; Nogai, S. D.; Karaghiosoff, K.; Schmidbaur, H. Insignificance of P−H···P Hydrogen Bonding: Structural Chemistry of Neutral and Protonated 1,8-Di(Phosphinyl)Naphthalene. *J. Am. Chem. Soc.* **2004**, *126*, 15833−15843.

(22) Sánchez-Sanz, G.; Trujillo, C.; Alkorta, I.; Elguero, J. Intramolecular Pnicogen Interactions in Phosphorus and Arsenic Analogues of Proton Sponges. *Phys. Chem. Chem. Phys.* **2014**, *16*, 15900−15909.

(23) Malkina, O. L.; Křístková, A.; Malkin, E.; Komorovský, S.; Malkin, V. G. Illumination of the Effect of the Overlap of Lone-Pairs on Indirect Nuclear Spin−Spin Coupling Constants. *Phys. Chem. Chem. Phys.* **2011**, *13*, 16015−16021.

(24) Sanz Camacho, P.; McKay, D.; Dawson, D. M.; Kirst, C.; Yates, J. R.; Green, T. F. G.; Cordes, D. B.; Slawin, A. M. Z.; Woollins, J. D.; Ashbrook, S. E. Investigating Unusual Homonuclear Intermolecular "Through-Space" J Couplings in Organochalcogen Systems. *Inorg. Chem.* **2016**, *55*, 10881−10887.

(25) Chalmers, B. A.; Nejman, P. S.; Llewellyn, A. V.; Felaar, A. M.; Griffiths, B. L.; Portman, E. I.; Gordon, E.-J. L.; Fan, K. J. H.; Woollins, J. D.; Bühl, M.; et al. A Study of Through-Space and Through-Bond J_{PP} Coupling in a Rigid Nonsymmetrical Bis-(Phosphine) and Its Metal Complexes. *Inorg. Chem.* **2018**, *57*, 3387−3398.

(26) Favaro, D. C.; Contreras, R. H.; Tormena, C. F. Unusual Through-Space, TS, Pathway for the Transmission of J_{FHF} Coupling: 2-Fluorobenzaldehyde Study Case. *J. Phys. Chem. A* **2013**, *117*, 7939−7945.

(27) Hierso, J.-C. Indirect Nonbonded Nuclear Spin−Spin Coupling: A Guide for the Recognition and Understanding of "Through-Space" NMR J Constants in Small Organic, Organometallic, and Coordination Compounds. *Chem. Rev.* **2014**, *114*, 4838−4867.

(28) Davis, D. R.; Lutz, R. P.; Roberts, J. D. Nuclear Magnetic Resonance Spectroscopy. Long-Range Spin-Spin Couplings in Saturated Molecules1. *J. Am. Chem. Soc.* **1961**, *83*, 246−247.

(29) Contreras, R. H.; Gotelli, G.; Ducati, L. C.; Barbosa, T. M.; Tormena, C. F. Analysis of Canonical Molecular Orbitals to Identify Fermi Contact Coupling Pathways. 1. Through-Space Transmission by Overlap of ^{31}P Lone Pairs. *J. Phys. Chem. A* **2010**, *114*, 1044−1051.

(30) Mallory, F. B.; Mallory, C. W.; Ricker, W. M. Nuclear Spin-Spin Coupling Via Nonbonded Interactions. 4. Fluorine-Fluorine and Hydrogen-Fluorine Coupling in Substituted Benzo[C]Phenanthrenes. *J. Org. Chem.* **1985**, *50*, 457−461.

(31) Mallory, F. B.; Mallory, C. W.; Butler, K. E.; Lewis, M. B.; Xia, A. Q.; Luzik, E. D.; Fredenburgh, L. E.; Ramanjulu, M. M.; Van, Q. N.; Francl, M. M.; et al. Nuclear Spin−Spin Coupling Via Nonbonded Interactions. 8.1 the Distance Dependence of Through-Space Fluorine−Fluorine Coupling. *J. Am. Chem. Soc.* **2000**, *122*, 4108−4116.

(32) Bowmaker, G.; Williams, J. Synthesis and N.M.R. Studies of New Unsymmetrically Substituted Ditertiary Phosphines. *Aust. J. Chem.* **1994**, *47*, 451−460.

(33) Heinicke, J.; He, M.; Kadyrov, R.; Jones, P. G. Sterically Stressed Amino- and Ph-Functional Di-T-Butyl-O-Phosphinophe-

DOI: 10.1021/acs.jpca.8b09425
J. Phys. Chem. A 2019, 123, 1372−1379

nols—Intramolecular Interaction and Formation of Benzoxadiphosphoholes. *Heteroat. Chem.* **1998**, *9*, 183−193.
(34) Hierso, J.-C. Palladium Complexes of Constrained Polyphosphines - Discovery and Investigation of "Through-Space" NMR Spin-Spin Couplings in Organometallic Compounds. *Curr. Org. Chem.* **2011**, *15*, 3197−3213.
(35) Griffin, J. M.; Yates, J. R.; Berry, A. J.; Wimperis, S.; Ashbrook, S. E. High-Resolution ^{19}F MAS NMR Spectroscopy: Structural Disorder and Unusual J Couplings in a Fluorinated Hydroxy-Silicate. *J. Am. Chem. Soc.* **2010**, *132*, 15651−15660.
(36) Ashbrook, S. E.; McKay, D. Combining Solid-State NMR Spectroscopy with First-Principles Calculations − a Guide to NMR Crystallography. *Chem. Commun.* **2016**, *52*, 7186−7204.
(37) Moran, R. F.; Dawson, D. M.; Ashbrook, S. E. Exploiting NMR Spectroscopy for the Study of Disorder in Solids. *Int. Rev. Phys. Chem.* **2017**, *36*, 39−115.
(38) Arras, J.; Eichele, K.; Maryasin, B.; Schubert, H.; Ochsenfeld, C.; Wesemann, L. Intermolecular ^{119}Sn,^{31}P Through-Space Spin−Spin Coupling in a Solid Bivalent Tin Phosphido Complex. *Inorg. Chem.* **2016**, *55*, 4669−4675.
(39) Sanz, D.; Claramunt, R. M.; Mathey, F.; Alkorta, I.; Sánchez-Sanz, G.; Elguero, J. Intermolecular Spin−Spin Coupling Constants between ^{31}P Atoms. *C. R. Chim.* **2013**, *16*, 937−944.
(40) Kaupp, M.; Patrakov, A.; Reviakine, R.; Malkina, O. L. Understanding the Conformational Dependence of Spin−Spin Coupling Constants: Through-Bond and Through-Space J(^{31}P,^{31}P) Coupling in Tetraphosphane-1,4-Diides [M(L)X]2[P4r4]. *Chem. - Eur. J.* **2005**, *11*, 2773−2782.
(41) Dračínský, M.; Buchta, M.; Buděšínský, M.; Vacek-Chocholoušová, J.; Stará, I. G.; Starý, I.; Malkina, O. L. Dihydrogen Contacts Observed by Through-Space Indirect NMR Coupling. *Chem. Sci.* **2018**, *9*, 7437−7446.
(42) Xiao, Y.; Mague, J. T.; Pascal, R. A. An Exceptionally Close, Non-Bonded Hydrogen−Hydrogen Contact with Strong Through-Space Spin−Spin Coupling. *Angew. Chem., Int. Ed.* **2018**, *57*, 2244−2247.
(43) Provasi, P. F.; Aucar, G. A.; Sauer, S. P. A. Large Long-Range F−F Indirect Spin−Spin Coupling Constants. Prediction of Measurable F−F Couplings over a Few Nanometers. *J. Phys. Chem. A* **2004**, *108*, 5393−5398.
(44) Swift, M. W.; Van de Walle, C. G.; Fisher, M. P. A. Posner Molecules: From Atomic Structure to Nuclear Spins. *Phys. Chem. Chem. Phys.* **2018**, *20*, 12373−12380.
(45) Frisch, M. J.; Trucks, G. W.; Schlegel, H. B.; Scuseria, G. E.; Robb, M. A.; Cheeseman, J. R.; Scalmani, G.; Barone, V.; Mennucci, B.; Petersson, G. A., et al. *Gaussian 09*; Gaussian, Inc.: Wallingford, CT, 2013.
(46) Provasi, P. F.; Sauer, S. P. A. Optimized Basis Sets for the Calculation of Indirect Nuclear Spin-Spin Coupling Constants Involving the Atoms B, Al, Si, P, and Cl. *J. Chem. Phys.* **2010**, *133*, 054308.
(47) Weigend, F.; Ahlrichs, R. Balanced Basis Sets of Split Valence, Triple Zeta Valence and Quadruple Zeta Valence Quality for H to Rn: Design and Assessment of Accuracy. *Phys. Chem. Chem. Phys.* **2005**, *7*, 3297−3305.
(48) Kutzelnigg, W.; Fleischer, U.; Schindler, M. The IGLO-Method: Ab-initio Calculation and Interpretation of NMR Chemical Shifts and Magnetic Susceptibilities. *NMR Basic Principles Prog.* **1990**, *23*, 165.
(49) Jensen, F. The Optimum Contraction of Basis Sets for Calculating Spin−Spin Coupling Constants. *Theor. Chem. Acc.* **2010**, *126*, 371−382.
(50) Chesnut, D. B.; Moore, K. D. Locally Dense Basis Sets for Chemical Shift Calculations. *J. Comput. Chem.* **1989**, *10*, 648−659.
(51) Provasi, P. F.; Aucar, G. A.; Sauer, S. P. A. The Use of Locally Dense Basis Sets in the Calculation of Indirect Nuclear Spin−Spin Coupling Constants: The Vicinal Coupling Constants in H_3C-CH_2X (X = H, F, Cl, Br, I). *J. Chem. Phys.* **2000**, *112*, 6201−6208.
(52) Sanchez, M.; Provasi, P. F.; Aucar, G. A.; Sauer, S. P. A. On the Usage of Locally Dense Basis Sets in the Calculation of NMR Indirect Nuclear Spin−Spin Coupling Constants: Vicinal Fluorine−Fluorine Couplings. *Adv. Quantum Chem.* **2005**, *48*, 161−183.
(53) Reid, D. M.; Kobayashi, R.; Collins, M. A. Systematic Study of Locally Dense Basis Sets for NMR Shielding Constants. *J. Chem. Theory Comput.* **2014**, *10*, 146−152.
(54) Reid, D. M.; Collins, M. A. Calculating Nuclear Magnetic Resonance Shieldings Using Systematic Molecular Fragmentation by Annihilation. *Phys. Chem. Chem. Phys.* **2015**, *17*, 5314−5320.
(55) Faber, R.; Sauer, S. P. A.; Gauss, J. Importance of Triples Contributions to NMR Spin−Spin Coupling Constants Computed at the CC3 and CCSDT Levels. *J. Chem. Theory Comput.* **2017**, *13*, 696−709.
(56) Helgaker, T.; Jaszuński, M.; Ruud, K. Ab Initio Methods for the Calculation of NMR Shielding and Indirect Spin−Spin Coupling Constants. *Chem. Rev.* **1999**, *99*, 293−352.
(57) Rocha, E. P.; Ramalho, T. C. Probing the Esipt Process in 2-Amino-1,4-Naphthoquinone: Thermodynamics Properties, Solvent Effect and Chemometric Analysis. *Theor. Chem. Acc.* **2016**, *135*, 39.
(58) Pudasaini, B.; Janesko, B. G. Evaluation of Approximate Exchange-Correlation Functionals in Predicting One-Bond 31 P− 1 H NMR Indirect Spin−Spin Coupling Constants. *J. Chem. Theory Comput.* **2013**, *9*, 1443−1451.
(59) Ramsey, N. F. Electron Coupled Interactions between Nuclear Spins in Molecules. *Phys. Rev.* **1953**, *91*, 303−307.
(60) Contreras, R. H.; Esteban, Á. L.; Díez, E.; Lochert, I. J.; Della, E. W.; Tormena, C. F. Experimental and DFT Studies on the Transmission Mechanisms of Analogous NMR J_{CH} and J_{CC} Couplings in 1-X- and 1-X-3-Methylbicyclo[1.1.1]-Pentanes. *Magn. Reson. Chem.* **2007**, *45*, 572−577.
(61) Ladd, T. D.; Jelezko, F.; Laflamme, R.; Nakamura, Y.; Monroe, C.; O'Brien, J. L. Quantum Computers. *Nature* **2010**, *464*, 45−53.
(62) Jameson, C. J.; De Dios, A.; Keith Jameson, A. Absolute Shielding Scale for ^{31}P from Gas-Phase Nmr Studies. *Chem. Phys. Lett.* **1990**, *167*, 575−582.
(63) van Wüllen, C. A Comparison of Density Functional Methods for the Calculation of Phosphorus-31 NMR Chemical Shifts. *Phys. Chem. Chem. Phys.* **2000**, *2*, 2137−2144.
(64) Vandersypen, L. M. K.; Chuang, I. L. NMR Techniques for Quantum Control and Computation. *Rev. Mod. Phys.* **2005**, *76*, 1037−1069.
(65) Ito, S.; Momozaki, T.; Kishimoto, Y.; Abe, J.; Iwahori, F. Demonstrations of NMR Quantum Information Processing Utilizing ^{31}P Nuclei of Phosphorus Heterocycles. *Chem. Lett.* **2009**, *38*, 1194−1195.

DOI: 10.1021/acs.jpca.8b09425
J. Phys. Chem. A 2019, 123, 1372−1379

Supporting information

Exploring Through-Space Spin-Spin Couplings for Quantum Information Processing: Facing the challenge of coherence time and control quantum states

Supporting Information

Exploring Through-Space Spin-Spin Couplings for Quantum Information Processing: Facing the Challenge of Coherence Time and Control Quantum States

Jéssica Boreli dos Reis Lino,[a]* Teodorico Castro Ramalho[a,b+]

[a]Chemistry Department, Federal University of Lavras, 37200-000 Lavras,MG, Brazil
[b]Center for Basic and Applied Research, Faculty of Informatics and Management, University Hradec Kralove, 50003 Hradec Kralove,

* jessicaboreli@outlook.com
+ teo@dqi.ufla.br

Table S1 ^{31}P Chemical Shifts δ (ppm) and P–P Though Space Coupling Constants TS J (Hz) for the P Atom of PPN Molecule

PPN molecule	OP1		OP2		OP3	
Theoretical level	δ P	TS $J_{P\text{-}1,P\text{-}2}$	δ P	TS $J_{P\text{-}1,P\text{-}2}$	δ P	TS $J_{P\text{-}1,P\text{-}2}$
B3LYP/aug-cc-pVTZ-J	-104.9	277.9	-105.6	281.1	-104.9	277.7
B3LYP/aug-cc-pVTZ-J$^{LDBS\text{-}1}$	-103.5	279.9	-104.3	283.2	-103.6	279.8
B3LYP/aug-cc-pVTZ-J$^{LDBS\text{-}2}$	-104.7	277.7	-105.4	281.0	-104.7	277.5
B3LYP/Def2-TZVP	-99.5	200.4	-102.1	202.4	-101.5	199.7
B3LYP/Def2-TZVP$^{LDBS\text{-}1}$	-104.0	203.7	-106.6	206.1	-105.9	203.4
B3LYP/IGLO-III	-102.4	279.9	-105.0	283.2	-104.3	279.9
B3LYP/IGLO-III$^{LDBS\text{-}1}$	-104.0	203.7	-106.6	206.1	-105.9	203.4
B3LYP/pcJ-2	-105.6	286.6	-106.1	289.9	-105.5	286.4
B3LYP/pcJ-2$^{LDBS\text{-}1}$	-113.8	263.2	-114.2	266.4	-113.8	263.2
B3LYP/pcJ-2$^{LDBS\text{-}2}$	-105.2	286.6	-105.7	290.3	-105.1	286.8
B3LYP/TZVP	-113.6	206.4	-116.2	206.7	-115.9	206.3
PBE1PBE/aug-cc-pVTZ-J	-110.1	250.8	-111.1	253.8	-110.4	251.2
PBE1PBE/aug-cc-pVTZ-J$^{LDBS\text{-}1}$	-109.3	252.8	-110.3	255.9	-109.6	253.3
PBE1PBE/aug-cc-pVTZ-J$^{LDBS\text{-}2}$	-110.0	250.6	-110.9	253.7	-110.2	251.0
PBE1PBE/Def2-TZVP	-105.4	179.7	-107.9	181.6	-107.3	179.5
PBE1PBE/Def2-TZVP$^{LDBS\text{-}1}$	-109.5	183.8	-112.0	186.0	-111.3	184.0
PBE1PBE/pcJ-2	-111.2	258.5	-112.0	261.6	-111.4	258.9
PBE1PBE/pcJ-2$^{LDBS\text{-}1}$	-119.3	236.4	-120.0	239.4	-119.5	237.0
PBE1PBE/pcJ-2$^{LDBS\text{-}2}$	-110.9	258.9	-111.7	262.1	-111.1	259.4
PBE1PBE/TZVP	-118.6	184.8	-121.2	187.0	-120.8	185.3
Experimental[a]	δ P-1	*-104.9*		TS $J_{P\text{-}1,P\text{-}2}$	*221.6*	

[a]From Reiter, S. A.; Nogai, S. D.; Karaghiosoff, K.; Schmidbaur, H. J. Am. Chem. Soc. 2004, 126 (48), 15833-15843; at CD_2Cl_2, 298 K.

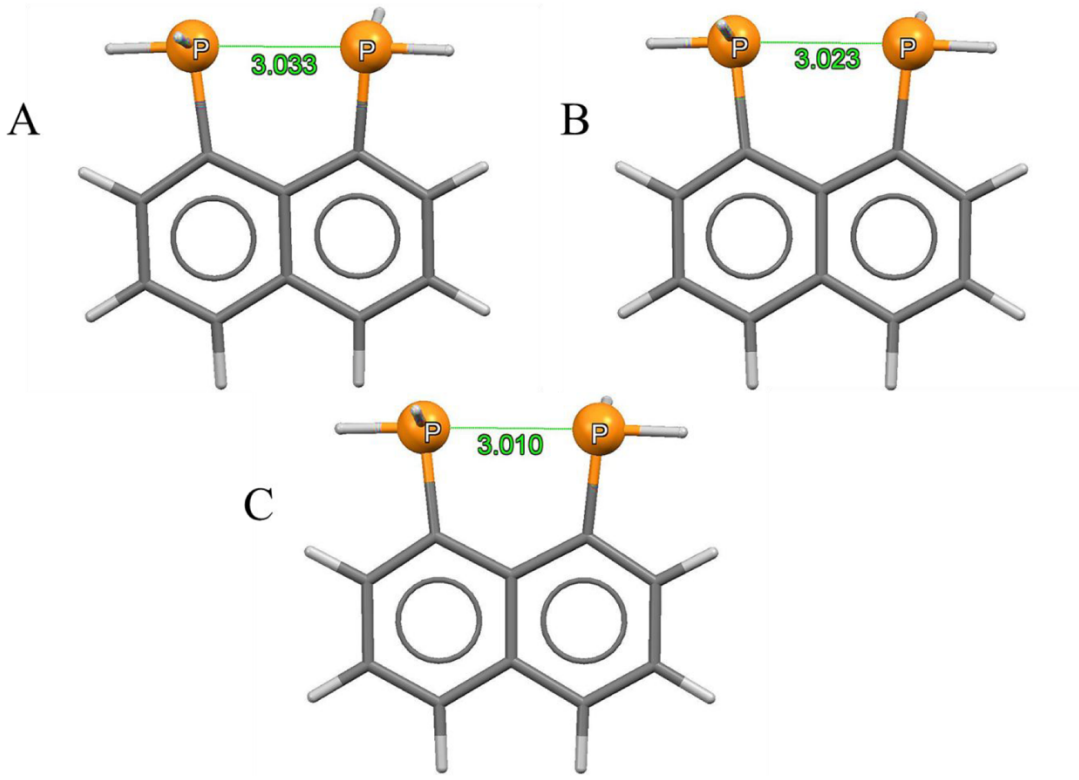

Figure S1 1,8-di(phosphinyl)naphthalene molecule, PPN molecule. Optimized at: (A) OP1-B3LYP/6-311G(d,p); (B) OP2-B3LYP/6-31+G(d,p); and (C) OP3-B3LYP/6-31+G(3df,2pd).

Table S2 ^{31}P Chemical Shifts [δ (ppm)] for the Studied Molecules

Compounds	δ P-1	δ P-2
PPN	-104.9	-104.9
PPN_o-F	-106.8	-178.3
PPN_m-F	-106.3	-105.7
PPN_p-F	-107.2	-108.5
PPN_o-Cl	-102.8	-139.7
PPN_m-Cl	-105.6	-105.2
PPN_p-Cl	-105.7	-106.6
PPN_o-Br	-102.2	-116.0
PPN_m-Br	-105.5	-104.8
PPN_p-Br	-105.2	-106.0
PPN_o-methyl	-109.1	-153.4
PPN_m-methyl	-105.0	-103.9
PPN_p-methyl	-104.7	-105.1
PPN_o-ethyl	-103.6	-160.1
PPN_m-ethyl	-105.8	-106.2
PPN_p-ethyl	-104.6	-104.8
PPN_o-phenyl	-112.1	-122.4
PPN_m-phenyl	-105.0	-103.7
PPN_p-phenyl	-103.7	-104.4
PPN_o-NH_2	-105.4	-160.4
PPN_m-NH_2	-106.6	-107.0
PPN_p-NH_2	-106.7	-106.5
PPN_o-NO_2	-91.7	-124.4
PPN_m-NO_2	-106.1	-104.5
PPN_p-NO_2	-105.0	-103.7
NTP	-3.1	2.2
NTP_o-F	-12.7	-10.7
NTP_o-Cl	-8.7	-3.9
NTP_o-methyl	-5.9	-3.3
NTP_o-ethyl	-7.8	-3.2
NTP_o-NH_2	-6.8	-2.9

For the calculated geometry coordinates, please go to J. Phys. Chem. A 2019, 123, 7, 1372–1379. DOI: 10.1021/acs.jpca.8b09425.

PAPER 2

Enhancing NMR quantum computation by exploring heavy metal complexes as multiqubit systems: a theoretical investigation

Published article at The Journal of Physical Chemistry A

THE JOURNAL OF PHYSICAL CHEMISTRY A

pubs.acs.org/JPCA Article

Enhancing NMR Quantum Computation by Exploring Heavy Metal Complexes as Multiqubit Systems: A Theoretical Investigation

Jéssica Boreli dos Reis Lino, Stephan P. A. Sauer, and Teodorico Castro Ramalho*

Cite This: J. Phys. Chem. A 2020, 124, 4946−4955 Read Online

ACCESS | Metrics & More | Article Recommendations | Supporting Information

ABSTRACT: Assembled together with the most common qubits used in nuclear resonance magnetic (NMR) quantum computation experiments, spin-1/2 nuclei, such as ^{113}Cd, ^{199}Hg, ^{125}Te, and ^{77}Se, could leverage the prospective scalable quantum computer architectures, enabling many and heteronuclear qubits for NMR quantum information processing (QIP) implementations. A computational design strategy for prescreening recently synthesized complexes of cadmium, mercury, tellurium, selenium, and phosphorus (called MRE complexes) as suitable qubit molecules for NMR QIP is reported. Chemical shifts and spin−spin coupling constants (SSCCs) in five MRE complexes were examined using the spin−orbit zeroth order regular approximation (ZORA) at the density functional theory level and the four-component relativistic Dirac−Kohn−Sham approach. In particular, the influence of different conformers, basis sets, exchange−correlation functionals, and methods to treat the relativistic as well as solvent effects were studied. The differences in the chemical shifts and SSCCs between different low energy conformers of the studied complexes were found to be very small. The TZ2P basis set was found to be the optimum choice for the studied chemical shifts, while the TZ2P-J basis set was the best for the couplings studied in this work. The PBE0 exchange−correlation functional exhibited the best performance for the studied MRE complexes. The addition of solvent effects has not improved on the gas phase results in comparison to the experiment, with the exception of the phosphorus chemical shift. The use of MRE complexes as qubit molecules for NMR QIP could face the challenges in single qubit control and multiqubit operations. They exhibit chemical shifts appropriately dispersed, allowing qubit addressability and exceptionally large spin−spin couplings, which could reduce the time of quantum gate operations and likely preserve the coherence.

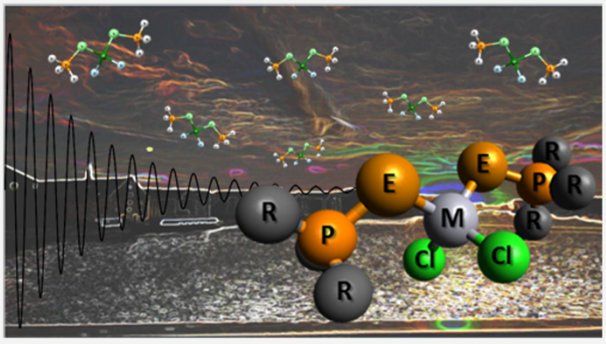

INTRODUCTION

Rapid developments in quantum information processing (QIP) have been made in laboratories around the world, both in theory and experiments. Quantum computers could one day provide breakthroughs for some of today's unsolvable problems in areas such as chemistry and artificial intelligence.[1]

Real quantum computing devices, built on a variety of physical implementations, are available nowadays for business and scientific applications. IBM Q,[2] Center for quantum photonics, quantum in the cloud,[3] and NMRCloudQ[4] are making small-sized quantum simulators or processors available to the public through the cloud. In the latter, nuclear resonance magnetic (NMR)[5−7] is used for implementing the computing tasks.[8] NMR is a powerful tool for studying QIP, indeed, it is one of the pioneer platforms with mature techniques in experimental quantum computing.[1,8−16]

Finding a suitable candidate for a quantum bit (qubit) is the major challenge for the physical implementation of QIP, as well as bringing them together in an organized, scalable, and addressable way to implement the quantum gates.[17,18] Nuclear spins (I = 1/2) in molecules are quantum systems with two well-characterized states, which therefore can act naturally as a qubit.[19] Although there is a limited number of different spin-1/2 nuclei, among which ^{1}H, ^{13}C, ^{19}F, ^{29}Si, and ^{31}P are the most common qubits used in NMR quantum computation experiments,[20,21] other spin-1/2 nuclei, such as ^{113}Cd, ^{199}Hg, ^{125}Te, and ^{77}Se, could in principle be used. Furthermore, assembled together with the most common spin-1/2 nuclei, the new complexes could leverage the prospective scalable quantum computer architectures. Once in an ensemble of identical independent molecules, which can, for most practical purposes, be treated as a single molecule in a mixed spin state,[22] it is interesting to use a heteronuclear spin system, with different nuclear species. In NMR−QIP, logic gates can be constructed based on some sort of spin−spin interaction. This makes it

Received: February 24, 2020
Revised: May 26, 2020
Published: May 28, 2020

https://dx.doi.org/10.1021/acs.jpca.0c01607
J. Phys. Chem. A 2020, 124, 4946−4955

necessary that the nuclei are distinct, such that the qubits can be separately addressed.

This work focuses, therefore, on heteronuclear systems with heavy metals as qubits for NMR−QIP. So far, the cadmium nucleus has already been suggested and studied for quantum computing and information processing.[23−25] Also, mercury telluride (HgTe) was pointed out as auspicious in constructing novel devices for QIP,[26] as well as Te crystal materials.[27] On the other hand, the nuclei ^{113}Cd, ^{199}Hg, ^{125}Te, and ^{77}Se were to the best of our knowledge not yet investigated as qubits for NMR−QIP.

A class of compounds, which could fulfill the requirements[14,28,29] for NMR−QIP (large differences in the chemical shift of the involved nuclei and large spin−spin coupling constants (SSCCs) between them), are metal complexes with phosphine chalcogenide ligands, in the following abbreviated as MRE, of the type $MCl_2(R_3PE)_2$ with M = Cd or Hg, R = *n*-Bu or (Me_2N), and E = Se or Te. They have recently attracted considerable attention because of their increasing use as suitable single-source precursors for the production of thin films ME (M = Cd or Hg; E = Se or Te) as well as quantum dots.[30] Profiting from this, there are some recently synthesized complexes[31−33] (Figure 1) that also show interesting values of

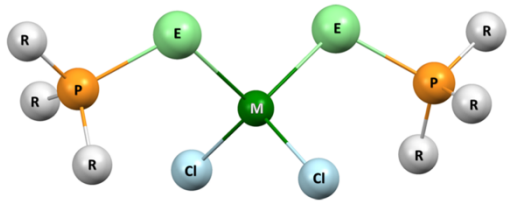

Figure 1. Metal complex with MRE of the type $MCl_2(R_3PE)_2$ (M = Cd or Hg; R = *n*-Bu or (Me_2N); E = Se or Te).

their NMR parameters which are remarkable and meet the requirements of NMR−QIP. However, to the best of our knowledge, no computational study of the NMR parameters of these complexes has so far been reported.

Previous computational studies of molecules suitable for NMR−QIP include, for example, the work of Mawhinney and Schreckenbach,[34] who have used density functional theory (DFT) and the zeroth order regular approximation (ZORA), a two-component relativistic approach, to examine the chemical shifts and SSCCs of 10 smaller organic compounds commonly used in NMR quantum computing experiments. Tamulis et al.[35] investigated Cu, Co, Zn, Mn, and Fe biliverdin derivatives as qubit molecules, whose proton chemical shift values were obtained using Hartree−Fock and DFT methods. Lino and Ramalho[9,36] studied previously phosphorus-based compounds interesting for QIP and thus calculated the NMR parameters of phosphorus heterocycles,[9] 1,8−diphosphanaphthalenes, and naphtho[1,8-cd]-1,2-dithiole phenylphosphine derivatives[36] at the DFT level.

In the present work, we will examine the NMR parameters, chemical shift, and the SSCC of cadmium, mercury, tellurium, selenium, and phosphorus in five MRE complexes using spin−orbit ZORA and four-component relativistic methods. The main objective of the present study is to develop a computational design strategy for prescreening molecules that could enable many and heteronuclear qubits for NMR−QIP implementations. In particular, the influence of different conformers, basis sets, functionals, and methods to treat the relativistic as well as solvent effects has been studied.

■ COMPUTATIONAL DETAILS

Geometry optimizations and vibrational frequency calculations of all compounds were performed with the GAUSSIAN G16 program[37] at the DFT level with the B3LYP exchange−correlation functional and the cc-pVDZ[38,39] basis set. The relativistic effects of the heavy atoms (^{77}Se, ^{125}Te, ^{113}Cd, and ^{199}Hg) on the geometries were taken care of by employing the Stuttgart−Dresden small-core relativistic effective core potentials[38,40] together with the cc-pVDZ-pp basis set[38,40] for the valence electrons, as such an approach was previously shown to reproduce geometries obtained by four-component calculations.[41] Corresponding frequency calculations confirmed that the geometries were indeed minima. Cartesian coordinates of all optimized structures in the gas phase and calculated harmonic frequencies for the discussed optimized geometries are given in the Supporting Information.

Starting from the optimized geometry (opt-1) of each MRE complex, a conformer search was carried out using the Open Babel 2.4.1[42] generic algorithm and up to 50 conformers were generated with the "minenergy" scoring function. Geometry optimizations were carried out on subsets of these conformers using the same theoretical level as outlined above.

The population of the conformers of each MRE complex was calculated from a Boltzmann distribution (25 °C) using the relative Gibbs free energies (ΔG) obtained in the frequency calculations. The calculated G includes molecular electronic, translational, rotational, and vibrational contributions.

The NMR parameters of the MRE complexes have been investigated in the gas phase at the DFT level in both nonrelativistic calculations (NR) and in the framework of the two-component relativistic zeroth-order regular approximation (ZORA),[43] including spin−orbit effects and a Gaussian finite nucleus, as implemented in the ADF (Amsterdam density functional) program.[44]

The calculations of the absolute nuclear magnetic shielding constants σ and the indirect spin−spin coupling constants (SSCC or J) were carried out with the exchange−correlation functionals, PB86, PBE, B3LYP, and PBE0, which are widely used in the prediction of NMR parameters,[45−49] together with triple-ζ (TZ2P) and quadruple-ζ (QZ4P) Slater-type basis sets. These basis sets are optimized for their use in ZORA calculations, which is an excellent approximation to the fully relativistic Dirac equation.[50] The J calculations were correspondingly performed with the TZ2P-J and QZ4P-J basis sets,[51] which are specially designed for NMR SSCC calculations. Gauge including atomic orbitals were employed in the calculation of the shieldings. The solvent effects were predicted using the conductor-like screening model (COSMO)[52] together with dichloromethane as the solvent for the HgBuTe complex, similar to the solvents used in the experimental measurements.

The NMR chemical shifts and SSCCs were also calculated at the nonrelativistic level (NR) and using the four-component Dirac−Kohn−Sham (DKS) relativistic Hamiltonian as implemented in a development version of the ReSpect[53] program package. The PBE0 exchange correlation functional together with the Dyall's relativistic all electron valence triple-ζ (dyall-vtz) basis set[54−61] was used in these four-component relativistic DFT calculations. The finite-size Gaussian-type

https://dx.doi.org/10.1021/acs.jpca.0c01607
J. Phys. Chem. A 2020, 124, 4946−4955

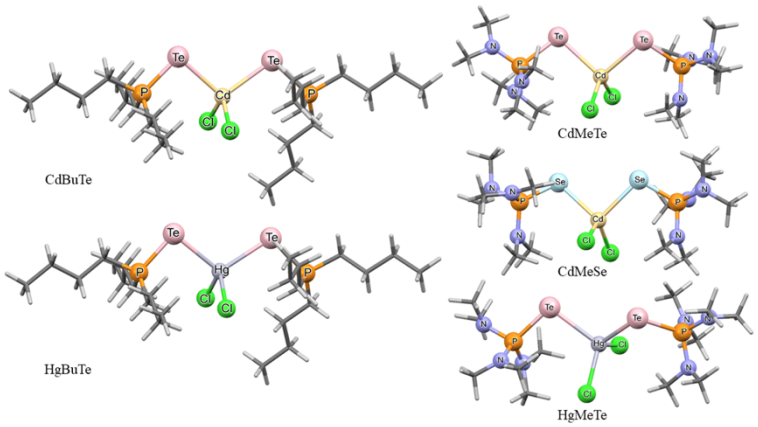

Figure 2. Studied complexes $CdCl_2[n\text{-}Bu_3PTe]_2$ (CdBuTe), $HgCl_2(n\text{-}Bu_3PTe)_2$ (HgBuTe), $CdCl_2[(Me_2N)_3PTe]_2$ (CdMeTe), $HgCl_2[(Me_2N)_3PTe]_2$ (HgMeTe), and $CdCl_2[(Me_2N)_3PSe]_2$ (CdMeSe).

Table 1. Effect of Different Conformers on the M (^{113}Cd or ^{199}Hg), E (^{77}Se or ^{125}Te), and ^{31}P Chemical Shifts, δ [ppm] and M−P and E−P SSCC, J [Hz] Calculated with the ZORA Method Using the PBE0 Exchange−Correlation Functional and the TZ2P Basis Set[a]

		δM	δE	δP	$^2J_{M-P}$	$^1J_{E-P}$
CdBuTe	opt-1	441	−659	−9.78	33.6	1299
	Boltz.[b]	444	−648	−7.05	33.6	1281
	exp.[c,f]	508	−720	−1.79	50.2	1287
CdMeTe	opt-1	439	−539	54.5	39.8	1742
	conf-1	433	−531	50.2	38.7	1722
	exp.[c,f]	484	−728	45.7	57.2	1617
CdMeSe	opt-1	440	−200	86.2	32.0	−701
	Boltz.[b]	440	−214	84.8	29.2	−698
	exp.[d,*]	385	−250	71.5	40.57	634
HgBuTe	opt-1	−1583	−508	−6.70	−113.3	1288
	Boltz.[b]	−1585	−507	−4.31	−113.2	1274
	exp.[e,f]	−1361	−478	−1.14	128.8	1262
HgMeTe	opt-1	−1554	−389	54.7	−139.3	1746
	conf-12[d]	−1554	−389	54.7	−139.2	1746
	exp.[e,f]	−1301	−480	44.8	195.6	1606

[a]For atoms in similar chemical environments, the average chemical shifts and SSCCs are reported. [b]Boltzmann average of the values in the main conformers. [c]From ref 31. [d]From ref 33. [e]From ref 32. [f]In CD_2Cl_2 at 188 K.

model was used for the nuclear charge distribution but not for the magnetic moment distribution of the nucleus. For the NR calculations in the ReSpect program, the scaling factor (cscale) for the speed of light was set to 20.0.

Vibrational corrections[62,63] to the absolute shieldings or SSCCs were not included. Although not negligible in general, their size is normally less than 10% of the total value. For some simple ^{125}Te-compounds, the vibrational corrections to the ^{125}Te chemical shifts were, for example, calculated to amount to 6%.[64] However, for molecules of the size studied here, these calculations would be exceedingly expensive. Besides, the question arises whether the usually employed second-order vibrational perturbation theory approach is sufficient for molecules with flexible side-chains as studied here.

In order to calculate the NMR chemical shifts (δ) of ^{31}P, ^{77}Se, ^{125}Te, ^{113}Cd, and ^{199}Hg, the absolute shieldings of ^{31}P in PH_3, ^{77}Se in $SeMe_2$, ^{125}Te in $TeMe_2$, ^{113}Cd in $CdMe_2$, and 199Hg in $HgMe_2$ were calculated at the same computational level. All reference molecules were also optimized at the same level aforementioned. Table S6 shows the respective absolute shieldings. The chemical shifts (δ_S in ppm) of nucleus (N) were then calculated as

$$\delta_N = \frac{\sigma_{reference} - \sigma_N}{1 - \sigma_{reference}} \times 10^6 \quad (1)$$

where for ^{31}P and ^{113}Cd the chemical shifts were afterward corrected by the gas phase experimental value of $CdMe_2$, −706.15,[65] and PH_3, −266.1.[66]

RESULTS AND DISCUSSION

The complexes studied in this work are $CdCl_2[n\text{-}Bu_3PTe]_2$,[31] $HgCl_2(n\text{-}Bu_3PTe)_2$,[32] $CdCl_2[(Me_2N)_3PTe]_2$,[31] $HgCl_2[(Me_2N)_3PTe]_2$,[32] and $CdCl_2[(Me_2N)_3PSe]_2$,[33] which will be denoted as CdBuTe, HgBuTe, CdMeTe, HgMeTe, and CdMeSe throughout the article (Figure 2).

Effect of Different Conformers. Starting from an optimized geometry of each MRE complex (opt-1), a conformer study was carried out in order to identify other conformations. With OBabel 2.4.1,[42] 50 conformers were generated using a generic search algorithm with the "minenergy" scoring function. All the conformers were then

https://dx.doi.org/10.1021/acs.jpca.0c01607
J. Phys. Chem. A 2020, 124, 4946−4955

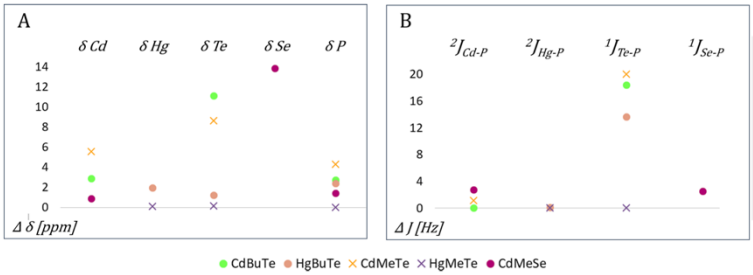

Figure 3. Changes in chemical shifts (A) and SSCCs (B) relative to the values for the preoptimized geometries opt-1. The ● symbol represents the results of the Boltzmann averaging, while the × symbol represents the values in the complexes with the biggest probability p_i.

re-optimized at the DFT level. From the Gibbs free energies relative to the conformer with the lowest Gibbs free energy, the population p_i of each conformer according to the Boltzmann distribution was calculated. Tables S1−S5 present the values of the Gibbs free energies, the change in the free Gibbs energy, ΔG, relative to the lowest energy conformer and the calculated Boltzmann population p_i at 25 °C for the MRE complex conformers.

According to the Boltzmann distribution, the CdBuTe, HgBuTe, and CdMeSe complexes have three main conformations (p_i more than 0.1), and in all three cases, the preoptimized starting geometry (opt-1) belongs to them and has even the largest population p_i. The three main conformers were: for CdBuTe, opt-1, conf-9, and conf-12; for HgBuTe, opt-1, conf-5, and conf-14, and; for CdMeSe, opt-1, conf-22, and conf-41. At the same time, the Boltzmann distributions for CdMeTe and HgMeTe showed more than three main conformers, in which, respectively, conf-1 and conf-12 have the largest p_i.

Taking into account these molecules and the calculated NMR parameter values, (calculated with the PBE0 functional and the TZ2P basis set) (Table S7) it was possible to observe an improvement of the symmetry of the MRE geometries. Table 1 shows the NMR parameters calculated in the conformer study.

The values of the NMR parameters were averaged over the Boltzmann distribution, where for each MRE complex the probability distribution has been normalized using the three main conformers. For example, for the CdBuTe complex, the normalized p_i were 50.6, 25.6, and 23.8% for opt-1, conf-12, and conf-9, respectively. Then, the averaged δ(Cd) was calculated as (opt-1 × 0.506) + (conf-12 × 0.256) + (conf-9 × 0.238). All NMR parameter values averaged over the Boltzmann distribution were obtained in the same way. For that, the normalized p_i for HgBuTe were 68.7, 20.2, and 11.1% for opt-1, conf-14, and conf-5, respectively. Likewise, for CdMeSe were 35.3, 34.7, and 29.9% for opt-1, conf-22, and conf-41, respectively.

The Cd chemical shifts change by 1−3 ppm on carrying out the Boltzmann averaging or in the case of CdMeTe, where the preoptimized structure opt-1 was not the global minimum, the change is 6 ppm, which has to be compared to the difference from the experimental values, which is between 55 and 64 ppm. For the Hg, the chemical shift changes by 2 ppm on Boltzmann averaging in HgBuTe and does not show any change in the case of HgMeTe, although the preoptimized structure was not the global minimum. The difference from the experimental values is about 224 ppm. Concerning the Te chemical shifts, the change is between 1 and 11 ppm running the Boltzmann averaging or around 0−9 ppm when the preoptimized structure is not the global minimum, differing around 30−70 ppm from the experimental value. The Se chemical shift changes by 14 ppm carrying out the Boltzmann averaging, and the difference from the experimental values is 36 ppm. For the P chemical shifts, the change is around 2−3 ppm performing the Boltzmann averaging or around 0−4 ppm in the case where the preoptimized structure is not the global minimum. The differences from the experimental values for P are about 3−13 ppm.

Turning to the SSCCs, the Cd−P SSCCs change by 0−3 Hz because of the Boltzmann averaging or in the case of CdMeTe, the change is 1 Hz, while the difference from the experimental values is between 11 and 17 Hz. The Hg−P SSCCs change by only 0.1 Hz, both on carrying out the Boltzmann averaging and in the case where the preoptimized structure was not the global minimum, while the difference from the experimental values is between 16 Hz. For the Te−P SSCCs, carrying out the Boltzmann average changes the SSCC values by 6−18 Hz, while they change by 0−20 Hz in the case where the preoptimized structure was not the global minimum; in this case, the difference from the experimental value is between 6 and 12 Hz. Finally, the Se−P SSCC changes by 3 Hz on Boltzmann averaging, and the difference from the experimental value is 64 Hz.

The changes in the calculated chemical shifts because of conformational averaging, relative to the values in opt-1, are also shown in Figure 3A. On average of the absolute values of the changes, δ changes by 2 ppm for Cd, 2 ppm for Hg, 6 ppm for Te, 14 ppm for Se, and 6 ppm for P, when all the main conformers are taken into account. By considering the complexes with the biggest Boltzmann factor, the δ calculated values change by 6 ppm for Cd, 0.1 ppm for Hg, 4 ppm for Te, and 2 ppm for P. In the same way, the changes in the SSCC values were, concerning all the main conformers, around 1 Hz for Cd−P, 0.1 Hz for Hg−P, 16 Hz for Te−P, and 3 Hz for Se−P and 1 Hz for Cd−P, 0.1 Hz for Hg−P, and 10 Hz for Te−P, given the complexes with the biggest p_i (Figure 3B).

Summarizing only these small variations in both δ and J because of Boltzmann averaging for CdBuTe, HgBuTe, and CdMeSe complexes, and in the same way, on changing to the complexes with the biggest p_i, that is, for the CdMeTe and HgMeTe complexes, there seems to be no need to perform calculations of the NMR parameters for all main MRE conformers. In the following, we will therefore only discuss the results for the originally optimized geometries, opt-1.

Effect of Basis Sets. In the second step, the effect of varying the basis set on the NMR parameters for the three smallest MRE complexes, CdMeTe, HgMeTe, and CdMeSe, in

https://dx.doi.org/10.1021/acs.jpca.0c01607
J. Phys. Chem. A 2020, 124, 4946−4955

their opt-1 geometries was investigated (Table 2). As expected,[48,67−69] the switch from TZ2P to QZ4P still brings about changes in the chemical shifts. For the heavier elements, the changes are negative: around −78 ppm for Cd, −544 ppm for Hg, close to −26 ppm for Te, and −24 ppm for Se, whereas it is with 4.5 ppm positive for P, which corresponds approximately to 18% for Cd, 35% for Hg, 12% for Se, 6% for Te, and between 5 and 8% for P. These changes are thus significantly larger than the variation in the chemical shifts for the different conformers with the exception of the chemical shifts of P, where the changes are in the same order of magnitude.

Table 2. Effect of the Basis Set on the M (^{113}Cd or ^{199}Hg), E (^{77}Se or ^{125}Te), and ^{31}P Chemical Shifts, δ [ppm], Calculated with the ZORA Method Using the PBE0 Exchange−Correlation Functional and Either the TZ2P or QZ4P Basis Set[a]

		δM	δE	δP
CdMeSe	TZ2P	440	−200	86.2
	QZ4P	365	−224	90.6
	exp.[b,e]	385	−250	71.5
CdMeTe	TZ2P	439	−539	54.5
	QZ4P	359	−567	59.1
	exp.[c,e]	484	−728	45.7
HgMeTe	TZ2P	−1554	−389	54.7
	QZ4P	−2098	−413	59.3
	exp.[d,e]	−1301	−480	44.8

[a]For atoms in similar chemical environments, the average chemical shifts are reported. [b]From ref 33. [c]From ref 31. [d]From ref 32. [e]In CD_2Cl_2 at 188 K.

Concerning the SSCCs of the three smaller complexes CdMeSe, CdMeTe, and HgMeTe (Table 3), the biggest change is observed on going from the TZ2P to the specialized coupling constant basis set TZ2P-J, on which $^2J_{Cd-P}$ is changed by about 6.0 Hz, $^2J_{Hg-P}$ by 30 Hz, $^1J_{Te-P}$ by about 300 Hz, and $^1J_{Se-P}$ by 145 Hz. Slightly smaller changes are observed on going from the TZ2P to the QZ4P basis: around 4.5 Hz for $^2J_{Cd-P}$, 26 for $^2J_{Hg-P}$, about 203 Hz for $^1J_{Te-P}$, and 109 Hz for $^1J_{Se-P}$. This implies that the QZ4P basis set must include some of the functions, which are important for the calculation of coupling constants and which were missing in the TZ2P basis set. When moving them from the QZ4P to the corresponding coupling constant basis set QZ4P-J, the further changes are only small with 1.7 Hz for $^2J_{Cd-P}$, 5.5 for $^2J_{Hg-P}$, about 77 Hz for $^1J_{Te-P}$, and 44 Hz for $^1J_{Se-P}$. Similarly, the differences between TZ2P-J and QZ4P-J are even smaller: around 0.1 Hz for $^2J_{Cd-P}$, 1.6 for $^2J_{Hg-P}$, −20 Hz for $^1J_{Te-P}$ and 8.9 Hz for $^1J_{Se-P}$.

For the two larger complexes CdBuTe and HgBuTe, the effect of changing from the TZ2P basis set to the specialized coupling constant basis set TZ2P-J was also evaluated. Similar large changes for the smaller complexes are observed again: 5.8 Hz for $^2J_{Cd-P}$, −24 Hz for $^2J_{Hg-P}$, and 225 Hz for $^1J_{Te-P}$.

Summarizing, one can say that the TZ2P-J basis set appears to be the optimal choice for the couplings studied in this work.

Comparing again to the differences in the coupling constants of different conformers, one observes that the latter are either similar in size to the changes on going from the TZ2P-J to the QZ4P-J basis set or even smaller than those. This shows that also for the coupling constants, the proper choice of the basis set is more important than investigating several conformers. In light of this, the starting geometry, that is, the geometry gathered by the first optimization of each MRE complex (opt-1), can be considered suitable for further theoretical studies.

Table 3. Effect of the Basis Set on the M−P (M = ^{113}Cd or ^{199}Hg) and E−P (E = ^{77}Se or ^{125}Te) SSCC, J [Hz] Calculated with the ZORA Method Using the PBE0 Exchange−Correlation Functional and the TZ2P, QZ4P, TZ2P-J, and QZ4P-J Basis Sets[a]

		$^2J_{M-P}$	$^1J_{E-P}$
CdMeSe	TZ2P	32.0	−701
	TZ2P-J	37.3	−845
	QZ4P	35.2	−810
	QZ4P-J	37.0	−854
	exp.[b,e]	40.57	634
CdMeTe	TZ2P	39.8	1742
	TZ2P-J	46.6	2041
	QZ4P	45.5	1945
	QZ4P-J	47.1	2021
	exp.[c,e]	57.2	1617
HgMeTe	TZ2P	−139.3	1746
	TZ2P-J	−168.8	2045
	QZ4P	−165.0	1948
	QZ4P-J	−170.4	2025
	exp.[d,e]	195.6	1606
CdBuTe	TZ2P	33.6	1299
	TZ2P-J	39.4	1525
	exp.[c,e]	50.2	1287
HgBuTe	TZ2P	−113.3	1288
	TZ2P-J	−137.2	1512
	exp.[d,e]	−128.8	1262

[a]For atoms in similar chemical environments, the average SSCCs are reported. [b]From ref 33. [c]From ref 31. [d]From ref 32. [e]In CD_2Cl_2 at 188 K.

Comparing the results with the different basis sets for the chemical shifts with the experimental data (Tables 2 and 3), there appears no systematic trend on going from the TZ2P to the QZ4P basis set. In general, the use of the TZ2P basis set in combination with the PBE0 exchange−correlation functional gives chemical shifts closer to the experimental values for Hg and P, whereas QZ4P gives closer values for Te and Se. Concerning the Cd chemical shifts, the TZ2P basis set leads to a closer value in the HgMeTe complex while QZ4P gives a closer value in the CdMeSe complex.

Regarding the SSCC results, the smallest basis set, TZ2P, in combination with the PBE0 exchange−correlation functional predicts more accurately the $^1J_{E-P}$ (E = Te or Se) couplings, while the larger basis sets and, in particular, the specialized coupling constant basis sets TZ2P-J and QZ4P-J give results in much better agreement with the experiment for the $^2J_{M-P}$ (M = Cd or Hg) coupling constants.

The conclusion from the basis set study is, thus, that the results, which are more converged with respect to the basis set, are not necessarily in better agreement with experimental values, but rather show the true performance of the given exchange−correlation functional.

Effect of Different Exchange−Correlation Functionals. Up to this point, the NMR parameters were evaluated only using the hybrid exchange−correlation functional PBE0 with 25% Hartree−Fock exchange. In this section, we investigate now for the HgBuTe complex how much the chemical shifts

https://dx.doi.org/10.1021/acs.jpca.0c01607
J. Phys. Chem. A 2020, 124, 4946−4955

and coupling constants change on varying the functional. The results obtained with two general gradient approximation (GGA) functionals, BP86 and PBE, and the popular hybrid functional B3LYP with 20% Hartree−Fock exchange will be compared with the PBE0 results and experimental values. The opt-1 geometry of the HgBuTe complex is used in these DFT calculations, which are performed using the TZ2P basis set for the chemical shifts and TZ2P-J for the SSCCs (Table 4).

Table 4. Effect of Different Exchange−Correlation Functionals on the ^{199}Hg, ^{125}Te, and ^{31}P Chemical Shifts, δ [ppm] and M−P and E−P SSCC, J [Hz] in HgBuTe Calculated with the ZORA Method Using the TZ2P Basis Set for Chemical Shifts and TZ2P-J for SSCCs[a]

	δHg	δTe	δP	$^2J_{Hg-P}$	$^1J_{Te-P}$
PBE0	−1583	−508	−6.7	−135.0	1192
B3LYP	−1803	−485	−2.3	−200.3	1770
PBE	−1711	−465	13	−95.8	1300
BP86	−1796	−418	10	−98.8	1310
exp.[b]	−1361	−478	−1.14	−128.8	1262

[a]For atoms in similar chemical environments, the average chemical shifts and SSCCs are reported. [b]From ref 31 in CD_2Cl_2 at 188 K.

Naturally, the use of different functionals leads to different chemical shift values. The biggest variation is observed for the heavier elements, which was also expected because of the magnitude of their chemical shifts. The spread of results is 221 ppm for Hg and 90 ppm for Te, which is about 16% for Hg and 19% for Te of the experimental value. The smallest variation occurs for the P nucleus, 19 ppm; however, this is about 17 times its experimental value, −1.14 ppm. Furthermore, the two GGA functionals predict even the wrong sign for the P chemical shift. For Hg, B3LYP yields the most negative chemical shift value, while PBE0 gives the least negative value and also the most accurate result. On the other hand, for Te and P, PBE0 presents the most negative chemical shift value, while the B3LYP result is in best agreement with the experiment. The BP86 and PBE GGA functionals lead to the largest chemical shift values for Te and P, respectively. All the four functionals underestimate the Hg experimental chemical shift value. For Te and P, the hybrids PBE0 and B3LYP also underestimate the experimental data, while the GGAs PBE and BP86 overestimate them.

Calculated with the specialized coupling constant basis set TZ2P-J, sizable differences are observed for the coupling constants. The calculated geminal Hg−P SSCC varies by 104.6 Hz using the different functionals, which represents about 81% of the experimental data. B3LYP presents the largest deviation from the experiment while PBE0 gives the closest result. Both functionals overestimate the experimental value. Meanwhile, the two GGA functionals have almost the same performance, underestimating the experimental result. Regarding the effect of varying the functional on the Te−P SSCC calculation, the values change by 578 Hz, which represents about 46% of the experimental result. Interestingly, PBE presents the most accurate result, although it overestimates it by 38 Hz. BP86 and B3LYP also overestimate the experimental data, and the latter yields the poorest result. Finally, the hybrid PBE0 underestimates the SSCC value by 70 Hz, which is only 5.5% of the experimental value.

In general, the hybrid functional PBE0 gives the most accurate results for the Hg chemical shift and Hg−P SSCC and performs reasonably for the other parameters. For the Te chemical shift and the Te−P SSCC, PBE0 differs by 6% from the experimental value, while for the P chemical shift the same functional deviates by 6 ppm from it. We can thus conclude that from the four investigated functionals PBE0 exhibits the overall best performance, and we will continue using this functional in the following.

Solvent Effect. Previous studies showed that solvent effects can play an important role for the accurate prediction of SSCCs.[70−73] The solvent effects were investigated for the HgBuTe complex using the COSMO[52] with dichloromethane as a solvent, similar to the solvents used in the experimental measurements. The results for the solvent calculation are shown in Table 5. In general, the addition of the solvent effects

Table 5. Effect of the Solvent on the ^{199}Hg, ^{125}Te, and ^{31}P Chemical Shifts, δ [ppm], M−P, and E−P SSCC, J [Hz] in HgBuTe Calculated with the ZORA Method Using the PBE0 Functional and the TZ2P Basis Set for Chemical Shifts and TZ2P-J for SSCCs[a]

	gas phase	solvent[b]	Δsolv.	exp.[c]
δHg	−1583	−1598	−15	−1361
δTe	−508	−452	56	−478
δP	−6.7	−1.6	5.1	−1.14
$^2J_{Hg-P}$	−135.0	−163.3	−28.3	128.8
$^1J_{Te-P}$	1192	1400	208	1262

[a]Δsolv. is the solvent effect correction. For atoms in similar chemical environments, the average chemical shifts and SSCCs are reported. [b]Using COSMO of solvation. Dichloroethane, Eps = 10.66 and Rad = 3.15. [c]From ref 31 in CD_2Cl_2 at 188 K.

using the COSMO model in ZORA/PBE0 calculations does not improve the agreement with the experiment compared to the gas phase results, with the exception of the phosphorus chemical shift.

Again, the biggest change is observed for the heavier elements. For the Hg chemical shift, the solvent effect correction is 15 ppm, which is only 1% of the experimental value, but the correction brings the PBE0 result further away from the experimental value. The solvent effect correction is 56 ppm for the Te chemical shift, which is about twice the difference between the gas phase result and experimental value, meaning that the gas phase and solvent results sandwich the experimental value with almost equal deviations. Only in the case of the P chemical shift, the solvent effect correction, although only 5.1 ppm, leads to a real improvement in the theoretical result. The δP result obtained from the gas phase calculation is −6.7 ppm, whereas the solvent result is −1.6 ppm, which is to be compared with an experimental value of −1.14 ppm. The conclusions are similar to the coupling constants. For the Hg−P SSCC, the solvent effect correction is 28.3 Hz but again adding it makes the agreement with the experiment worse, so that the solvent result now differs by about 27% from the experimental value. For the Te−P SSCC, the solvent effect correction is larger, 208 Hz, but like for δP adding the solvent corrections overshoots the experimental value such that the solvent result is in worse agreement than the gas phase result.

Relativistic Effects: ZORA Versus 4-Component Calculations. Finally, in this section, we compare the performance of spin−orbit ZORA and four-component relativistic methods in the theoretical calculation of NMR

https://dx.doi.org/10.1021/acs.jpca.0c01607
J. Phys. Chem. A 2020, 124, 4946−4955

parameters of HgBuTe. This complex contains Hg, the nucleus which is expected to present the most pronounced relativistic effects. Because of the size of the HgBuTe complex, it was necessary to reduce its size in the four-component calculations by replacing the *n*-butyl groups by methyl groups starting from its opt-1 geometry. Figure 4 shows the used structure, which is called HgBuTe-4c.

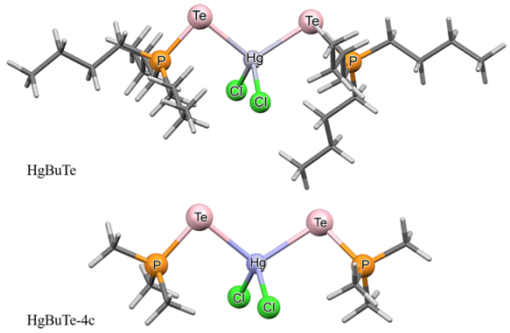

Figure 4. HgBuTe complex and the reduced structure for the 4-component calculations.

The ZORA and the nonrelativistic (NR) calculations with the ADF program are performed using the PBE0 exchange–correlation functional with the TZ2P basis set for chemical shifts and TZ2P-J for SSCCs. For the 4-component calculations and the corresponding nonrelativistic calculations with the ReSpect program, the PBE0 functional is again used together with the dyall-vtz basis set for chemical shifts and SSCCs.

From the two-component ZORA/TZ2P results in Table 6, it becomes clear that replacing the *n*-butyl groups by methyl groups affects the chemical shifts more than the SSCCs. Again, the effect is more pronounced on the heavier elements, which is also expected because of the magnitude of their chemical shifts. The Hg chemical shift changes by −490 ppm and the Te chemical shift by −278 ppm. The effect on the P nucleus is less pronounced, 44 ppm. Reducing the length of the alkyl substituents changes the value of the calculated Te–P SSCC by 65 Hz. For the Hg–P SSCC, the change is less expressive, only about 12 Hz. Both were calculated with the specialized coupling constant basis set ZORA/TZ2P-J. These changes are obviously too large for replacing HgBuTe by HgBuTe-4c in general in our study, but for studying the performance of different relativistic methods HgBuTe-4c will be a sufficient model.

For HgBuTe, the relativistic corrections to chemical shifts are 1258 ppm for mercury, 240 ppm for tellurium, and 70 ppm for phosphorus, at the ZORA/TZ2P level. These relativistic corrections correspond to 92% of the experimental data for Hg chemical and 50% for Te chemical shift and are thus very significant. For the P chemical shift, the NR/TZ2P calculation even predicts the wrong sign and gives the result with the largest percentage error, about 53 times the experimental data. This is probably due to the HALA effect (heavy atom effect on the shielding of a light atom) from the neighboring Te and Hg atoms, which is in a good agreement with the conclusion made by Krivdin[45] that HALA relativistic corrections to ^{31}P chemical shifts are strongly dependent on the substituents at phosphorus. For the SSCCs in HgBuTe, the relativistic corrections are 105 Hz from Hg–P and 149 for Te–P, also at the ZORA/TZ2P level. The former relativistic correction is with 81% of the experimental value again very large, while the latter is about 12% of the experimental value.

In the following, we investigate the relativistic corrections for the HgBuTe-4c complex and how much the chemical shifts and coupling constants change on varying from the two-component ZORA to four-component DKS approach. For the Hg chemical shift, the relativistic corrections are 951 ppm in the ZORA/TZ2P and 1512 ppm in the DKS/dyall-vtz calculation. The ZORA approach reproduces thus 63% of the relativistic corrections of the four-component DKS approach for Hg. The ZORA/TZ2P relativistic correction for the Te chemical shift is 212 ppm while DKS/dyall-vtz is 184 ppm. This means a change of results of 28 ppm, upon going from ZORA/TZ2P to DKS/dyall-vtz. The difference between the relativistic corrections at the two levels for the P chemical shift is significantly smaller, 102 ppm for ZORA/TZ2P and 107 ppm for DKS/dyall-vtz, which corresponds to a difference in relativistic corrections of 5 ppm.

Using the specialized coupling constant basis set ZORA–TZ2P–JCPL, the relativistic corrections in SSCCs are 96 Hz for Hg–P and 125 Hz for Te–P, while with the four-component DKS approach, the relativistic corrections are 120 Hz and 218 Hz for Hg–P and Te–P SSCCs, respectively. The ZORA/TZ2P level reproduces thus 80% of the DKS/dyall-vtz relativistic corrections for Hg–P SSCC and 57% for Te–P SSCC.

Suitable Qubit Molecules. Most conventional NMR studies are conducted on the spin $I = 1/2$ nuclei, which also provide a natural method of implementing QIP. In conjunction with the most commonly used qubits, ^{1}H, ^{13}C, ^{19}F, ^{29}Si, and ^{31}P, the use of heavy metal complexes can hold the

Table 6. ^{199}Hg, ^{125}Te, and ^{31}P Chemical Shifts, δ [ppm] and Hg–P and Te–P SSCC, J [Hz] Calculated Using Nonrelativistic, Two-Component ZORA and Four-Component DKS Approach[a]

		δHg	δTe	δP	$^{2}J_{Hg-P}$	$^{1}J_{Te-P}$
HgBuTe	NR/TZ2P	−324.2	−748	63.7	−32.4	1363
	ZORA/TZ2P	−1583	−508	−6.70	−137.2	1512
	exp.[b]	−1361	−478	−1.14	128.8	1262
HgBuTe-4c	NR/TZ2P	−141	−442	51.3	−28.5	1452
	ZORA/TZ2P	−1093	−230	−50.9	−124.9	1577
	NR/dyall-vtz	−84	−428	48.3	−39.4	1586
	DKS/dyall-vtz	−1596	−244	−58.7	−159.8	1804

[a]All calculations were carried out with the PBE0 exchange–correlation functional and the shown basis sets, where in the case of the ZORA SSCC calculations, the respective ZORA–JCPL basis sets were employed. For atoms in similar chemical environments, the average chemical shifts and SSCCs are reported. [b]From ref 31 in CD_2Cl_2 at 188 K.

https://dx.doi.org/10.1021/acs.jpca.0c01607
J. Phys. Chem. A 2020, 124, 4946–4955

forthcoming scalable heteronuclear spin system in NMR quantum computation experiments.

In NMR QIP, irradiating the nuclei with resonant radio frequency (RF) pulses allows to manipulate the nuclei, giving rise to generic single-qubit gates.[19,22] In a heteronuclear spin system, in which the nuclei have distinct nuclear g-factors, the qubits can easily be individually addressed through RF pulses.[74] In larger heteronuclear spin systems, as every spin will be a long way from resonance with every other spin,[22] simple hard pulses applied on resonance can be used.[75] Enabling the logic gate implementations in a qubit-selective manner, so that only a single-qubit is affected by the RF field.[22]

Table 7 shows the differences in the Larmor frequencies for the coupled nuclei. As expected, the use of different nuclear species provides a huge dispersion in the Larmor frequencies of the involved nuclei. The Te−P pair presents the smallest difference $\Delta\nu$ (Te−P), 38 MHz, while the Hg−P pair shows the highest, 96 MHz, only slightly larger than for Se−P in CdMeSe, 91 MHz. The Cd−P pair has also a considerable difference in the Larmor frequencies, 78 MHz.

Table 7. Differences in the Larmor Frequencies (for a 10 T Magnet) between the M (^{113}Cd or ^{199}Hg) Nucleus and ^{31}P or between the E (^{77}Se or ^{125}Te) Nucleus and ^{31}P, $\Delta\nu$ [MHz] and M−P (M = ^{113}Cd or ^{199}Hg), and E−P (E = ^{77}Se or ^{125}Te) SSCC, J [Hz] Calculated Using the Two-Component ZORA[a]

	$\Delta\nu$ (M−P)	$^{2}J_{M-P}$	$\Delta\nu$ (E−P)	$^{1}J_{E-P}$
CdBuTe	78.0	39.4	37.6	1525
CdMeTe	78.0	46.6	37.6	2041
CdMeSe	78.0	37.3	91.1	−845
HgBuTe	96.2	−137	37.5	1512
HgMeTe	96.2	−169	37.5	2045

[a]All calculations were carried out with the PBE0 exchange−correlation functional and the TZ2P basis set, where in the case of the ZORA SSCC calculations ZORA−JCPL basis set was employed. For atoms in similar chemical environments, the average chemical shifts and SSCCs are reported.

As the number of qubits increases the qubit addressability becomes difficult because the chemical shift differences become smaller, thereby hampering selective operations of qubits.[22] In this way, exploring the ^{113}Cd, ^{199}Hg, ^{125}Te, and ^{77}Se complexes is a starting point for the construction of more complex heteronuclear systems, which can beat some of the challenges for large-scale NMR QIP.

Another complexity, which arises in larger spin systems, is that the quantum register becomes difficult once the spin−spin coupling differences become smaller. Two-qubit interactions arise from indirect couplings.[19] In this way, spin−spin couplings in a molecule are essential for NMR QIP implementations, they promote interactions among the individual qubits that are required for a quantum register consisting of an ensemble of qubits.[19,25,76,77]

Table 7 shows the SSCCs for the studied MRE complexes. The Cd−P SSCCs have the lowest magnitude, around 41 Hz for the Cd complexes, while Hg−P SSCCs exhibits an appreciable value, about 144 Hz for the Hg complexes. Te−P SSCCs have exceptionally large values, the smallest is 1512 Hz for HgBuTe and the biggest 2045 Hz for HgMeTe. Se−P SSCC also presents a notable value, 845 Hz.

Again, exploring the remarkably large SSCCs of the MRE complexes studied in this work (Table 7) can afford an efficient manner to control two-qubit operations. Additionally, a large SSCC could be useful to overcome potential sources of quantum information loss, suggesting the use of relatively short-pulse sequences. Moreover, under these circumstances, coherence could likely be preserved.[9]

As said above, the MRE complexes are multiple−spin systems which can enable many qubits NMR QIP implementations, presenting a well-defined qubit which can be easily distinguished through their Larmor frequencies which are appropriately dispersed, allowing qubit addressability and the exceptionally large spin−spin coupling between the pair of spins, enabling the two-qubit operations. For two-qubit operations, this stronger coupling between spins reduces the time of quantum gate operations.[9]

At this point, it is worth mentioning that despite the partially low natural abundance of the ^{113}Cd (12.3% natural abundance), ^{199}Hg (16.84% natural abundance), ^{125}Te (7.07% natural abundance), and ^{77}Se (7.6% natural abundance) nuclei the samples could easily be isotopically enriched; moreover their resonances are readily accessible with modern NMR instrumentation.[31,33,78]

For a practical quantum computer, the qubits must have long relaxation times to prevent quantum effects from decohering away. NMR systems have fairly long relaxation times, currently used sample preparations for liquid state NMR quantum computers result in nuclear spin relaxation times of up to several seconds.[15]

The longitudinal relaxation of ^{77}Se and ^{125}Te at high fields is governed by the spin−rotation mechanism with typical T_1 values in the range of 1−30 s.[79] For ^{199}Hg spin−lattice relaxation times, the chemical-shielding anisotropy mechanism was shown to be important at high fields.[80] Up to 10 s were found for spin−lattice relaxation times of the ^{199}Hg nucleus.[81] Finally, a ^{113}Cd T_1 relaxation time for Cd in complexes of 4.8 s was found.[82] These times might be sufficient considering the minimum time required for a given single-spin quantum gate, once in heteronuclear spin systems, for example, typical single-spin gate durations are of the order of 10^{-5} s.[83] Hence, these nucleus times are feasible based on current liquid state NMR technology.

Given this scenario, the use of MRE complexes as qubit molecules for NMR QIP could face the challenges on single qubit control and multiqubit operations, broadening the forthcoming scalable quantum computer.

■ ASSOCIATED CONTENT

Supporting Information

The Supporting Information is available free of charge at https://pubs.acs.org/doi/10.1021/acs.jpca.0c01607.

Cartesian coordinates, calculated harmonic frequencies, Gibbs free energies, relative Gibbs free energies, calculated Boltzmann distribution, absolute shieldings, and calculated NMR parameter values of the MRE complexes (PDF)

■ AUTHOR INFORMATION

Corresponding Author

Teodorico Castro Ramalho − *Department of Chemistry, Federal University of Lavras, 37200-000 Lavras, Minas Gerais, Brazil; Center for Basic and Applied Research, Faculty of*

https://dx.doi.org/10.1021/acs.jpca.0c01607
J. Phys. Chem. A 2020, 124, 4946−4955

Informatics and Management, University Hradec Kralove, 50003 Hradec Kralove, Czech Republic; orcid.org/0000-0002-7324-1353; Phone: +55 35 3829-1522; Email: teodorico.ramalho@gmail.com; Fax: +55 35 3829-1271

Authors

Jéssica Boreli dos Reis Lino − *Department of Chemistry, Federal University of Lavras, 37200-000 Lavras, Minas Gerais, Brazil;* orcid.org/0000-0002-2141-3440

Stephan P. A. Sauer − *Department of Chemistry, University of Copenhagen, DK-2100 Copenhagen, Denmark;* orcid.org/0000-0003-4812-0522

Complete contact information is available at: https://pubs.acs.org/10.1021/acs.jpca.0c01607

Notes

The authors declare no competing financial interest.

■ ACKNOWLEDGMENTS

The authors thank the Brazilian financial agency Coordenação de Aperfeiçoamento de Pessoal de Nível Superior/Ministério da Defesa (CAPES/MD) for financial support, the Federal University of Lavras (UFLA) for providing work space, and SPAS thanks the Danish Center for Scientific Computing (DCSC) for financial support and the Department of Chemistry, University of Copenhagen for access to its high-performance computer cluster.

■ REFERENCES

(1) Xin, T.; Wang, B.-X.; Li, K.-R.; Kong, X.-Y.; Wei, S.-J.; Wang, T.; Ruan, D.; Long, G.-L. *Chin. Phys. B* **2018**, *27*, 020308.
(2) http://research.ibm.com/ibm-q (accessed March 9, 2019).
(3) https://cnotmz.appspot.com/doc (accessed March 9, 2019).
(4) http://nmrcloudq.com/zh-hans (accessed March 9, 2019).
(5) Ramalho, T. C.; Taft, C. A. *J. Chem. Phys.* **2005**, *123*, 054319.
(6) Ramalho, T. C.; Rocha, M. V. J.; da Cunha, E. F. F.; Oliveira, L. C. A.; Carvalho, K. T. G. *J. Biomol. Struct. Dyn.* **2010**, *28*, 227−238.
(7) Gonçalves, M. A.; Santos, L. S.; Peixoto, F. C.; Ramalho, T. C. *Int. J. Quantum Chem.* **2019**, *119*, No. e25896.
(8) Xin, T.; Huang, S.; Lu, S.; Li, K.; Luo, Z.; Yin, Z.; Li, J.; Lu, D.; Long, G.; Zeng, B. *Sci. Bull.* **2018**, *63*, 17−23.
(9) Lino, J. B. d. R.; Ramalho, T. C. *Rev. Virtual Quim.* **2018**, *10*, 940−962.
(10) Cory, D. G.; Price, M. D.; Havel, T. F. *Phys. D* **1998**, *120*, 82−101 , Proceedings of the Fourth Workshop on Physics and Consumption.
(11) Jones. *Fortschr. Phys.* **2000**, *42*, 909−924.
(12) Gershenfeld, N. A.; Chuang, I. L. *Science* **1997**, *275*, 350−356.
(13) Warren, W. S. *Science* **1997**, *277*, 1688−1690.
(14) Cory, D. G.; Laflamme, R.; Knill, E.; Viola, L.; Havel, T. F.; Boulant, N.; Boutis, G.; Fortunato, E.; Lloyd, S.; Martinez, R.; et al. *Fortschr. Phys.* **2000**, *48*, 875−907.
(15) Jones, A. *J. Phys. Chem. Comm.* **2001**, *4*, 49−56.
(16) Abe, E.; Itoh, K. M.; Ladd, T. D.; Goldman, J. R.; Yamaguchi, F.; Yamamoto, Y. *J. Supercond.* **2003**, *16*, 175−178.
(17) Ferrando-Soria, J.; Pineda, E. M.; Chiesa, A.; Fernandez, A.; Magee, S. A.; Carretta, S.; Santini, P.; Vitorica-Yrezabal, I. J.; Tuna, F.; Timco, G. A.; et al. *Nat. Commun.* **2016**, *7*, 1−10.
(18) Lino, J. B. R.; Rocha, E. P.; Ramalho, T. C. *J. Chem. Phys. A* **2017**, *121*, 4486−4495.
(19) Ladd, T. D.; Jelezko, F.; Laflamme, R.; Nakamura, Y.; Monroe, C.; O'Brien, J. L. *Nature* **2010**, *464*, 45−53.
(20) Lu, D.; Brodutch, A.; Park, J.; Katiyar, H.; Jochym-O'Connor, T.; Laflamme, R. In *Electron Spin Resonance (ESR) Based Quantum Computing*; Takui, T., Berliner, L., Hanson, G., Eds.; Springer New York: New York, NY, 2016; pp 193−226.
(21) Vind, F. A.; Foerster, A.; Oliveira, I. S.; Sarthour, R. S.; Soares-Pinto, D. O.; Souza, A. M.; Roditi, I. *Sci. Rep.* **2016**, *6*, 1−8.
(22) Jones, J. A. *Prog. Nucl. Magn. Reson. Spectrosc.* **2011**, *59*, 91−120.
(23) Leibrandt, D. R.; Labaziewicz, J.; Clark, R. J.; Chuang, I. L.; Epstein, R. J.; Ospelkaus, C.; Wesenberg, J. H.; Bollinger, J. J.; Leibfried, D.; Wineland, D. J.; et al. *Quant. Inf. Comput.* **2009**, *9*, 901−919.
(24) Tanaka, U.; Urabe, S.; Watanabe, M. *Appl. Phys. B: Lasers Opt.* **2004**, *78*, 43−47.
(25) Blinov, B. B.; Deslauriers, L.; Lee, P.; Madsen, M. J.; Miller, R.; Monroe, C. *Phys. Rev. A: At., Mol., Opt. Phys.* **2002**, *65*, 040304.
(26) Roth, A.; Brüne, C.; Buhmann, H.; Molenkamp, L. W.; Maciejko, J.; Qi, X.-L.; Zhang, S.-C. *Science* **2009**, *325*, 294−297.
(27) Bouleghlimat, O.; Hocini, A. *Phys. Scr.* **2014**, *89*, 105502.
(28) Glaser, S. J. *Angew. Chem., Int. Ed.* **2001**, *40*, 147−149.
(29) Mádi, Z. L.; Brüschweiler, R.; Ernst, R. R. *J. Chem. Phys.* **1998**, *109*, 10603−10611.
(30) Nordheider, A.; Woollins, J. D.; Chivers, T. *Chem. Rev.* **2015**, *115*, 310378−310406.
(31) Mallek, R.; Sanhoury, M. A. K.; Ben Dhia, M. T.; Khaddar. *J. Coord. Chem.* **2014**, *67*, 1541−1549.
(32) Mallek, R.; Sanhoury, M. A. K.; Bahri, L.; Khaddar, M. R.; Ben Dhia. *J. Coord. Chem.* **2016**, *69*, 726−734.
(33) Dhia, M. T. B.; Sanhoury, M. A. M. K.; Zenati, C.; Khaddar, M. R. *Phosphorus, Sulfur, Silicon Relat. Elem.* **2009**, *184*, 3082−3089.
(34) Mawhinney, R. C.; Schreckenbach, G. *Magn. Reson. Chem.* **2004**, *42*, S88−S98.
(35) Tamulis, A.; Tamulis, V.; Ziriakoviene, A. *Solid State Phenom.* **2004**, *97*−*98*, 173−180.
(36) Lino, J. B. d. R.; Ramalho, T. C. *J. Phys. Chem. A* **2019**, *123*, 1372−1379.
(37) Frisch, M. J.; Trucks, G. W.; Schlegel, H. B.; Scuseria, G. E.; Robb, M. A.; Cheeseman, J. R.; Scalmani, G.; Barone, V.; Petersson, G. A.; Nakatsuji, H. et al. *Gaussian 16*, Revision B.01; Gaussian Inc: Wallingford CT, 2016.
(38) Peterson, K. A.; Figgen, D.; Goll, E.; Stoll, H.; Dolg, M. *J. Chem. Phys.* **2003**, *119*, 11113−11123.
(39) Peterson, K. A.; Puzzarini, C. *Theor. Chem. Acc.* **2005**, *114*, 283−296.
(40) Figgen, D.; Rauhut, G.; Dolg, M.; Stoll, H. Relativistic Effects in Heavy-Element Chemistry and Physics. In Memoriam Bernd A. Hess (1954−2004). *Chem. Phys.* **2005**, *311*, 227−244.
(41) Dohn, A. O.; Møller, K. B.; Sauer, S. P. A. *Curr. Inorg. Chem.* **2013**, *3*, 213−219.
(42) O'Boyle, N. M.; Banck, M.; James, C. A.; Morley, C.; Vandermeersch, T.; Hutchison, G. R. *J. Cheminf.* **2011**, *3*, 33.
(43) Lenthe, E. v.; Baerends, E. J.; Snijders, J. G. *J. Chem. Phys.* **1993**, *99*, 4597−4610.
(44) Baerends, E. J.; Ziegler, T.; Atkins, A. J.; Autschbach, J.; Bashford, D.; Baseggio, O.; Bérces, A.; Bickelhaupt, F. M.; Bo, C.; Boerritger, P. M. et al. *ADF2017, SCM, Theoretical Chemistry*; Vrije Universiteit: Amsterdam, The Netherlands, 2017. https://www.scm.com.
(45) Rusakov, Y. Y.; Rusakova, I. L.; Krivdin, L. B. *Magn. Reson. Chem.* **2018**, *56*, 1061−1073.
(46) Rusakova, I. L.; Krivdin, L. B. *Mendeleev Commun.* **2018**, *28*, 1−13.
(47) Casella, G.; Ferrante, F.; Saielli, G. *Polyhedron* **2016**, *117*, 48−56.
(48) Arcisauskaite, V.; Melo, J. I.; Hemmingsen, L.; Sauer, S. P. A. *J. Chem. Phys.* **2011**, *135*, 044306.
(49) Pagola, G. I.; Larsen, M. A. B.; Ferraro, M.; Sauer, S. P. A. *J. Comput. Chem.* **2018**, *39*, 2589−2600.
(50) Van Lenthe, E.; Baerends, E. J. *J. Comput. Chem.* **2003**, *24*, 1142−1156.
(51) Bryce, D. L.; Autschbach, J. *Can. J. Chem.* **2009**, *87*, 927−941.

(52) Pye, C. C.; Ziegler, T.; van Lenthe, E.; Louwen, J. N. *Can. J. Chem.* **2009**, *87*, 790−797.
(53) Repisky, M.; Komorovsky, S.; Malkin, V. G.; Malkina, O. L.; Kaupp, M.; Ruud, K. *ReSpect 5.1.0, relativistic spectroscopy DFT program*, with contributions from Bast, R., Di Remigio, R., Ekstrom, U., Kadek, M., Knecht, S., Konecny, L., Malkin, E., Malkin−Ondik, I., 2019: (see http://www.respectprogram.org).
(54) Dyall, K. G. *Theor. Chem. Acc.* **2002**, *108*, 335−340.
(55) Dyall, K. G. *Theor. Chem. Acc.* **2004**, *112*, 403−409.
(56) Dyall, K. G. *Theor. Chem. Acc.* **2006**, *115*, 441−447.
(57) Dyall, K. G. *Theor. Chem. Acc.* **2007**, *117*, 483−489.
(58) Dyall, K. G. *Theor. Chem. Acc.* **2007**, *117*, 491−500.
(59) Dyall, K. G. *J. Phys. Chem. A* **2009**, *113*, 12638−12644.
(60) Dyall, K. G. *Theor. Chem. Acc.* **2011**, *129*, 603−613.
(61) Dyall, K. G. *Theor. Chem. Acc.* **2016**, *135*, 128.
(62) Ruden, T. A.; Ruud, K. In *Calculation of NMR and EPR Parameters: Theory and Applications*; Kaupp, M., Malkin, V. G., Bühl, M., Eds.; Wiley-VCH, Weinheim, 2004; Chapter 10, pp 153−173.
(63) Faber, R.; Kaminsky, J.; Sauer, S. P. A. In *Gas Phase NMR*; Jackowski, K., Jaszunski, M., Eds.; Royal Society of Chemistry: London, 2016; Chapter 7, pp 219−268.
(64) Rusakova, I. L.; Rusakov, Y. Y.; Krivdin, L. B. *J. Phys. Chem. A* **2017**, *121*, 4793−4803.
(65) Cardin, A. D.; Ellis, P. D.; Odom, J. D.; Howard, J. W. *J. Am. Chem. Soc.* **1975**, *97*, 1672−1679.
(66) Pecul, M.; Urbańczyk, M.; Wodyński, A.; Jaszuński, M. *Magn. Reson. Chem.* **2011**, *49*, 399−404.
(67) Jankowska, M.; Kupka, T.; Stobiński, L.; Faber, R.; Lacerda, E. G., Jr.; Sauer, S. P. A. *J. Comput. Chem.* **2016**, *37*, 395−403.
(68) Haase, P. A. B.; Repisky, M.; Komorovsky, S.; Bendix, J.; Sauer, S. P. A. *Chem.—Eur. J.* **2018**, *24*, 5124−5133.
(69) Arcisauskaite, V.; Knecht, S.; Sauer, S. P. A.; Hemmingsen, L. *Phys. Chem. Chem. Phys.* **2012**, *14*, 2651−2657.
(70) Autschbach, J.; Ziegler, T. *J. Am. Chem. Soc.* **2001**, *123*, 3341−3349.
(71) Cammi, R.; Frediani, L.; Mennucci, B.; Ruud, K. *J. Chem. Phys.* **2003**, *119*, 5818−5827.
(72) Møgelhøj, A.; Aidas, K.; Mikkelsen, K. V.; Sauer, S. P. A.; Kongsted, J. *J. Chem. Phys.* **2009**, *130*, 134508.
(73) Ramalho, T. C.; Pereira, D. H.; Thiel, W. *J. Phys. Chem. A* **2011**, *115*, 13504−13512.
(74) Criger, B.; Park, D.; Baugh, J. *Quantum Information and Computation for Chemistry*; John Wiley I& Sons, Inc: Hoboken, New Jersey, 2014; pp 193−227.
(75) Jones, J. A.; Mosca, M. *J. Chem. Phys.* **1998**, *109*, 1648−1653.
(76) Peng, X.-h.; Suter, D. *Front. Phys. China* **2010**, *5*, 1−25.
(77) Suter, D.; Mahesh, T. S. *J. Chem. Phys.* **2008**, *128*, 052206.
(78) Rozovsky, S. *Biochalcogen Chemistry: The Biological Chemistry of Sulfur, Selenium, and Tellurium*; American Chemical Society, 2013; Chapter 6, pp 127−142.
(79) Gerothanassis, I. P. In *Encyclopedia of Spectroscopy and Spectrometry*; Lindon, J. C., Ed.; Elsevier: Oxford, 1999; pp 722−729.
(80) Wasylishen, R. E.; Lenkinski, R. E.; Rodger, C. *Can. J. Chem.* **1982**, *60*, 2113−2117.
(81) Maliarik, M.; Persson, I. *Magn. Reson. Chem.* **2005**, *43*, 835−842.
(82) Dixon, A. M.; Larive, C. K.; Nantsis, E. A.; Carper, W. R. *J. Phys. Chem. A* **1998**, *102*, 10573−10578.
(83) Glaser, S. J.; Marx, R.; Reiss, T.; Schulte-Herbrüggen, T.; Khaneja, N.; Myers, J. M.; Fahmy, A. F. *Quantum Information Processing*; Wiley-VCH: Weinheim, 2005; pp 58−69.

https://dx.doi.org/10.1021/acs.jpca.0c01607
J. Phys. Chem. A 2020, 124, 4946−4955

Supporting information

Enhancing NMR quantum computation by exploring heavy metal complexes as multiqubit systems: a theoretical investigation

Supporting Information

Enhancing NMR Quantum Computation by Exploring Heavy Metal Complexes as Multiqubit Systems: a Theoretical Investigation

Jéssica Boreli dos Reis Lino,[a‡] Stephan P. A. Sauer,[b#] Teodorico Castro Ramalho[a,c]*

[a]Department of Chemistry, Federal University of Lavras, 37200-000 Lavras,MG, Brazil
[b]Department of Chemistry, University of Copenhagen, Universitetsparken 5,DK-2100 Copenhagen, Denmark.
[c]Center for Basic and Applied Research, Faculty of Informatics and Management, University Hradec Kralove, 50003 Hradec Kralove,

‡ jessicaboreli@outlook.com
# sauer.kiku@gmail.com
*teodorico.ramalho@gmail.com

Table of contents

Tables S1-S5 show the calculated Boltzmann distribution. The Boltzmann distribution is a probability distribution that gives the probability of a certain state as a function of that state's energy and temperature of the system to which the distribution is applied.[1] The calculation is made following the equation:

$$p_i = \frac{e^{-\Delta G_i/kT}}{\sum_{j=1}^{M} e^{-\Delta G_j/kT}}$$

where p_i is the Boltzmann factor, ΔG is the relative Gibbs energy, regarding to the lowest energy conformer, k is the Boltzmann constant, T is the temperature of the system and M is the number of all conformers.

[1] Atkins, P. W.; De Paula, J.; Friedman, R. S. *Physical Chemistry: Quanta, Matter, and Change*; Oxford: Oxford University Press, U.K., 2014.

Table S1 Gibbs Free Energy values, G [kJ.mol-1], relative G (ΔG), regarding to the lowest energy conformer and calculated Boltzmann distribution, p_i (25 °C) for CdBuTe conformer

Conformer	G	ΔG	p_i factor
opt-1	-8543044.0	0	0.30020
conf-12	-8543042.4	1.7	0.15210
conf-9	-8543042.2	1.9	0.14108
conf-19	-8543040.3	3.7	0.06658
conf-27	-8543039.5	4.5	0.04866
conf-4	-8543039.5	4.6	0.04744
conf-11	-8543038.8	5.3	0.03557
conf-50	-8543037.0	7.0	0.01760
conf-8	-8543036.7	7.3	0.01560
conf-7	-8543036.7	7.4	0.01544
conf-5	-8543036.4	7.7	0.01368
conf-2	-8543036.2	7.9	0.01257
conf-21	-8543036.0	8.0	0.01171
conf-14	-8543036.0	8.1	0.01150
conf-47	-8543035.6	8.4	0.01009
conf-18	-8543035.6	8.4	0.01001
conf-22	-8543035.5	8.6	0.00949
conf-3	-8543035.3	8.8	0.00865
conf-34	-8543035.2	8.8	0.00860
conf-24	-8543035.2	8.8	0.00852
conf-1	-8543035.0	9.1	0.00770
conf-25	-8543034.5	9.6	0.00632
conf-32	-8543033.8	10.3	0.00474
conf-10	-8543033.3	10.7	0.00399
conf-35	-8543033.2	10.8	0.00382
conf-45	-8543033.0	11.0	0.00351
conf-26	-8543032.9	11.2	0.00331
conf-16	-8543032.9	11.2	0.00329
conf-13	-8543031.9	12.1	0.00227
conf-6	-8543031.9	12.2	0.00220
conf-17	-8543031.8	12.2	0.00218
conf-36	-8543031.6	12.4	0.00200
conf-33	-8543031.6	12.5	0.00196
conf-39	-8543031.5	12.6	0.00188
conf-29	-8543029.8	14.2	0.00097
conf-41	-8543029.8	14.2	0.00096
conf-44	-8543029.0	15.1	0.00069
conf-42	-8543028.4	15.6	0.00055
conf-15	-8543028.0	16.0	0.00047
conf-23	-8543027.9	16.1	0.00045
conf-20	-8543027.3	16.7	0.00035
conf-40	-8543027.1	16.9	0.00033
conf-48	-8543026.1	18.0	0.00021
conf-31	-8543025.7	18.3	0.00018
conf-37	-8543025.2	18.8	0.00015
conf-28	-8543024.3	19.7	0.00011
conf-30	-8543024.2	19.8	0.00010
conf-46	-8543023.9	20.1	0.00009
conf-38	-8543023.5	20.5	0.00008
conf-49	-8543021.5	22.6	0.00003
conf-43	-8543020.1	23.9	0.00002

Table S2 Gibbs Free Energy values, G [kJ.mol-1], relative G (ΔG), regarding to the lowest energy conformer and calculated Boltzmann population, p_i (25 °C) for HgBuTe conformer

Conformer	G	ΔG	p_i factor
opt-1	-8505517.5	0	0.61894
conf-14	-8505514.4	3.0	0.18233
conf-5	-8505512.9	4.5	0.09969
conf-3	-8505509.5	8.0	0.02487
conf-16	-8505508.6	8.9	0.01698
conf-1	-8505508.4	9.1	0.01602
conf-7	-8505507.9	9.6	0.01288
conf-10	-8505505.8	11.7	0.00554
conf-18	-8505505.2	12.2	0.00443
conf-37	-8505504.9	12.6	0.00384
conf-42	-8505504.8	12.7	0.00373
conf-32	-8505504.2	13.3	0.00289
conf-34	-8505503.0	14.4	0.00184
conf-12	-8505501.2	16.3	0.00087
conf-2	-8505500.8	16.7	0.00073
conf-33	-8505500.7	16.8	0.00070
conf-46	-8505500.5	17.0	0.00066
conf-47	-8505500.2	17.3	0.00058
conf-29	-8505499.4	18.0	0.00043
conf-11	-8505499.0	18.4	0.00036
conf-31	-8505497.7	19.8	0.00021
conf-49	-8505497.6	19.9	0.00020
conf-6	-8505497.6	19.9	0.00020
conf-23	-8505496.9	20.5	0.00016
conf-30	-8505496.8	20.7	0.00015
conf-9	-8505496.3	21.2	0.00012
conf-35	-8505495.9	21.6	0.00010
conf-43	-8505495.7	21.8	0.00009
conf-28	-8505495.5	22.0	0.00009
conf-21	-8505494.8	22.6	0.00007
conf-40	-8505494.5	23.0	0.00006
conf-50	-8505493.5	24.0	0.00004
conf-27	-8505493.0	24.5	0.00003
conf-17	-8505492.5	24.9	0.00003
conf-20	-8505492.4	25.1	0.00003
conf-24	-8505492.1	25.4	0.00002
conf-48	-8505491.6	25.9	0.00002
conf-38	-8505491.5	26.0	0.00002
conf-39	-8505490.8	26.6	0.00001
conf-4	-8505490.5	27.0	0.00001
conf-44	-8505489.2	28.3	0.00001
conf-15	-8505488.6	28.9	0.00001
conf-8	-8505487.9	29.6	0.00000
conf-22	-8505487.7	29.8	0.00000
conf-19	-8505484.7	32.8	0.00000
conf-41	-8505481.4	36.1	0.00000
conf-13	-8505479.7	37.7	0.00000
conf-36	-8505479.3	38.2	0.00000
conf-45	-8505478.5	38.9	0.00000
conf-25	-8505478.0	39.5	0.00000

Table S3 Gibbs Free Energy values, G [kJ.mol-1], relative G (ΔG), regarding to the lowest energy conformer and calculated Boltzmann population, p_i (25 °C) for CdMeTe conformer.

Conformer	G	ΔG	p_i factor
conf-1	-8176811.4	0	0.08557
conf-27	-8176811.4	0.0	0.08387
conf-8	-8176811.4	0.1	0.08378
conf-25	-8176811.4	0.1	0.08342
conf-4	-8176811.3	0.1	0.08246
conf-34	-8176811.3	0.2	0.08013
conf-6	-8176810.1	1.3	0.05002
conf-30	-8176809.9	1.5	0.04694
conf-37	-8176809.7	1.7	0.04299
conf-47	-8176808.6	2.9	0.02683
conf-12	-8176808.5	2.9	0.02652
opt-1	-8176808.1	3.3	0.02232
conf-41	-8176808.1	3.3	0.02218
conf-36	-8176808.1	3.4	0.02213
conf-7	-8176807.7	3.7	0.01922
conf-40	-8176807.2	4.2	0.01558
conf-29	-8176807.2	4.3	0.01536
conf-50	-8176807.0	4.5	0.01400
conf-45	-8176806.9	4.5	0.01397
conf-28	-8176806.6	4.8	0.01228
conf-39	-8176806.6	4.9	0.01201
conf-44	-8176806.6	4.9	0.01200
conf-26	-8176806.6	4.9	0.01195
conf-17	-8176806.5	4.9	0.01171
conf-43	-8176805.4	6.1	0.00744
conf-2	-8176805.4	6.1	0.00741
conf-21	-8176805.4	6.1	0.00740
conf-14	-8176805.3	6.1	0.00734
conf-11	-8176805.3	6.1	0.00733
conf-49	-8176805.1	6.4	0.00653
conf-22	-8176804.9	6.5	0.00618
conf-38	-8176804.4	7.0	0.00503
conf-9	-8176804.4	7.1	0.00498
conf-3	-8176804.4	7.1	0.00491
conf-42	-8176804.3	7.1	0.00490
conf-10	-8176804.3	7.2	0.00477
conf-15	-8176803.9	7.5	0.00409
conf-32	-8176803.9	7.6	0.00405
conf-23	-8176803.7	7.7	0.00381
conf-46	-8176803.4	8.0	0.00335
conf-19	-8176803.1	8.4	0.00292
conf-13	-8176803.1	8.4	0.00291
conf-20	-8176802.7	8.8	0.00249
conf-33	-8176802.5	9.0	0.00231
conf-31	-8176801.3	10.1	0.00145
conf-48	-8176798.1	13.4	0.00039
conf-18	-8176797.2	14.2	0.00028
conf-24	-8176797.0	14.5	0.00025
conf-35	-8176797.0	14.5	0.00025

Table S4 Gibbs Free Energy values, G [kJ.mol-1], relative G (ΔG), regarding to the lowest energy conformer and calculated Boltzmann population, p_i (25 °C) for HgMeTe conformer.

Conformer	G	ΔG	p_i factor
conf-12	-8139280.2	0	0.04749
conf-6	-8139280.2	0.0	0.04734
conf-14	-8139280.2	0.0	0.04714
opt-1	-8139280.2	0.0	0.04699
conf-9	-8139280.2	0.0	0.04694
conf-19	-8139280.1	0.2	0.04428
conf-21	-8139280.0	0.3	0.04249
conf-22	-8139279.9	0.3	0.04160
conf-8	-8139279.9	0.3	0.04134
conf-32	-8139279.6	0.6	0.03695
conf-31	-8139279.6	0.6	0.03660
conf-1	-8139279.6	0.7	0.03633
conf-35	-8139279.6	0.7	0.03629
conf-28	-8139279.2	1.0	0.03132
conf-17	-8139279.2	1.0	0.03129
conf-13	-8139279.2	1.0	0.03112
conf-2	-8139279.1	1.1	0.03073
conf-20	-8139278.6	1.6	0.02497
conf-15	-8139278.2	2.0	0.02097
conf-46	-8139278.2	2.1	0.02070
conf-39	-8139278.1	2.1	0.02012
conf-42	-8139278.1	2.1	0.02007
conf-30	-8139277.6	2.6	0.01650
conf-49	-8139277.6	2.6	0.01642
conf-7	-8139277.6	2.7	0.01629
conf-18	-8139277.2	3.0	0.01397
conf-48	-8139277.2	3.1	0.01384
conf-33	-8139276.9	3.3	0.01248
conf-34	-8139276.8	3.4	0.01211
conf-4	-8139276.8	3.4	0.01192
conf-10	-8139276.8	3.4	0.01187
conf-37	-8139276.5	3.7	0.01064
conf-38	-8139276.5	3.7	0.01064
conf-44	-8139276.5	3.7	0.01055
conf-41	-8139276.5	3.7	0.01054
conf-3	-8139275.9	4.3	0.00824
conf-43	-8139275.9	4.3	0.00822
conf-11	-8139275.9	4.4	0.00821
conf-25	-8139275.9	4.4	0.00820
conf-50	-8139275.3	5.0	0.00644
conf-16	-8139272.6	7.7	0.00216
conf-36	-8139272.5	7.7	0.00214
conf-40	-8139269.9	10.3	0.00073
conf-24	-8139269.9	10.3	0.00073
conf-29	-8139269.9	10.4	0.00073
conf-26	-8139269.9	10.4	0.00073
conf-5	-8139269.8	10.4	0.00072
conf-23	-8139269.8	10.4	0.00072
conf-45	-8139269.4	10.8	0.00060
conf-47	-8139268.6	11.7	0.00043
conf-27	-8139265.7	14.5	0.00013

Table S5 Gibbs Free Energy values, G [kJ.mol-1], relative G (ΔG), regarding to the lowest energy conformer and calculated Boltzmann population, p_i (25 °C) for CdMeSe conformer.

Conformer	G	ΔG	p_i factor
conf-22	-8728847.4	0	0.10589
conf-41	-8728847.4	0.0	0.10411
opt-1	-8728847.0	0.4	0.08967
conf-45	-8728845.4	2.0	0.04760
conf-18	-8728844.9	2.5	0.03819
conf-23	-8728844.5	2.9	0.03261
conf-8	-8728844.3	3.1	0.03083
conf-32	-8728844.3	3.1	0.03080
conf-25	-8728844.1	3.3	0.02791
conf-48	-8728844.0	3.4	0.02715
conf-19	-8728843.9	3.5	0.02532
conf-35	-8728843.9	3.5	0.02532
conf-31	-8728843.9	3.6	0.02527
conf-40	-8728843.8	3.6	0.02521
conf-14	-8728843.8	3.6	0.02516
conf-46	-8728843.2	4.2	0.01916
conf-3	-8728843.2	4.2	0.01910
conf-50	-8728843.0	4.4	0.01781
conf-44	-8728843.0	4.4	0.01770
conf-39	-8728842.8	4.6	0.01665
conf-9	-8728842.8	4.6	0.01658
conf-36	-8728842.8	4.6	0.01656
conf-6	-8728842.8	4.6	0.01644
conf-34	-8728842.8	4.6	0.01638
conf-7	-8728842.8	4.6	0.01637
conf-15	-8728842.8	4.6	0.01637
conf-43	-8728841.8	5.6	0.01124
conf-12	-8728841.8	5.6	0.01091
conf-33	-8728841.6	5.8	0.01035
conf-4	-8728841.6	5.8	0.01026
conf-38	-8728841.6	5.8	0.01020
conf-47	-8728841.6	5.8	0.01017
conf-5	-8728841.6	5.8	0.01014
conf-28	-8728841.6	5.8	0.01013
conf-42	-8728841.0	6.5	0.00785
conf-11	-8728840.8	6.6	0.00751
conf-20	-8728840.2	7.2	0.00569
conf-21	-8728839.9	7.5	0.00513
conf-17	-8728839.9	7.5	0.00509
conf-49	-8728839.9	7.5	0.00509
conf-37	-8728839.9	7.5	0.00508
conf-30	-8728839.8	7.6	0.00485
conf-1	-8728839.8	7.6	0.00484
conf-29	-8728839.7	7.7	0.00479
conf-10	-8728839.7	7.7	0.00475
conf-26	-8728839.3	8.1	0.00408
conf-24	-8728835.1	12.3	0.00075
conf-16	-8728833.1	14.3	0.00034
conf-13	-8728832.1	15.3	0.00022
conf-27	-8728832.1	15.3	0.00022
conf-2	-8728831.5	15.9	0.00017

Table S6 ^{31}P, ^{77}Se, ^{125}Te, ^{113}Cd and ^{199}Hg NMR absolute shieldings (σ) of the PH_3, $SeMe_2$, $TeMe_2$, $CdMe_2$ and $HgMe_2$ reference molecules

	σ $CdMe_2$	σ $HgMe_2$	σ $TeMe_2$	σ $SeMe_2$	σ PH_3
ZORA/PBE0/TZ2P	3594.24	9374.91	3456.38	1871.72	598.22
ZORA/PBE0/QZ4P	3542.64	9605.64	3468.34	1865.69	584.70
NR/PBE0/TZ2P		6533.74	2779.65		585.87
ZORA/PBE0/TZ2P/Solvent *		9496.48	3532.62		597.98
ZORA/B3LYP/TZ2P		9286.78	3302.47		576.03
ZORA/PBE/TZ2P		8998.75	3260.57		588.99
ZORA/BP86/TZ2P		8968.24	3254.02		582.99
DKS/PBE0/dyall-VTZ		11097.37	3846.83		601.79
NR/PBE0/dyall-VTZ		6475.91	2799.02		582.76

* Using conductor like screening model (COSMO) of solvation. Dichloroethane, Eps = 10.66 and Rad = 3.15.

Table S7 M (^{113}Cd or ^{199}Hg), E (^{77}Se or ^{125}Te) and ^{31}P chemical shifts, δ [ppm] and M−P and E−P spin-spin coupling constant, J [Hz] calculated with the ZORA method using the PBE0 exchange-correlation functional and the shown basis set

		δ M	δ E		δ P		$^{2}J_{M-P}$		$^{1}J_{E-P}$		$^{2}J_{M-P}$*		$^{1}J_{E-P}$*	
						CdBuTe								
TZ2P	opt-1	441	-642	-675	-7.2	-12	32.1	35.2	1278	1321	37.7	41.1	1500	1550
	conf-12	446	-635	-635	-4.5	-4.0	33.6	33.6	1262	1261	39.5	39.4	1483	1482
	conf-9	449	-637	-637	-4.3	-4.3	33.4	33.4	1263	1263	39.2	39.2	1484	1484
	Boltz.[a]	444	-639	-656	-5.8	-8.3	32.8	34.3	1270	1292	38.5	40.2	1492	1517
						CdMeTe								
TZ2P	opt-1	439	-567	-511	52.5	56.4	37.4	42.2	1751	1733	43.7	49.4	2053	2029
	conf-1	433	-530	-531	50.2	50.1	38.7	38.7	1722	1722	45.1	45.1	2019	2019
QZ4P		359	-598	-536	57.0	61.1	42.7	48.3	1954	1935	44.2	50.0	2032	2010
						CdMeSe								
TZ2P	opt-1	440	-185	-216	83.7	88.8	29.1	34.9	-700	-702	33.8	40.7	-844	-847
	conf-22	442	-227	-228	84.5	84.5	26.7	26.7	-696	-696	31.0	31.0	-840	-840
	conf-41	437	-216	-217	83.7	83.7	29.0	29.0	-700	-700	33.8	33.7	-845	-845
	Boltz.[b]	440	-209	-220	83.9	85.7	28.2	30.2	-698	-698	32.8	35.2	-842	-843
QZ4P		365	-206	-242	87.8	93.5	31.9	38.5	-809	-811	33.5	40.4	-853	-855
						HgBuTe								
TZ2P	opt-1	-1583	-489	-526	-3.3	-10	-105	-121	1310	1265	-128	-147	1539	1486
	conf-14	-1578	-521	-517	2.0	3.5	-113	-114	1243	1246	-137	-138	1460	1464
	conf-5	-1608	-462	-490	-0.6	-4.1	-115	-109	1241	1246	-140	-132	1460	1464
	Boltz.[c]	-1585	-493	-520	-1.9	-6.7	-108	-118	1289	1259	-131	-143	1514	1479
						HgMeTe								
TZ2P	opt-1	-1554	-422	-356	52.1	57.3	-134	-145	1756	1735	-162	-176	2059	2031
	conf-12	-1554	-422	-356	52.1	57.3	-133	-145	1756	1735	-161	-176	2059	2031
QZ4P		-2098	-449	-377	56.5	62.1	-158	-172	1959	1936	-163	-178	2037	2013

[a] From Boltzmann Distribution opt-1 (50.6 %), conf-12 (25.6 %) and conf-9 (23.8 %).
[b] From Boltzmann Distribution opt-1 (35.3 %), conf-22 (34.7 %) and conf-41 (29.9 %).
[c] From Boltzmann Distribution opt-1 (68.7 %), conf-14 (20.2 %) and conf-5 (11.1 %).
*Calculated using the specialized coupling constant basis set ZORA-JCPL.

Table S8 M (^{113}Cd or ^{199}Hg), E (^{77}Se or ^{125}Te) and ^{31}P absolute shieldings, σ [ppm] calculated with the ZORA method using the PBE0 exchange-correlation functional and the shown basis set

		σ M	σ E		σ P	
CdBuTe						
TZ2P	opt-1	3858.0	4096.0	4129.5	339.5	344.6
	conf-12	3853.8	4088.8	4089.4	336.8	336.3
	conf9	3850.3	4091.5	4091.5	336.5	336.6
CdMeTe						
TZ2P	opt-1	3860.4	4021.5	3965.9	279.8	275.9
	conf-1	3866.0	3985.0	3985.1	282.2	282.2
QZ4P		3889.0	4063.9	4002.3	261.7	257.7
CdMeSe						
TZ2P	opt-1	3859.0	2056.3	2087.3	248.7	243.5
	conf-22	3857.3	2098.8	2098.9	247.9	247.9
	conf-41	3862.5	2086.9	2087.8	248.6	248.6
QZ4P		3882.9	2071.5	2107.7	231.0	225.3
HgBuTe						
TZ2P	opt-1	10942.7	3944.0	3980.8	335.6	342.4
	conf-14	10938.4	3975.6	3972.0	330.3	328.8
	conf-5	10968.1	3916.4	3944.7	332.9	336.4
HgMeTe						
TZ2P	opt-1	10914.4	3876.9	3811.4	280.2	275.0
	conf-12	10914.3	3876.9	3811.0	280.2	275.0
QZ4P		11683.2	3915.6	3844.4	262.3	256.7

Table S9 Effect of different exchange–correlation functionals and solvent on the ^{199}Hg, ^{125}Te and ^{31}P absolute shieldings, σ [ppm] in HgBuTe calculated with the ZORA method using TZ2P basis set

	σ Hg	σ Te		σ P	
PBE0	10942.7	3944.0	3980.8	335.6	342.4
PBE0 /solvent*	11079.8	3971.4	3995.2	331.5	335.7
B3LYP	11073.3	3765.1	3807.4	308.5	316.3
PBE	10694.4	3706.6	3740.8	306.4	314.5
BP86	10748.0	3653.9	3687.1	302.7	311.0

*Using conductor like screening model (COSMO) of solvation. Dichloroethane, Eps = 10.66 and Rad = 3.15.

Table S10 ^{199}Hg, ^{125}Te and ^{31}P absolute shieldings, σ [ppm] calculated using nonrelativistic (NR), the two-component ZORA and the four-component DKS approach. All calculations were carried out with the PBE0 exchange-correlation functional and the shown basis sets

		σ Hg	σ Te		σ P-1	
HgBuTe	ZORA/TZ2P	10942.7	3944.0	3980.8	335.6	342.4
	NR/TZ2P	6855.8	3506.9	3544.6	256.1	256.4
HgBuTe-4c	NR/TZ2P	6674.3	3205.8	3235.2	270.5	266.7
	ZORA/TZ2P	10457.2	3676.7	3694.2	383.5	382.8
	DKS/PBE0/dyall-vtz	12675.4	4081.3	4098.9	395.1	394.0
	DKS/dyall-vtz	6559.4	3210.3	3241.2	270.8	266.4

Calculated harmonic frequencies (cm^{-1}) for the discussed optimized geometries (B3LYP/cc–pVDZ). For heavy atoms (SDD–cc–pVDZ–pp).

CdBuTe-opt-1		
6.7429	10.5946	15.1684
20.6889	25.6919	27.9866
30.5770	32.2655	33.9912
37.1880	42.6729	46.5973
49.7179	52.4859	55.4329
57.2506	57.8077	63.7587
65.2766	70.5574	71.6815
72.6248	74.6271	78.6713
86.0018	88.4384	99.6511
109.6569	110.4987	117.7209
119.5794	122.0239	125.2957
128.5222	132.2716	148.0148
151.1474	162.8063	165.0514
186.1615	192.9806	199.4693
204.4773	213.8411	217.7001
221.8104	229.2290	234.0530
234.8718	242.0729	252.6963
253.0739	253.4794	256.0118
256.2373	257.5932	258.1951
297.9112	322.3328	352.0189
383.6218	388.5850	390.2119
403.3863	406.1268	425.3485
435.1808	446.8683	451.9600
678.6277	688.9235	702.3593
706.4119	728.7559	730.5439
735.6533	738.7818	739.4348
746.3468	761.0922	763.3837
774.4779	779.9622	781.4913
783.3446	790.4280	791.6136
888.5098	892.5422	897.1605
898.7414	900.0883	902.4285
907.9245	910.5585	912.9132
916.0746	917.8010	919.5010
1019.9616	1020.2335	1020.7659
1022.8432	1025.6170	1031.2445
1047.7766	1052.4132	1056.5464
1065.0036	1065.3845	1066.1878
1066.4390	1067.8766	1068.1881
1068.7443	1074.6721	1079.3926
1106.5440	1106.7830	1109.1877
1112.6812	1116.5190	1119.9315
1214.5160	1215.0330	1218.1075
1219.4523	1220.9673	1221.7609
1224.2439	1227.4664	1228.5990
1235.5883	1248.2725	1250.7955
1295.4384	1296.0921	1296.7615
1300.9998	1304.9768	1307.4412
1324.0465	1324.4080	1324.9485
1325.2101	1326.5138	1328.4272
1328.9180	1329.0355	1332.1233
1332.2631	1337.1878	1338.0742
1382.2808	1382.8063	1387.1811
1388.4405	1389.9335	1391.0359
1398.9127	1399.5282	1399.5550
1400.8197	1400.9939	1404.8149
1422.8387	1424.2272	1433.5729
1433.9000	1434.5343	1435.2907
1459.5640	1461.0630	1462.3250
1463.1694	1464.0160	1464.3156
1467.0515	1468.1257	1468.1664
1469.4844	1470.2298	1470.2618
1470.4625	1470.5318	1470.6044
1471.0552	1471.2251	1474.7182
1481.5779	1483.0957	1483.1661
1484.2737	1484.7576	1487.5292
2998.4019	3005.1050	3007.0993
3008.5973	3009.5197	3009.7969
3010.4832	3012.7152	3013.9842
3014.2155	3014.6440	3017.7685
3021.1039	3021.2016	3021.3514
3021.7926	3023.9511	3024.5205
3026.4191	3026.8399	3027.9648
3030.3772	3041.6447	3042.3658
3043.9968	3046.8314	3050.4193
3054.9453	3055.7574	3062.5982
3063.4836	3064.4220	3065.3281
3066.0138	3071.8777	3073.4609
3076.3325	3076.8991	3086.9361
3093.1234	3093.3860	3094.4972
3094.5213	3094.8988	3095.3836
3098.2092	3099.1366	3099.7239
3100.9157	3101.0127	3101.0917
3104.1435	3104.6988	3112.5749

CdBuTe-conf-12		
10.4705	12.1774	15.7957
22.7728	26.6500	27.6239
29.3696	31.0303	34.0223
36.1223	40.9068	44.2859
46.6189	49.3510	50.7572
53.3509	55.9786	57.6162
59.5803	63.6575	65.9999
73.2515	75.2916	79.7037
82.4726	92.2370	98.7738
111.3716	115.5411	116.6849
117.7110	123.1603	126.4775
129.5923	133.8215	157.9291
158.6321	163.1160	163.7584
191.8288	192.0253	198.3281
199.1862	218.1868	221.0548
225.4815	230.7220	238.7820
240.0640	243.8545	247.5105
253.3412	253.5892	257.7037
260.1771	282.0311	287.9598
311.9368	314.6295	347.2658
371.8128	385.7356	396.3023
410.5787	412.3795	434.3612
437.7239	454.8797	456.6857
678.3866	679.6960	703.7594
704.5851	730.6184	731.9126
732.3585	737.0206	748.5337
750.0947	761.9546	762.5284
776.7143	779.4692	784.9453
786.5961	791.6719	797.7592
874.3530	874.6521	895.2401
895.6542	898.2812	901.1386
904.8332	909.1099	910.8447
916.1635	921.7033	923.6171
981.5568	983.9416	1020.1159
1020.5731	1024.4359	1025.4581
1051.9175	1053.4854	1060.3557
1060.8193	1064.4308	1064.5988
1068.1206	1069.4922	1075.7273
1077.9319	1088.4432	1088.9628
1109.1698	1109.8372	1110.1378
1110.2791	1115.1403	1117.0186
1199.6157	1201.0945	1218.1204
1218.5140	1221.9338	1223.4035
1224.6249	1228.6515	1237.0916
1239.5601	1249.5355	1249.5723
1293.7223	1295.8560	1298.4287
1302.1332	1302.9503	1303.7705
1314.7179	1315.4941	1325.0418
1325.5512	1326.7137	1327.3679
1328.2214	1331.0347	1331.1433
1332.9751	1369.5710	1369.6240
1371.5700	1373.1327	1382.2713
1383.7188	1387.3369	1387.6545
1398.3854	1399.6590	1399.7100
1400.8610	1401.4492	1402.6113
1430.4684	1431.8817	1435.4207
1435.9186	1439.4286	1441.1892
1459.0445	1459.4460	1460.2884
1460.5127	1461.5686	1462.7798
1463.1208	1464.2028	1466.9268
1467.7149	1468.6713	1470.1631
1470.3546	1470.3688	1470.6892
1471.5610	1473.8059	1474.9023
1479.4583	1479.6884	1481.2596
1482.6896	1483.1245	1484.1828
3005.6664	3009.8572	3010.4715
3010.7445	3011.0634	3011.1896
3017.9129	3018.1556	3018.3802
3018.5557	3018.9601	3021.2946
3021.7638	3021.9877	3022.8366
3022.8839	3025.0926	3026.1605
3026.6262	3029.4289	3032.0881
3032.3084	3034.1264	3038.7145
3040.2878	3048.8925	3049.1547
3055.5667	3061.2210	3065.7630
3065.9663	3066.3327	3066.5104
3067.6292	3072.0636	3076.7813
3087.6762	3090.1283	3090.4239
3091.2972	3091.6566	3092.6293
3092.9937	3093.9525	3094.7501
3094.7895	3095.5473	3096.7768
3097.0091	3101.9322	3102.1414
3102.1909	3103.8052	3107.4997

CdBuTe-conf-9		
9.9416	11.6326	15.3872
22.7349	26.0784	27.2636
29.2468	30.3937	31.3061
35.4684	41.5394	45.3399
46.9788	49.5004	53.2035
53.9736	55.6348	56.2876
58.9521	64.1749	64.2080
73.2287	74.9967	79.9115
81.7817	92.9109	98.3814
111.1705	115.5035	116.3696
117.5613	123.6585	123.9796
129.4327	129.5119	159.3426
159.6842	163.4667	163.9601
192.4480	192.7572	198.4160
198.7688	216.0566	216.1162
230.6892	230.7788	238.9239
239.9606	244.5953	248.4810
253.7939	253.8133	257.7454
258.5269	287.9445	288.2322
314.1563	314.5249	346.6226
347.1803	396.0876	396.8513
412.2566	412.3003	437.3927
438.5170	454.6387	455.3192
679.2621	679.5888	704.8977
705.0972	731.6198	732.0229
732.5887	732.6338	749.0734
749.1801	761.7791	762.0851
779.1109	779.4156	786.5299
786.9273	791.5398	791.5926
874.8946	874.9480	895.0919
895.5404	898.3547	898.3966
904.8415	905.0325	915.9941
916.1600	921.5483	922.0064
981.6107	981.6717	1020.1155
1020.1340	1025.4581	1025.5203
1051.9782	1052.3156	1059.9807
1060.4385	1064.4256	1064.4316
1070.3579	1070.3885	1075.8960
1076.0785	1088.7015	1089.1056
1109.6548	1109.9494	1110.1629
1110.3883	1115.0708	1115.1269
1199.1848	1199.2566	1218.5179
1218.5733	1221.8758	1221.9654
1224.7920	1225.0767	1238.8434
1239.1170	1249.0953	1249.1350
1295.5850	1296.0113	1298.2830
1298.2866	1302.9088	1302.9181
1315.1580	1315.3777	1325.2891
1325.2940	1326.6830	1326.8064
1328.0080	1328.1714	1330.7729
1330.7946	1369.3803	1369.5268
1372.4261	1372.8890	1382.2781
1382.3400	1387.3659	1387.4549
1399.6909	1399.7008	1400.8189
1400.8204	1401.6162	1401.6500
1430.7342	1430.8090	1435.4057
1435.8542	1440.4034	1440.5215
1460.1934	1460.4223	1460.4906
1460.5871	1462.8401	1462.8836
1463.1851	1463.2265	1467.7995
1467.8033	1470.2372	1470.2403
1470.4102	1470.4110	1470.7468
1470.7488	1473.9548	1474.0282
1479.7717	1479.8353	1482.7585
1482.7658	1484.1764	1484.1798
3009.7467	3009.8456	3010.6274
3010.6330	3011.4231	3011.4615
3018.1600	3018.1820	3018.6622
3018.6873	3021.7193	3021.7224
3022.8108	3022.8541	3026.1080
3026.1208	3026.2841	3026.3673
3029.5760	3029.6895	3031.9670
3032.0357	3034.1432	3034.1863
3040.1797	3040.1831	3049.0196
3049.0322	3065.8454	3065.8509
3066.3637	3066.3751	3066.3788
3066.4264	3076.7140	3076.7526

3090.2350	3090.2852	3090.4505
3090.4962	3091.4514	3091.5133
3092.8480	3092.8583	3094.8890
3094.9325	3096.7095	3096.7175
3097.0933	3097.1311	3102.0936
3102.1018	3103.8099	3103.8274

CdMeTe-opt-1

12.2384	13.4244	19.2188
31.6750	37.9393	42.1785
48.2870	52.0547	58.0062
62.2362	65.5457	73.6739
77.5562	84.4521	87.1194
94.8383	96.1544	98.0802
108.3992	116.3629	120.8432
122.2905	126.1336	133.5116
135.4841	138.5928	142.7088
148.3224	157.1591	168.1116
178.1304	182.5437	184.7112
187.3753	195.2440	205.7587
210.6573	213.8447	225.5440
241.4847	243.7638	248.9746
251.9949	258.4936	262.2136
271.4369	278.1277	292.4095
296.1262	316.6243	323.3936
337.3471	339.6204	341.9686
357.2850	357.6113	360.6296
424.1819	424.7313	434.6096
437.0334	482.1960	489.5399
635.0735	642.6919	692.9384
701.3194	712.6539	713.0215
958.5140	964.4105	974.1383
977.5404	987.1610	994.7969
1062.2132	1064.2361	1064.5261
1070.6725	1073.0671	1079.9736
1102.1959	1105.0844	1108.2350
1110.1122	1113.8301	1113.9182
1150.5409	1151.4293	1152.1874
1153.5508	1154.2144	1157.6499
1182.8980	1188.8840	1203.4044
1214.3035	1217.2714	1218.7018
1271.7838	1279.4151	1286.2420
1297.6474	1299.5014	1314.1475
1415.0631	1417.9091	1419.6624
1421.3686	1422.1212	1428.6803
1441.2866	1445.1356	1445.6337
1446.7421	1447.8511	1450.0288
1450.1665	1450.3816	1452.7865
1453.0331	1456.8240	1457.1080
1462.4989	1464.0694	1467.9939
1468.1809	1470.3429	1472.3109
1473.5118	1474.6195	1474.9520
1478.0543	1481.6183	1483.8491
1491.8981	1496.0638	1498.8306
1499.0703	1500.7558	1504.0478
2984.1055	2985.6014	2989.4536
2993.6410	2996.6285	2997.8961
3003.9294	3008.4379	3011.5740
3011.8740	3016.7828	3020.4339
3048.4703	3051.1347	3053.6933
3065.2383	3068.6491	3073.0689
3077.8084	3080.0752	3082.3920
3083.6730	3084.2430	3088.9765
3133.0715	3134.4277	3138.5834
3140.2428	3142.0043	3142.5407
3149.8589	3153.8417	3157.3514
3158.6407	3161.8994	3162.6979

CdMeTe-conf-1

6.4841	10.3392	14.9699
29.0233	32.6296	40.7016
48.9087	49.6221	53.2170
59.2842	59.3644	75.8290
82.5211	89.4893	91.1785
95.9918	98.3974	101.3894
101.6118	111.9796	113.3036
120.9443	121.6689	135.2881
136.8954	140.5850	144.0810
156.0856	156.8264	176.5866
176.7925	185.3045	185.4526
185.8498	185.9199	208.1297
208.2000	220.1043	220.1502
239.1375	239.3989	250.3009
250.3351	252.3665	260.4181
270.8800	271.1938	288.4562
288.7436	321.7130	321.9263
341.3488	341.4334	355.7015
356.0178	360.3276	360.3896
425.3405	425.3922	436.3775
436.8187	482.8677	486.3169
636.6763	642.3181	702.5250
702.7747	709.9866	710.8935
956.4577	957.1597	976.9733
978.2936	987.6808	990.4409
1063.7095	1063.7421	1070.8564
1071.3319	1072.9387	1072.9638
1104.3191	1104.3459	1109.9363
1110.0087	1112.5208	1112.5424
1151.7334	1151.7389	1154.6477
1154.7507	1156.4908	1156.6374
1180.0405	1180.3190	1211.6116
1211.8814	1220.2666	1220.5228
1269.0862	1269.2250	1297.9976
1298.1733	1303.4884	1304.0944
1419.5457	1419.6910	1421.1587
1421.1845	1424.7218	1424.7653
1444.8397	1444.9127	1448.3328
1448.4121	1449.8194	1449.8516
1450.5795	1450.6031	1451.9936
1452.0333	1457.7355	1457.7641
1463.2414	1463.2468	1467.8208
1468.1851	1470.5386	1471.0228
1473.3720	1473.3735	1476.8050
1476.8273	1486.5289	1486.6812
1492.1833	1492.5997	1498.9655
1499.1002	1504.3019	1505.2315
2983.3309	2983.3815	2985.9298
2985.9519	2991.1429	2991.4627
3000.4159	3000.4701	3011.9964
3012.0356	3016.0829	3016.3590
3050.5461	3050.5749	3056.1301
3056.1469	3073.1296	3073.2484
3075.8484	3075.8903	3079.8653
3079.9091	3087.6112	3087.6512
3132.4258	3132.4556	3133.3765
3133.4341	3139.2946	3139.3373
3145.6169	3145.6871	3150.1020
3150.1094	3159.6177	3159.6609

CdMeSe-opt-1

7.7639	10.1476	18.0690
31.4669	36.1417	37.4008
46.4283	51.4300	54.3928
57.8146	63.5606	73.1898
76.4432	84.3712	90.6248
96.4056	98.2286	102.3652
107.9515	111.3128	121.6632
122.3237	125.9336	134.7845
143.8800	147.8270	156.4714
160.0096	170.8920	172.4963
181.7229	185.9433	188.7071
192.9188	199.6087	208.2654
212.6768	215.9018	229.7474
249.8770	250.8283	256.3229
259.7694	270.7208	275.3525
278.4619	287.2066	296.0302
299.3994	318.6874	324.0850
336.1708	341.7480	342.2057
358.8002	359.7078	364.2376
427.0857	429.0399	438.7418
441.1448	492.9041	497.0850
646.0895	654.1225	697.3386
705.6470	716.2674	716.6723
959.2224	967.0032	978.0446
980.5226	989.2928	993.1942
1065.0918	1065.5788	1066.8081
1070.6486	1072.7068	1073.6789
1104.5547	1104.7237	1108.4873
1110.5839	1113.3888	1114.5596
1152.3730	1152.5145	1154.2653
1155.2954	1155.6154	1156.5131
1182.8150	1192.5132	1205.0806
1215.3613	1218.6002	1222.4487
1271.4032	1280.3732	1291.7448
1299.8663	1301.6586	1310.3855
1415.1334	1419.3108	1420.1145
1420.5397	1423.4211	1428.1906
1441.1811	1443.9299	1444.7757
1447.8810	1448.0074	1449.3368
1450.4285	1450.7250	1451.7898
1452.8418	1456.7466	1458.5405
1463.0781	1463.3876	1467.2653
1467.9087	1470.2355	1470.6871
1471.8829	1473.8288	1474.3382
1477.2084	1480.0642	1486.2362
1492.5715	1493.0970	1499.4261
1499.4783	1500.8658	1504.7434
2983.0291	2985.2191	2985.5110
2989.2224	2996.3731	2999.3376
3001.2546	3008.2164	3012.3199
3012.7828	3016.4423	3018.3668
3048.4059	3048.5203	3053.7711
3064.3568	3068.9634	3072.2487
3074.8219	3076.4639	3079.1916
3082.5631	3085.8537	3086.2614
3133.5625	3134.9134	3143.6521
3145.7070	3146.0796	3146.0930
3147.4901	3153.5633	3157.0605
3161.1639	3165.7223	3167.3462

CdMeSe-conf-22

4.9459	9.5620	18.2568
36.8432	37.7200	44.1665
47.4380	52.2437	58.5649
61.1912	63.8854	73.8094
76.8719	91.4126	91.9905
97.6228	98.1842	102.1136
102.3677	108.1826	111.1282
121.9847	122.8339	132.1153
133.6915	155.2769	156.6022
171.6761	174.0418	182.6588
183.6204	189.3135	190.6800
192.2573	192.8409	207.1413
207.2563	229.0417	229.5142
248.5882	249.2696	256.4419
260.4456	260.6622	270.1405
279.5294	279.9124	297.6012
298.6989	322.6711	322.8855
342.1887	342.2853	359.2935
359.5669	364.5963	364.7892
428.7580	428.9433	437.9135
438.3451	494.9805	498.5460
648.3314	655.2179	705.3139
705.6644	716.5125	717.5727
958.6095	959.3971	979.7772
981.3389	992.5535	995.3741
1065.4862	1065.5179	1073.2470
1073.2519	1074.5272	1074.6388
1105.0625	1105.0986	1110.6234
1110.6576	1113.5169	1113.5412
1152.3332	1152.3584	1155.5034
1155.5789	1156.4049	1156.4360
1182.5790	1182.9658	1215.5458
1215.6108	1221.9675	1222.4107
1271.5993	1271.7486	1299.8621
1300.0352	1311.6506	1312.1559
1420.0302	1420.1260	1420.7673
1420.9513	1423.1080	1423.2305
1444.5262	1444.5812	1448.1598
1448.3933	1449.4296	1449.4497
1451.1283	1451.3494	1452.7601
1452.8086	1457.7782	1457.8203
1463.2692	1463.3415	1467.2279
1467.4916	1469.7194	1470.1911
1473.3459	1473.4573	1477.1270
1477.1372	1486.1651	1486.2455
1493.0141	1493.4298	1499.3889
1499.5367	1503.9428	1504.7982
2982.7922	2982.8485	2985.1708
2985.2186	2988.8109	2989.1719
3001.0086	3001.0700	3006.6358
3006.8386	3011.3160	3011.5830
3048.4975	3048.5221	3053.6648
3053.6990	3072.1405	3072.2677
3074.6868	3074.6914	3075.7119
3075.8630	3085.2485	3085.3684
3133.3577	3133.4771	3143.7682
3143.7926	3144.9262	3145.0061
3146.6387	3146.6727	3146.9082
3146.9172	3161.9174	3162.1207

CdMeSe-conf-41

5.0062	9.5964	18.2674
36.8537	37.7386	44.1705
47.4445	52.2710	58.5761
61.1857	63.8798	73.8158
76.8733	91.4321	92.0043
97.5991	98.1948	102.1087
102.3794	108.1753	111.1257
121.9685	122.8327	132.1079
133.6876	155.2749	156.6068
171.6764	174.0410	182.6422
183.6023	189.3065	190.6854
192.2556	192.8359	207.1400
207.2512	229.0133	229.4987
248.5816	249.2644	256.4419
260.4316	260.6535	270.1229
279.5289	279.9146	297.5945
298.6926	322.6678	322.8836
342.1903	342.2887	359.2933
359.5846	364.5808	364.8234
428.7484	428.9506	437.9057
438.3452	494.9842	498.5511
648.3356	655.2219	705.3124
705.6696	716.5183	717.5823
958.6011	959.3888	979.7745
981.3373	992.5636	995.3838
1065.4788	1065.5153	1073.2476
1073.2531	1074.5166	1074.6550
1105.0602	1105.0982	1110.6200
1110.6644	1113.5198	1113.5456
1152.3225	1152.3662	1155.5033
1155.5789	1156.4046	1156.4386
1182.5463	1182.9491	1215.5506
1215.6153	1221.9684	1222.4147
1271.5951	1271.7491	1299.8581
1300.0346	1311.6400	1312.1848
1420.0117	1420.1448	1420.7742
1420.9587	1423.0941	1423.2419
1444.5309	1444.5857	1448.1631
1448.3971	1449.4228	1449.4516
1451.1361	1451.3567	1452.7477
1452.8144	1457.7784	1457.8247
1463.2525	1463.3469	1467.2278
1467.4936	1469.7175	1470.1882
1473.3447	1473.4572	1477.1286

1477.1378	1486.1417	1486.2550
1493.0134	1493.4311	1499.3896
1499.5374	1503.9312	1504.7911
2982.7748	2982.8561	2985.1856
2985.2325	2988.7994	2989.1661
3001.0117	3001.0912	3006.5728
3006.8740	3011.2677	3011.5926
3048.4883	3048.5021	3053.6530
3053.6882	3072.1403	3072.2773
3074.6834	3074.7109	3075.6919
3075.8884	3085.2823	3085.3899
3133.3529	3133.5130	3143.7492
3143.7865	3144.9200	3145.0206
3146.6410	3146.6675	3146.9174
3146.9267	3161.8872	3162.1765

HgBuTe-opt-1

7.8745	10.6193	14.2087
20.7218	25.2919	28.3356
29.8741	32.2970	34.4317
36.1219	41.8525	43.9663
49.1075	50.2976	53.7239
55.6664	56.9565	61.3382
63.7030	65.8245	70.0850
71.4268	72.5344	75.3110
78.4133	88.7951	101.3466
108.0170	108.8707	111.1904
113.8739	121.9269	124.5362
128.3921	131.6264	148.0361
151.3295	162.1302	164.0834
185.7762	192.7360	197.5839
203.2102	207.2534	213.6477
216.9495	221.5837	222.6157
230.5375	235.1610	235.4092
252.5455	253.2734	255.8528
256.3790	256.9473	257.5785
297.8309	322.3949	351.6499
383.7382	387.9308	389.1301
403.3012	406.0224	425.0076
435.1121	445.7682	450.5509
678.0719	688.1759	703.1481
706.5602	728.2110	730.3454
736.3453	738.6083	739.4007
746.6596	760.8723	763.5346
774.4834	780.5332	781.5084
783.1963	790.6941	791.3891
888.5782	892.5351	897.0274
898.7132	899.9640	902.1998
907.8590	910.5351	912.5515
915.9215	917.6040	919.2310
1019.8337	1019.9724	1020.4788
1022.4329	1025.5310	1031.2105
1048.5095	1052.9679	1056.8152
1064.8770	1065.2290	1065.9088
1066.4203	1067.7090	1067.9156
1068.4630	1075.3574	1079.5486
1106.4474	1106.7614	1108.8982
1112.8045	1116.7416	1120.0070
1214.3764	1214.8782	1218.3487
1219.4853	1221.2658	1221.5985
1223.9899	1227.4290	1228.7617
1236.9608	1249.0528	1251.0352
1295.5608	1296.1228	1296.6964
1301.4549	1305.2119	1307.6920
1324.1076	1324.3429	1324.5636
1324.8244	1326.9961	1328.5381
1329.2847	1329.5171	1332.2341
1333.3644	1338.5296	1338.8235
1382.0827	1382.4194	1387.2939
1388.5171	1389.8880	1392.4836
1398.8472	1399.3704	1399.5101
1400.7222	1400.9361	1404.5904
1422.0877	1423.6601	1432.8454
1434.0689	1434.5782	1435.0361
1459.4588	1461.0778	1462.3376
1462.8950	1463.9791	1464.4778
1467.0983	1468.0316	1468.1780
1469.2286	1470.2123	1470.2601
1470.3705	1470.5514	1470.6139
1470.9781	1471.1869	1474.1520
1481.7035	1483.0054	1483.2224
1484.1771	1484.8583	1487.2428
2996.7110	3003.8352	3003.9403
3008.1702	3008.6442	3009.3174
3009.5043	3011.8430	3012.9942
3014.1643	3014.4475	3016.4983
3020.0302	3020.7300	3020.9373
3021.5049	3023.5804	3023.9248
3026.3216	3026.8961	3027.4293
3029.3283	3041.7218	3042.4236
3046.3348	3046.8917	3050.1398
3054.4868	3056.5691	3062.5493
3062.6537	3063.3906	3065.5659
3065.9867	3071.6776	3072.1048
3075.1846	3075.9962	3084.5653
3093.1310	3093.1916	3094.1562
3094.5624	3095.0019	3096.4107
3098.1765	3099.6629	3100.4369
3100.7611	3100.7772	3100.9828
3104.2132	3104.8571	3113.2072

HgBuTe-conf-14

10.7275	12.1296	14.3219
21.3907	26.7697	27.5213
29.2447	32.2590	33.5782
35.6505	36.9889	39.5009
41.7327	47.0814	50.0310
53.9211	57.7302	61.4682
65.0472	66.8771	70.1749
73.8459	75.2797	79.2143
82.0556	94.7610	103.5137
110.9161	114.5771	118.5448
119.1354	122.6946	123.7196
137.7395	138.8574	147.9997
152.7448	190.3032	193.4763
195.8290	197.3968	203.2418
204.7293	205.7603	212.4768
215.8172	216.1763	219.6438
226.2540	233.2688	241.8144
252.9671	253.2919	258.1770
263.2932	276.4382	291.5610
302.6375	306.7087	374.1283
384.4622	388.3134	389.4090
405.1236	420.0983	440.3101
443.2842	444.5632	446.0462
682.5561	683.0449	702.1469
703.2194	723.1993	730.1990
735.7102	738.1477	739.6980
742.7384	765.3061	767.8992
776.8676	777.8503	780.4308
787.5035	801.5541	805.5103
870.3379	874.4470	882.3723
891.9185	896.9073	899.8030
905.6070	908.4270	913.9543
920.0991	923.8942	925.1018
979.6301	979.8693	984.4145
1020.3954	1026.0542	1031.2549
1047.5507	1048.9883	1066.3802
1066.9035	1068.3897	1069.0800
1069.1152	1073.5719	1074.6879
1081.6040	1085.8632	1086.4991
1105.3223	1105.9329	1107.8834
1108.2208	1120.8057	1120.9604
1200.4024	1200.7781	1204.3460
1214.9527	1219.1498	1221.5304
1227.0216	1227.5845	1237.0259
1238.7840	1253.8975	1258.8479
1291.1440	1292.7708	1293.0700
1298.5762	1302.4090	1306.2099
1311.5338	1312.0729	1318.9916
1324.6446	1325.9771	1326.4610
1331.9693	1333.6685	1336.0923
1366.6883	1366.8347	1367.9981
1368.8976	1369.0242	1372.4847
1386.3768	1387.6913	1388.8203
1398.0183	1398.0582	1399.8360
1403.5869	1403.6433	1408.6585
1432.7180	1433.8940	1435.6562
1435.8981	1443.6165	1443.9146
1457.3093	1457.4402	1459.3676
1459.5586	1461.3287	1462.1867
1462.4116	1464.0855	1465.2234
1465.8667	1466.6674	1469.8714
1470.6658	1470.8370	1470.9162
1474.3643	1475.0044	1476.9359
1479.5669	1479.7792	1480.0438
1480.0675	1482.2724	1484.4283
3004.9117	3004.9393	3005.7643
3007.2872	3007.6478	3008.1846
3011.0177	3013.1865	3015.4194
3016.9556	3016.9862	3017.4982
3018.6588	3019.6496	3020.9239
3021.0121	3022.9752	3024.8494
3024.9667	3027.9634	3028.0912
3029.0094	3046.5763	3047.9687
3051.3319	3051.5605	3054.5097
3054.5772	3057.7070	3060.2399
3065.5880	3065.8344	3065.8679
3066.2145	3072.6828	3072.8339
3074.8060	3076.8324	3087.6341
3087.7611	3093.3727	3094.1519
3094.2450	3097.4958	3098.0969
3098.2321	3101.7456	3103.1860
3103.3296	3106.7792	3106.8320
3107.8567	3107.9686	3110.6334

HgBuTe-conf-5

5.8466	13.0304	15.8094
22.2810	23.3861	27.1596
28.0960	30.5744	31.2188
37.0868	38.3643	41.0111
45.2586	47.3805	51.6118
55.4848	55.9142	57.2193
61.1945	63.3977	68.1357
71.7087	74.8942	77.3593
82.0152	89.6058	102.4330
106.6904	109.3681	113.9419
119.3780	124.5790	124.7756
135.2326	137.2977	153.0358
158.6081	163.4184	188.5053
192.5445	197.2352	198.6031
199.5509	202.0863	214.9771
217.1247	219.0357	227.0223
227.6961	231.3217	233.7083
253.0710	256.6571	259.2997
271.1282	285.7126	297.3110
318.7360	319.8556	351.9274
355.3118	389.0259	390.2954
405.3319	428.9967	433.7157
444.9587	451.1629	458.7877
672.8490	680.3875	696.6577
708.7326	723.2918	729.4294
731.7358	734.5499	746.9125
754.8788	759.7349	767.9928
771.9794	785.8697	785.8835
789.7470	792.5533	803.1800
868.7223	875.6064	881.9765
893.0066	897.2726	901.1129
906.6556	909.2875	913.1021
916.0613	920.6239	925.6638
979.3062	982.5046	984.8212
1019.9425	1023.4873	1026.0528
1051.3998	1053.7845	1060.8247
1061.1115	1064.3918	1067.8286
1069.9074	1073.9687	1080.9154
1081.0522	1084.8472	1089.9310
1104.8375	1109.3356	1109.9461
1111.9039	1115.4567	1117.4231
1198.8273	1202.4329	1209.9458
1215.4345	1219.6968	1223.0901
1224.3540	1230.0283	1236.5201
1246.8181	1250.2194	1254.9366
1290.8750	1293.0667	1297.9036
1302.0421	1304.0569	1306.7108
1313.3336	1315.0112	1319.6982
1323.5352	1325.2761	1326.9196
1328.2013	1332.5916	1334.5891
1365.5070	1368.5333	1369.3238
1370.6250	1372.8714	1375.8469
1382.2522	1387.2892	1387.9310
1397.9967	1399.6609	1400.8774
1401.2032	1403.6371	1410.1919
1428.8159	1430.6408	1432.7341
1432.9949	1434.5580	1436.2506
1457.8814	1459.0674	1460.2958
1460.8354	1461.7336	1462.3455
1462.9517	1464.1425	1465.8507
1466.0952	1467.7129	1470.2038
1470.3338	1470.4678	1470.9131
1474.5627	1474.7148	1476.7950
1479.3382	1479.6074	1480.2527
1482.6712	1484.0192	1485.8863
3004.1197	3006.2923	3009.4533
3009.9703	3010.0160	3011.0181
3013.8646	3014.0038	3017.9026
3018.3466	3018.6167	3019.0416
3021.2213	3021.8532	3022.7876
3024.9884	3025.9836	3026.2664
3027.0529	3028.6728	3028.9224
3031.7284	3032.0963	3040.2463
3045.4698	3046.9336	3049.8109
3054.1091	3058.6480	3065.0953
3065.7719	3066.0689	3066.4140
3068.4012	3069.6354	3075.1189
3083.9977	3089.3293	3090.7525
3091.4818	3091.6668	3093.7604
3094.6621	3094.8440	3095.2696
3096.8252	3097.6925	3098.9126
3101.0526	3101.8893	3103.7331
3104.1014	3107.6667	3112.3245

HgMeTe-opt-1

11.1120	13.4392	18.7301
29.9789	36.4814	43.2619
46.1559	46.7921	52.0615
59.3139	64.4861	69.6446
77.4706	81.1304	84.4213
86.6839	91.9360	97.3743
107.3899	112.6377	119.2150
123.4490	127.1008	134.0928
135.1910	139.6852	141.9151
147.7704	156.2615	169.4187
178.7303	182.6685	184.3243
186.0328	196.9291	205.5401
209.3465	212.7940	218.8678
224.7560	227.1090	240.1744
244.9184	251.6328	260.2079
271.9779	277.1986	291.8649
295.3513	316.0422	323.0352
336.2264	337.9861	341.7645
357.0307	357.0572	360.2651
423.5097	424.2982	434.3104
436.8577	481.1213	489.1855
633.7088	641.2891	694.2215
702.3325	713.9829	714.0982
957.9145	965.1689	974.6076

977.5163	986.4488	995.0813	3014.7668	3017.7407	3021.2637	271.9671	277.1752	291.8092	1462.3032	1464.2165	1468.0661
1061.5859	1063.7180	1064.9372	3048.3971	3052.2222	3053.7286	295.3880	315.9973	323.0243	1468.3089	1469.7794	1472.1411
1070.2881	1073.1004	1080.0212	3064.9534	3068.2655	3074.6548	336.2042	337.9241	341.7689	1473.4097	1473.8941	1475.3245
1102.4220	1105.3432	1108.1881	3078.2025	3083.8046	3084.8855	357.0148	357.0612	360.2439	1478.1350	1481.2654	1483.7396
1109.9176	1113.6883	1113.7824	3085.1843	3086.6409	3091.3807	423.4890	424.3032	434.2880	1492.3113	1495.4380	1498.9199
1150.2190	1151.3501	1152.2578	3131.9073	3132.9228	3139.0510	436.8605	481.0948	489.1908	1499.0057	1501.0681	1503.5605
1153.6151	1154.3502	1157.6915	3141.2185	3141.4434	3142.6857	633.7041	641.2961	694.2110	2984.2786	2986.5464	2989.6005
1181.7394	1188.1436	1203.3137	3150.0651	3153.0691	3157.5945	702.3485	714.0313	714.1048	2994.4276	2996.1999	2998.4906
1213.4879	1217.1566	1218.8213	3159.4321	3161.7161	3162.1413	957.9575	965.1633	974.5958	3004.1226	3008.6152	3012.4040
1272.1608	1280.4869	1286.6387				977.5292	986.4626	995.1226	3014.7857	3017.6640	3021.2838
1297.7583	1299.0432	1314.3783	HgMeTe-conf-12			1061.5868	1063.7187	1064.9359	3048.3727	3052.2126	3053.7116
1415.4967	1417.9250	1419.7362	11.1040	13.4471	18.7288	1070.2856	1073.1055	1080.0464	3064.9409	3068.2845	3074.6844
1421.5353	1422.3979	1428.6771	29.9585	36.4732	43.2675	1102.4369	1105.3417	1108.1992	3078.2385	3083.7901	3084.8702
1441.5015	1445.1515	1445.6803	46.1330	46.7894	52.0392	1109.9140	1113.6904	1113.7796	3085.2021	3086.5188	3091.4304
1446.8705	1447.9288	1449.8910	59.2719	64.4732	69.5930	1150.2116	1151.3495	1152.2652	3131.9429	3132.8950	3139.0344
1450.3087	1450.8222	1452.4495	77.5251	81.1232	84.3951	1153.6295	1154.3393	1157.6766	3141.1421	3141.4247	3142.6923
1453.0592	1456.8642	1457.0182	86.6542	91.9152	97.3840	1181.7634	1188.1562	1203.2993	3150.0985	3153.1456	3157.7782
1462.3226	1464.2311	1468.0630	107.2952	112.6151	119.1079	1213.5208	1217.1457	1218.8203	3159.4907	3161.5934	3162.1143
1468.3122	1469.7928	1472.1449	123.4693	127.0972	134.0166	1272.1733	1280.4951	1286.6150			
1473.3961	1473.8972	1475.3323	135.1739	139.6027	141.8803	1297.7868	1299.0996	1314.4217			
1478.1339	1481.2760	1483.7491	147.7217	156.2760	169.4178	1415.4960	1417.9214	1419.7327			
1492.3042	1495.4332	1498.9193	178.7373	182.6078	184.2139	1421.5532	1422.3994	1428.6742			
1498.9899	1501.0866	1503.5813	185.9947	196.9278	205.5065	1441.4993	1445.1072	1445.6938			
2984.2650	2986.5076	2989.5879	209.2712	212.7535	218.8256	1446.8810	1447.8992	1449.8913			
2994.4189	2996.1903	2998.5020	224.7615	227.1796	240.1522	1450.2850	1450.8257	1452.4455			
3004.1604	3008.6702	3012.4546	244.8951	251.6023	260.1951	1453.0719	1456.8698	1457.0124			

For the calculated geometry coordinates, please go to *J. Phys. Chem. A* 2020, 124, 24, 4946–4955. DOI: 10.1021/acs.jpca.0c01607.

3 CONCLUSION

NMR has emerged as one of the most promising experimental techniques for implementing quantum computing protocols. Precise and accurate control over the magnetic moments of nuclei provided the basis for NMR being used to manipulate information using the rules of quantum mechanics. The isolation of the nuclear spins and consequent long relaxation times, combined with RF pulses, led to important studies in the area.

Over the last decade, quantum computer with up to 12 qubits have been developed via liquid-NMR. However, in order to increase this number of qubits in NMR quantum computing, the qubit molecule should meet conditions such as: a) Large and appropriately dispersed chemical shifts (δ), which allows logic gate implementations by RF pulses, applied in the system resonance frequencies, making of the qubit individual manipulations; b) appreciable coupling constant (J) between the pair of spins, since this promotes the interaction between individual qubits in the QIP, and; c) a long relaxation time (T), so that the coherence of superposed states is maintained during the quantum processing and the information is not destroyed.

In this concern, exceptionally large "through space" spin-spin, TS J(^{31}P,^{31}P), coupling observed in 1,8-diphosphanaphthalenes (PPN) and in naphtho[1,8-cd]-1,2-dithiole phenylphosphines (NTP) were proposed and investigated to develop new promising molecules able to provide more accurate control in the large-scale QIP via NMR. The PPN structures were optimized was carried out employing the B3LYP functional among 6-311G(d,p), 6-31+G(d,p) or 6-31+G(3df,2pd) basis sets. B3LYP/6-311G(d,p) level has provided a good correlation between calculated and theoretical values. The spectroscopic properties of PPN and NTP derivatives, such as chemical shifts (δ) and TS spin-spin couplings were explored by theoretical strategies. The spectroscopic parameters (δ and J) were calculated with different DFT functionals for P-1 and P-2 atoms in both molecules within the “locally dense basis sets” approach. For the PPM molecule, the B3LYP/aug-cc-pVTZ-J level showed better agreement with experimental data of ^{31}P chemical shifts and PBE1PBE functional among pcJ-2 within the LDBS-1 scheme was the most accurate level for TS J(^{31}P,^{31}P) coupling. Differently, for the NTP dimer, PBE1PBE and pcJ-2 within the LDBS-2 scheme showed better agreement with the experimental data of ^{31}P chemical shifts; otherwise, for the TS J(^{31}P,^{31}P) coupling, the most accurate methodology was using the PBE1PBE functional with the Def2-TZVP basis set within the LDBS-1 scheme. From our results, the derivatives PPN$_o$-F, PPN$_o$-ethyl and PPN$_o$-NH$_2$ were

the best candidates for quantum information processing via NMR, where the large TS J could circumvent the need of long-time quantum gate implementations. Which could, in principle, overcome natural limitations related to the development of large-scale NMR.

A computational design strategy for prescreening recently synthesized complexes of cadmium, mercury, tellurium, selenium, and phosphorus, called MRE complexes, as suitable qubit molecules for NMR QIP was also reported. Assembled together with the most common qubits used in NMR quantum computation experiments, spin-1/2 nuclei, such as ^{113}Cd, ^{199}Hg, ^{125}Te, and ^{77}Se, could leverage the prospective scalable quantum computer architectures, enabling many and heteronuclear qubits for NMR quantum information processing (QIP) implementations. Chemical shifts and spin–spin coupling constants in five MRE complexes were examined using the spin–orbit zeroth order regular approximation (ZORA) at the DFT level and the four-component relativistic Dirac–Kohn–Sham approach. In this work, we have investigated the influence of different conformers, basis sets, exchange–correlation functionals, and methods to treat the relativistic as well as solvent effects. The differences in the chemical shifts and SSCCs between different low energy conformers of the studied complexes were very small. The TZ2P basis set was found to be the optimum choice for the studied chemical shifts, while the TZ2P-J basis set was the best for the couplings studied. The PBE0 exchange–correlation functional exhibited the best performance for the studied MRE complexes. The addition of solvent effects has not improved on the gas phase results in comparison to the experiment, except for the phosphorus chemical shift. Using MRE complexes as qubit molecules for NMR QIP could face the challenges in single qubit control and multiqubit operations. They exhibit chemical shifts appropriately dispersed, allowing qubit addressability and exceptionally large spin–spin couplings, which could reduce the time of quantum gate operations and likely preserve the coherence.

Given the above, it is evident that the theoretical study of NMR parameters is a promising tool in the field of quantum computing. Thus, with respect to promising molecules for QIP via NMR, it is possible to optimize them as well as to propose new structures which meets the optimal conditions for a qubit molecule. Our work introduced those derivatives toward suitable qubits molecules as a kick-off for the construction of more complex derivatives, which can meet the challenge of large-scale NMR QIP.

APPENDIX

Publications resulting from this thesis

Revista Virtual de Química

ISSN 1984-6835

Artigo

Informação Quântica e Parâmetros de Ressonância Magnética Nuclear

Lino, J. B. R.; Ramalho, T. C.*

Rev. Virtual Quim., **2018**, *10* (4), *no prelo*. Data de publicação na Web: 27 de julho de 2018

http://rvq.sbq.org.br

Quantum Information and Nuclear Magnetic Resonance Parameters

Abstract: Regarding the end of the 1900s, a small community of researchers in physics, computer science, mathematics and chemistry began to explore the fertile ground at the intersection of quantum mechanics with information theory, which led to a new and powerful paradigm of quantum computing. Quantum information processing promises to extend today's computing resources. Quantum computers, theoretically, could solve problems much more quickly than any classic computer. Intensive experimental efforts have been made to implement quantum computing since Shor and Grover developed their algorithms. In 1997, Nuclear Magnetic Resonance (NMR) emerged as one of the most promising experimental techniques for the implementation of quantum computing protocols. The isolation of nuclear spins and consequent long relaxation times, combined with the perfect dynamics implemented by radiofrequency pulses, led to important studies in the area. Therefore, nuclear spins are picked out as good candidates for quantum bits. In this scenario, quantum chemistry covers a vast field of quantum information science and can lead to advances in scientific research.

Keywords: Quantum computing; NMR parameters calculations; Hyperfine coupling constant; Theoretical calculations.

THE JOURNAL OF PHYSICAL CHEMISTRY A
Article
Cite This: J. Phys. Chem. A 2019, 123, 1372−1379
pubs.acs.org/JPCA

Exploring Through-Space Spin−Spin Couplings for Quantum Information Processing: Facing the Challenge of Coherence Time and Control Quantum States

Jéssica Boreli dos Reis Lino[†] and Teodorico Castro Ramalho*[,†,‡]

[†]Chemistry Department, Federal University of Lavras, 37200-000 Lavras, MG Brazil

[‡]Center for Basic and Applied Research, Faculty of Informatics and Management, University Hradec Kralove, 50003 Hradec Kralove, Czech Republic

Supporting Information

ABSTRACT: Nuclear magnetic resonance (NMR) is a powerful tool for studying quantum information processing (QIP). Recently quantum technologies have been proposed to overcome the challenges in large-scale NMR QIP. Furthermore, computational chemistry can promote its improvement. Nuclear spins-$^1/_2$ are natural qubits and have been used in most NMR quantum computation experiments. However, molecules that enable many qubits NMR QIP implementations should meet some requirements regarding their spectroscopic properties. Exceptionally large through-space (TS) P−P spin−spin coupling constants (SSCC or J) observed in 1,8-diphosphanaphthalenes (PPN) and in naphtho[1,8-*cd*]-1,2-dithiole phenylphosphines (NTP) were proposed and investigated to provide more accurate control within large-scale NMR QIP. Spectroscopic properties of PPN and NTP derivatives were explored by theoretical strategies using locally dense basis sets (LDBS). ^{31}P chemical shifts (δ) calculated at the B3LYP/aug-cc-pVTZ-J level and TS P−P SSCCs at the PBE1PBE/pcJ-2 (LDBS-1) level are very close to the experimental data for the PPN molecule. Differently, for the NTP dimer, PBE1PBE/pcJ-2 (LDBS-2) predicts more accurate ^{31}P δ, whereas PBE1PBE/Def2-TZVP (LDBS-1) forecasts more accurate TS P−P SSCCs. From our results, PPN$_o$-F, PPN$_o$-ethyl, and PPN$_o$-NH$_2$ were the best candidates for NMR QIP, in which the large TS SSCCS could face the need of long-time quantum gates implementations. Therefore, it could overcome natural limitations concerning the development of large-scale NMR.

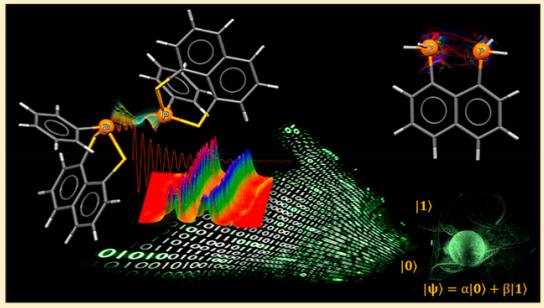

THE JOURNAL OF PHYSICAL CHEMISTRY A

pubs.acs.org/JPCA Article

Enhancing NMR Quantum Computation by Exploring Heavy Metal Complexes as Multiqubit Systems: A Theoretical Investigation

Jéssica Boreli dos Reis Lino, Stephan P. A. Sauer, and Teodorico Castro Ramalho*

Cite This: J. Phys. Chem. A 2020, 124, 4946−4955 Read Online

ACCESS | Metrics & More | Article Recommendations | Supporting Information

ABSTRACT: Assembled together with the most common qubits used in nuclear resonance magnetic (NMR) quantum computation experiments, spin-1/2 nuclei, such as ^{113}Cd, ^{199}Hg, ^{125}Te, and ^{77}Se, could leverage the prospective scalable quantum computer architectures, enabling many and heteronuclear qubits for NMR quantum information processing (QIP) implementations. A computational design strategy for prescreening recently synthesized complexes of cadmium, mercury, tellurium, selenium, and phosphorus (called MRE complexes) as suitable qubit molecules for NMR QIP is reported. Chemical shifts and spin−spin coupling constants (SSCCs) in five MRE complexes were examined using the spin−orbit zeroth order regular approximation (ZORA) at the density functional theory level and the four-component relativistic Dirac−Kohn−Sham approach. In particular, the influence of different conformers, basis sets, exchange−correlation functionals, and methods to treat the relativistic as well as solvent effects were studied. The differences in the chemical shifts and SSCCs between different low energy conformers of the studied complexes were found to be very small. The TZ2P basis set was found to be the optimum choice for the studied chemical shifts, while the TZ2P-J basis set was the best for the couplings studied in this work. The PBE0 exchange−correlation functional exhibited the best performance for the studied MRE complexes. The addition of solvent effects has not improved on the gas phase results in comparison to the experiment, with the exception of the phosphorus chemical shift. The use of MRE complexes as qubit molecules for NMR QIP could face the challenges in single qubit control and multiqubit operations. They exhibit chemical shifts appropriately dispersed, allowing qubit addressability and exceptionally large spin−spin couplings, which could reduce the time of quantum gate operations and likely preserve the coherence.

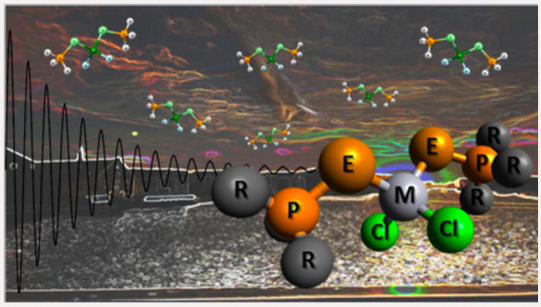

Theoretical Chemistry Accounts (2021) 140:8
https://doi.org/10.1007/s00214-020-02706-9

REGULAR ARTICLE

Value of NMR relaxation parameters of diamagnetic molecules for quantum information processing: optimizing the coherent phase

Jéssica Boreli dos Reis Lino[1] · Mateus Aquino Gonçalves[1] · Teodorico Castro Ramalho[1,2]

Received: 3 August 2020 / Accepted: 15 December 2020 / Published online: 12 January 2021

Abstract
Quantum computing is the science that studies the applications of quantum mechanics in computer science. Thus, a quantum computer is an entity which can store quantum information, which in turn is an innovative procedure that creates conditions to allow the implementation of quantum algorithms and simulations, wherein the decoherence is a key problem. Considering the unique qubits, the time of the coherence phase can be well measured by the time of transversal relaxation (T_2). In this line, we study the PPN derivatives, PPN-F, PPN-ethyl and PPN-NH_2, as candidates to carry out quantum information. Therefore, the structures were optimized at the B3LYP/6-311G(d,p) level; after the optimization, molecular dynamics (MD) simulations were performed and the structures obtained were selected by statistical inefficiency method to then obtain the relaxation parameters (T_1 and T_2). The modification in the PPN molecule increases the transverse relaxation rate phosphorus nuclear spins at most five times because of the hydrogen bonds. From our findings, the studied molecules showed excellent candidates for the processing of quantum information; however, it is important to rule out the PPN-NH_2 molecule that has more significant values of T_1 and T_2, and thus, this compound stands out from the others studied.

Keywords ^{31}P NMR · NMR parameters calculations · Quantum computation · Quantum information

Fwd: Virtual Issue on Qubits

Teodorico C. Ramalho <teodorico.ramalho@gmail.com>
Tue 21/11/16 09:44
To: Jéssica Boreli <jessicaboreli@outlook.com>

---------- Forwarded message ---------
De: **Gregory Hartland** <hartland-office@jpc.acs.org>
Date: dom., 14 de nov. de 2021 às 11:23
Subject: Virtual Issue on Qubits
To: teodorico.ramalho@gmail.com <teodorico.ramalho@gmail.com>

Dear Prof. Ramalho,

I am writing to you to let you know that your article "Enhancing NMR Quantum Computation by Exploring Heavy Metal Complexes as Multiqubit Systems: A Theoretical Investigation" has been included in a new Virtual Issue on "Recent Innovations in Solid-State and Molecular Qubits for Quantum Information Applications." This issue features recent experimental and theory papers from several ACS journals that describe research on the discovery of new qubit candidates and devices, elucidation of decoherence mechanisms to increase qubit lifetime, and computational applications of qubit-based quantum computers.

The Virtual Issue has been published in *The Journal of Physical Chemistry A/B/C/Letters* and can be found at:

https://pubs.acs.org/page/vi/qubits

Please feel free to share and distribute with your colleagues.

We thank you for contributing to ACS journals, and we hope that you will consider us for your future publications in this area, as well as other areas of research!

Yours sincerely,

Greg Hartland

Deputy Editor

The Journal of Physical Chemistry C

Anastassia Alexandrova

Senior Editor

The Journal of Physical Chemistry A/B/C